



Universitätsklinikum  
Hamburg-Eppendorf

Dissertation for the attainment of  
the academic title  
*doctor rerum naturalium*

# Antigen-specific therapies of membranous nephropathy

Presented by

**Sarah Mara Stella Köllner**

Department of Biology  
University of Hamburg

1. Reviewer: Prof. Dr. Wolfgang Streit
2. Reviewer: Priv.-Doz. Dr. Gunther Zahner

Defense: 30.06.2023

Hamburg, April 2023

The presented work was conducted from January 2020 until December 2022 externally in the III. Department of Medicine at the University Medical Center Hamburg-Eppendorf under the supervision of Priv.-Doz. Dr. Gunther Zahner. Prof. Dr. Wolfgang Streit supervised this work in the Department of Biology at the University of Hamburg.

## Eidesstattliche Erklärung

Hiermit versichere ich eidesstattlich, dass ich die Arbeit selbständig verfasst und keine anderen als die angegebenen Quellen und Hilfsmittel benutzt habe.

Hamburg, den 17.01.2023



---

Sarah Köllner

Ich versichere, dass dieses gebundene Exemplar der Dissertation und das in elektronischer Form eingereichte Dissertationsexemplar (über den Docata-Upload) und das bei der Fakultät (zuständiges Studienbüro bzw. Promotionsbüro Physik) zur Archivierung eingereichte gedruckte gebundene Exemplar der Dissertationsschrift identisch sind.

Hamburg, den 17.01.2023



---

Sarah Köllner

# 1 Table of Contents

I.	Acknowledgements .....	I
II.	Index of Figures .....	II
III.	Index of Tables .....	III
IV.	Summary .....	IV
V.	Zusammenfassung.....	V
1.	Introduction .....	1
1.1	Membranous nephropathy .....	1
1.2	Antigens in membranous nephropathy .....	2
1.3	Current treatments in MN.....	4
1.4	Engineered antibodies as a new therapeutic concept .....	5
1.5	Fc gamma receptors and their role in immunity.....	6
1.6	Liver sinusoidal endothelial cells as an endogenous degradation system.....	8
1.7	Experimental MN mouse models .....	9
1.8	Aim of this work.....	10
2	Material and Methods .....	11
2.1	Material.....	11
2.1.1	Equipment .....	11
2.1.2	Consumables .....	12
2.1.3	Chemicals .....	13
2.1.4	Enzymes and buffers .....	13
2.1.5	Antibodies .....	14
2.1.6	Commercial kits and markers.....	15
2.1.7	Bacterial strains .....	15
2.1.8	Cell lines.....	15
2.1.9	Plasmids and oligonucleotides .....	16
2.1.10	Proteins.....	17
2.1.11	Media and supplements.....	18
2.1.12	Buffers and solutions.....	19
2.1.13	Software and Databases .....	20
2.2	Methods .....	21
2.2.1	Cloning of AgFc constructs.....	21
2.2.2	Production of AgFc .....	24
2.2.3	Antibody-mediated cellular cytotoxicity assay (ADCC).....	25
2.2.4	Enzyme-linked immunosorbent assay (ELISA).....	26

2.2.5	Isolation of primary liver sinusoidal endothelial cells .....	27
2.2.6	Uptake assays fluorescence-coupled immune complexes.....	28
2.2.7	Immunofluorescence .....	28
2.2.8	Flow cytometry .....	29
2.2.9	Analysis of fluorescence in organs and blood samples with <i>in vivo</i> imaging systems (IVIS).....	31
2.2.10	Animal experiments .....	31
2.2.11	Statistics .....	35
3	Results.....	37
3.1	Characterization of AgFc constructs .....	37
3.2	Antibody-dependent cellular cytotoxicity mediated through AgFcs.....	40
3.3	In vitro immune complex uptake by primary LSECs.....	42
3.4	In vivo blocking of rabbit anti-THSD7A IgG with AgFcs .....	44
3.6	In vivo distribution of immune complexes 6 hours post injection .....	51
3.7	The FcRn's involvement in the rescue of immune complexes.....	53
3.8	Clearance of large amounts of polyclonal immune complexes.....	57
3.9	In vivo safety assessment of AgFcs.....	59
3.10	Blocking of actively THSD7A-immunized mice sera to determine a therapeutic dose.....	62
3.11	Pre-Treatment of actively THSD7A-immunized mice with AgFcs .....	63
3.12	Treatment of actively THSD7A-immunized mice with AgFc .....	65
3.13	Treatment of autoimmune hPLA2R mice.....	68
4	Discussion .....	71
4.1	In vitro characterization of AgFcs .....	72
4.2	SELF mutation leads to better uptake into LSECs in vitro but not in vivo.....	73
4.3	The impact of the SELF mutation on FcγRIII.....	74
4.4	Kinetics of immune complex uptake in LSECs .....	75
4.5	The neonatal Fc receptor impacts immune complex degradation .....	76
4.6	Administering AgFcs to healthy animals leads to mild antibody generation in a few mice.....	78
4.7	Clearance of large amounts of immune complexes does not lead to immune complex deposition .....	79
4.8	Treatment success depends on the limitations of the mouse models.....	79
4.9	Enhancements of AgFcs in combination with new antigen-specific therapies could increase therapeutic potency .....	82
5	Conclusion and Outlook.....	86
6	Annex .....	87
6.1	Supplementary data .....	87
6.2	Abbreviations .....	89
7	References .....	93

## I. Acknowledgements

Firstly, I would like to thank **Dr. Nicola Tomas**, who invited me into his laboratory and into his team, who took a lot of time to go over every little bit of data and was as invested emotionally in this thesis as I was. Thank you and I had a wonderful time with you all!

A special thanks goes to **Prof. Dr. Wolfgang Streit**, who agreed to be my first reviewer. Thank you for this opportunity and your trust.

Secondly, I would like to thank **Priv.-Doz. Dr. Gunther Zahner**, who not only agreed to be the second reviewer of my thesis but also provided guidance along the way. All your insights were deeply appreciated.

I want to acknowledge Prof. Dr. Friedrich Koch-Nolte as well: without your creativity and excitement this thesis would not have been possible.

I want to thank my colleagues that helped me during these years: Silke Dehde, Renke Lucas, Larissa Seifert, Ming Huang, Annabel Schnarre and Jana Abt. For all the group outings, dumpling nights and wine shared between us. A big thank you to Renke and Laura, who made this experience so much more fun! I want to thank co-workers like Pauline Sprezyna and Anastasios Giannou for showing me how to isolate LSECs, Kingsley Kumashie and Hans-Joachim Paust for helping with my FACS panel, Catherine Meyer-Schwesinger for the valuable insight on the confocal and IF stainings and the Nolte working group for sharing HEK cells and their expertise on antibodies.

I want thank friends and family for seeing this through with me but especially I want to thank my mom, without you and all your support I would not be here. I hope you are proud.

## II. Index of Figures

Figure 1: Histological features of membranous nephropathy .....	2
Figure 2: Antigens of membranous nephropathy .....	3
Figure 3: The sweeping antibody concept.....	6
Figure 4: Gating strategies for flow cytometry .....	30
Figure 5: Analyzing blood and organ samples with IVIS .....	31
Figure 6: Creating AgFc constructs.....	38
Figure 7: Characterization of anti-THSD7A and anti-PLA2R hybridomas.....	39
Figure 8: Binding characterization of AgFcs .....	40
Figure 9: ADCC through AgFcs.....	41
Figure 10: Immune complex uptake in primary LSECs .....	43
Figure 11: Blocking of rIgG with d1d2-AgFc in THSD7A <sup>-/-</sup> mice.....	45
Figure 12: Time course of <i>in vitro</i> formed immune complexes <i>in vivo</i> . .....	47
Figure 13: Time course of <i>in vivo</i> degradation.....	50
Figure 14: <i>In vivo</i> uptake in WT BALB/c mice. ....	52
Figure 15: Immune complex uptake in FcRn <sup>-/-</sup> mice .....	56
Figure 16: <i>In vivo</i> clearance of immune complexes.....	61
Figure 17: Safety assessment of AgFcs.....	58
Figure 18: Blocking of antibodies in sera from actively immunized mice in ELISA.....	62
Figure 19: Pre-Treatment of actively immunized mice.....	64
Figure 20: Analysis of IgG deposition in pre-treated THSD7A-EAMN mice.....	65
Figure 21: Treatment of THSD7A-MN mice. ....	67
Figure 22: Treatment of hPLA2R autoimmune mice.....	69
Figure 23: Antigen-specific therapies for MN .....	85
Figure 24: Non-reducing SDS-PAGE of remaining AgFcs .....	89

### III. Index of Tables

Table 2-1: List of equipment .....	11
Table 2-2: List of consumables .....	12
Table 2-3: List of enzymes .....	13
Table 2-4: List of commercial antibodies.....	14
Table 2-5: List of used Antibodies .....	14
Table 2-6: List of commercial kits .....	15
Table 2-7: List of markers .....	15
Table 2-8: Used bacterial strains .....	15
Table 2-9: Used cell lines .....	16
Table 2-10: Used plasmids .....	16
Table 2-11: Used oligonucleotides .....	17
Table 2-12: Used proteins .....	17
Table 2-13: Recipe for LB medium.....	18
Table 2-14: Recipe of SOC medium .....	18
Table 2-15: Medium supplements used.....	19
Table 2-16: List of buffers and solutions .....	19
Table 2-17: List of software and databases .....	21
Table 2-18: Composition of digestion mix.....	21
Table 2-19: Composition of ligation mix .....	22
Table 2-20: Reagents for the colony PCR.....	22
Table 2-21: Colony PCR protocol.....	23
Table 2-22: PCR amplification for md1d20 and hd1d20 .....	23
Table 2-23: PCR protocol.....	24
Table 6-1: Degree of labelling for fluorochrome coupled AgFcs .....	89
Table 6-2: List of abbreviations used in this study.....	89

#### IV. Summary

Membranous nephropathy (MN) is a rare but potentially severe kidney disease and a major cause of nephrotic syndrome in adults. It is defined by immune deposits at the glomerular basement membrane and destruction of the podocyte. Immune deposits are formed through autoantibodies targeting antigens on the podocyte surface such as PLA2R and THSD7A and subsequent binding of complement factors. The resulting proteinuria can result in hyperlipidemia, hypoalbuminemia and ultimately kidney failure. So far, patients have been treated with drugs that generally suppress the immune system leaving patients susceptible to secondary infections. In an effort to create antigen-specific therapies that target pathogenic autoantibodies exclusively, antibody Fc fusion constructs (AgFc) were generated. These AgFc consist of a mouse Fc region fused to the epitope-containing domains of the respective podocyte antigens PLA2R and THSD7A. Consequently, these AgFc can form immune complexes with the circulating pathogenic antibodies preventing the binding of autoantibodies to their podocyte targets inside the kidneys. A mutation was inserted in the Fc region to increase the affinity to the Fc gamma receptor IIB (Fc $\gamma$ RIIB), which amplifies the intrinsic quality of this receptor: the uptake and subsequent degradation of immune complexes into specialized scavenger cells of the liver (LSECs). With this, pathogenic autoantibodies can be depleted in an antigen-specific manner without influencing the immune system globally.

*In vitro* characterization showed specific binding of the AgFc to their corresponding monoclonal antibodies and an enhanced affinity to Fc $\gamma$ RIIB compared to the WT AgFc. Additionally, an increased uptake into LSECs as immune complexes could be observed. To test the therapeutic potential of our AgFc in different disease models, we treated MN in different mouse models: actively THSD7A-immunized WT BALB/c and in transgenic hPLA2R-expressing mice that develop autoantibodies intrinsically. The effect on other Fc $\gamma$ Rs was investigated as well as the ability to deplete autoantibodies from the circulation and the deposition of immune complexes along the glomerular basement membrane. Proteinuria could be decreased efficiently in actively THSD7A-immunized mice. Further characterization of the constructs included safety and toxicity assessment in healthy mice, where we injected animals with several small doses over consecutive weeks and monitored their response. Moreover, to study if large amounts of polyclonal immune complexes might cause immune complex disease (ICD), THSD7A<sup>-/-</sup> mice were immunized with domains of THSD7A, causing an immune response with high anti-THSD7A antibody titers. The depletion of the antibody titers *in vivo* with a large dose of AgFc revealed no changes in serum parameters indicating the onset of ICD.

Overall, these preclinical experiments demonstrate the potential of AgFcS to efficiently decrease antibody levels in an antigen-specific way, which could represent a highly specific, less toxic treatment for MN and other antibody-mediated autoimmune diseases in the future.

## V. Zusammenfassung

Die membranöse Nephropathie (MN) ist eine seltene, aber potentiell schwer verlaufende Nierenerkrankung, sowie die häufigste Ursache eines nephrotischen Syndroms bei Erwachsenen. Sie ist durch Immunablagerungen an der glomerulären Basalmembran und Zerstörung der Podozyten charakterisiert. Die Immunablagerungen bestehen aus Autoantikörpern, die Antigene auf der Podozytenoberfläche wie beispielsweise PLA2R oder THSD7A binden, sowie Komplementfaktoren. Die daraus resultierende Proteinurie kann zu Hyperlipidämie, Hypoalbuminämie und schließlich zu Nierenversagen führen. Bisher werden Patienten mit einer allgemeinen Suppression des Immunsystems behandelt, was diese allerdings anfällig für Sekundärinfektionen macht. Prinzipiell ermöglicht die genaue Kenntnis der renalen Autoantigene jedoch eine zielgerichtete Therapie. Um Antigen-spezifische Therapien zu entwickeln, wurden Antikörper-Fc-Fusionskonstrukte (AgFcS) generiert. Diese Fusionsproteine bestehen aus einem Maus-Fc-Teil und Domänen der Podozyten-Antigene, welche Epitope der Autoantikörper enthalten, anstatt des Fab-Parts. Dadurch können die AgFcS zirkulierende Autoantikörper in Immunkomplexen binden und verhindern, dass diese ihre Target-Proteine auf den Podozyten in der Niere erreichen können. Eine Mutation im Fc-Teil erhöht die Affinität zum Fc-Gamma-Rezeptor IIB (Fc $\gamma$ RIIB) und verstärkt dessen intrinsischen Eigenschaften: Aufnahme und Abbau von Immunkomplexen durch spezialisierte Fresszellen in der Leber (LSECs). Folglich können Autoreaktive Antikörper abgefangen werden, ohne das Immunsystem global zu beeinflussen.

Die *in vitro* Charakterisierung der AgFcS zeigte sowohl eine spezifische Bindung an die passenden monoklonalen Antikörper als auch eine erhöhte Affinität der mutierten AgFcS zum Fc $\gamma$ RIIB. Ebenso konnte gezeigt werden, dass Immunkomplexe aus monoklonalen Antikörpern und AgFcS vermehrt in die LSECs aufgenommen wurden. Das therapeutische Potenzial der AgFcS wurde in verschiedenen Krankheitsmodellen getestet: in THSD7A-immunisierten WT BALB/c Mäusen und in transgenen hPLA2R exprimierenden Mäusen, die *in situ* Autoantikörper gegen PLA2R bilden. Die Wirkung auf andere Fc $\gamma$ Rs wurde ebenso untersucht wie die Fähigkeit Autoantikörper aus dem Blutkreislauf zu entfernen und Ablagerungen von Immunkomplexen entlang der glomerulären Basalmembran zu verhindern. Die Proteinurie konnte bei THSD7A-immunisierten Mäusen gegenüber transgenen humanen PLA2R-Mäusen effizient gesenkt werden. Zusätzlich

wurden die Effekte der AgFcs auf gesunde Mäuse bestimmt als auch untersucht, ob große Mengen polyklonaler Immunkomplexe eine Immunkomplexkrankheit (ICD) verursachen können. Diese Untersuchungen sind entscheidend für die Verträglichkeit der AgFcs und in beiden Versuchsreihen konnten keine ungewollten Nebenwirkungen festgestellt werden.

Zusammenfassend haben diese präklinischen Experimente gezeigt, dass AgFcs Autoantikörper-Titer Antigen-spezifisch und effizient verringern können und könnten sich dadurch zu einer erfolgreichen alternativen Therapiemethode für MN Patienten und Patienten anderer Antikörper-vermittelten Autoimmunerkrankungen entwickeln.

## 1. Introduction

### 1.1 Membranous nephropathy

Membranous nephropathy (MN) is an antibody-mediated autoimmune kidney disease. The autoantibodies developed by patients damage the filtration barrier of the glomerulus through mechanisms of action that are still poorly understood. After diagnosis, 40 % of cases undergo spontaneous remission, while 30 % develop end-stage kidney disease after 10 years, causing a highly heterogeneous outcome in patients. Clinically MN is characterized by proteinuria exceeding 3.5 grams per day, low serum albumin and the risk of renal failure [1]. In some cases, this can lead to nephrotic syndrome. Circulating antibodies against podocyte antigens like thrombospondin type 1 domain containing 7A (THSD7A) or phospholipase A2 receptor (PLA2R) can be found in the majority of patients [1]. Even though both proteins are expressed in several tissues throughout the body, to date it is not clear why the disease is limited to the kidney [2]. In electron microscopy, patients show a broadening of the glomerular basement membrane (GBM), podocyte foot process effacement and subepithelial deposition of immune complexes (Figure 1A). The structure of the glomerular filtration barrier is made up of podocytes, the GBM, and the endothelium. Podocytes enwrap the outer glomerular capillaries creating a functional slight diaphragm [3]. In case of podocyte injury, proteins can escape the filtration barrier creating proteinuria. Immunohistochemically, patients can show an increased THSD7A or PLA2R staining, depending on the antibody involved, as can be seen in Figure 1B compared to healthy individuals. Additionally, immune deposits can be that consist of different IgG subtypes and complement factors. When there is no underlying cause to be found such as infection, autoimmune disease or malignancies defining secondary MN [4], patients are diagnosed with primary or idiopathic MN. In primary MN, deposits along the GBM are made up predominantly of IgG4. The other subtypes IgG1, IgG2, and IgG3 were found in 72, 26, and 87 % of patients, respectively [5]. IgG4 is a peculiar antibody for it normally does not bind the complement factor C1q and behaves like a monovalent antibody because it can undergo Fab-arm exchange, creating bispecific antibodies. This usually has a tolerogenic effect by binding IgG1 or competing with IgE and the reason why the immune deposits are mostly made up of IgG4 remains unknown. Haddad et al. [6] found that altered glycosylation of IgG4 in PLA2R-positive MN patients can activate the lectin pathway *in vitro*, providing an idea how the complement system might be activated even with low amounts of other activating subtypes such as IgG1, IgG2 and IgG3 being present. Moreover, recent investigations in complement-deficient mice suggest that complement-independent mechanisms

also play a role in the mediation of glomerular damage and proteinuria (Seifert et al., unpublished).

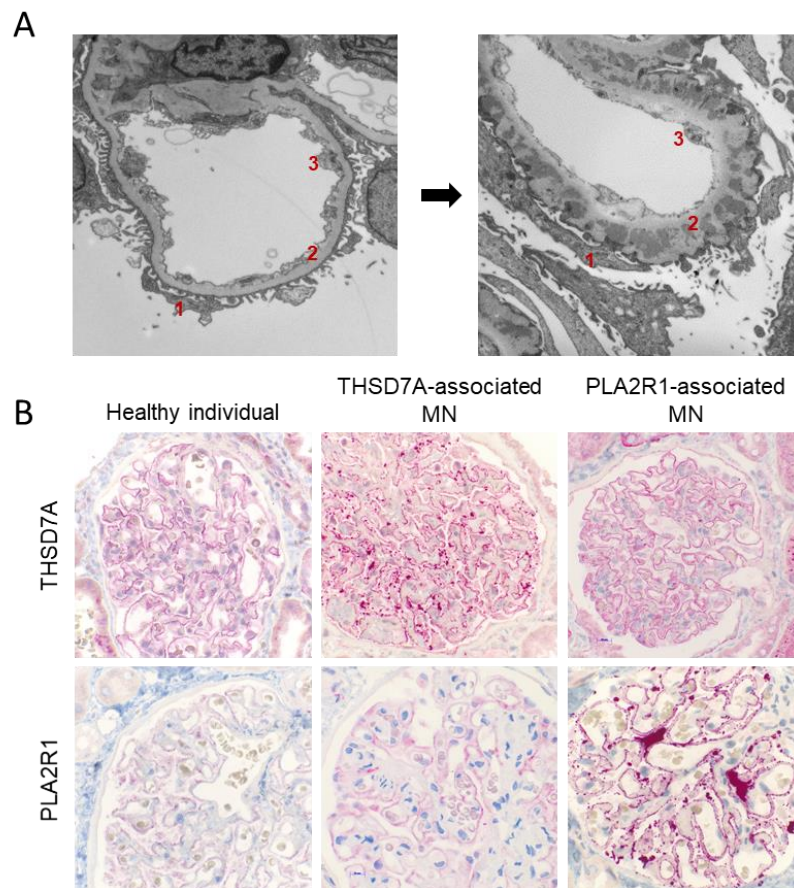


**Figure 1: Histological features of membranous nephropathy.** (A) Electron microscopic image of a normal (left) and diseased (right) glomerular filtration barrier. The structure of the glomerular filtration barrier is made up of 1: podocytes, 2: glomerular basement membrane (GBM), and 3: the endothelium. In MN, the GBM is broadened, podocyte foot processes are effaced and deposition of immune complexes is found in the subepithelial space. (B) Immunohistochemical staining for THSD7A and PLA2R1 in renal biopsy specimens from healthy controls and from patients with MN. MN patients can present with circulating autoantibodies against either THSD7A or PLA2R. The upper row shows THSD7A staining in biopsies from healthy individuals, THSD7A-associated MN patients and PLA2R1-associated patients. The staining for THSD7A is increased and granular deposits can be observed in the THSD7A-associated MN patient but not in the PLA2R-associated MN patient (upper row, middle and right pictures). The lower row shows increased and granular deposits for the PLA2R1-associated patient, while the healthy control and THSD7A-associated MN patient show basal staining (lower row, far right picture). All images were kindly provided by Prof. Dr. Thorsten Wiech. Own Figure, based on Seifert et al. [7].

## 1.2 Antigens in membranous nephropathy

Until recently, only two major antigens were known to be involved in this disease, THSD7A [8] and PLA2R [9], making up about 85% of the cases worldwide. The rise of new approaches in antigen discovery expanded the field of MN tremendously, adding exostosin 1/exostosin 2 (EXT1/EXT2) [10], Semaphorin-3B (SEMA3B) [11], neural EGF-like-1 protein (NEL-1) [12] and protocadherin 7 (PCDH7) [13] among others to the list of antigens. Since our group has successfully established the mouse models for the antigens THSD7A and PLA2R, investigations were limited to these two antigens.

PLA2R is a large type I transmembrane protein (185 kDa) and is expressed on human podocytes [14]. It is part of the mannose receptor family that includes 4 members and promotes the internalizing of secreted phospholipase A2 (sPLA2) [15]. All members of the family contain a cysteine-rich domain (CysR), a fibronectin type II (FnII) domain and multiple sequential C-type lectin domains (CTLD) [16–18]. The immune-dominant epitope recognized by autoantibodies of PLA2R-positive MN patients is located inside the CysR domain [19], while lower titers have been found to bind CTLD1, 7, and 8 as depicted in Figure 2A [20–22]. These findings are conclusive with the newly published high-resolution structure of PLA2R. Fresquet et al. [23] found that PLA2R is elongated and flexible at neutral pH, but becomes more rigid and compact at lower pH. They also reported that the immune-dominant domains (CysR, CTLD1, 7, and 8) are in close proximity to one another and are all accessible near the cell surface (Figure 2B).

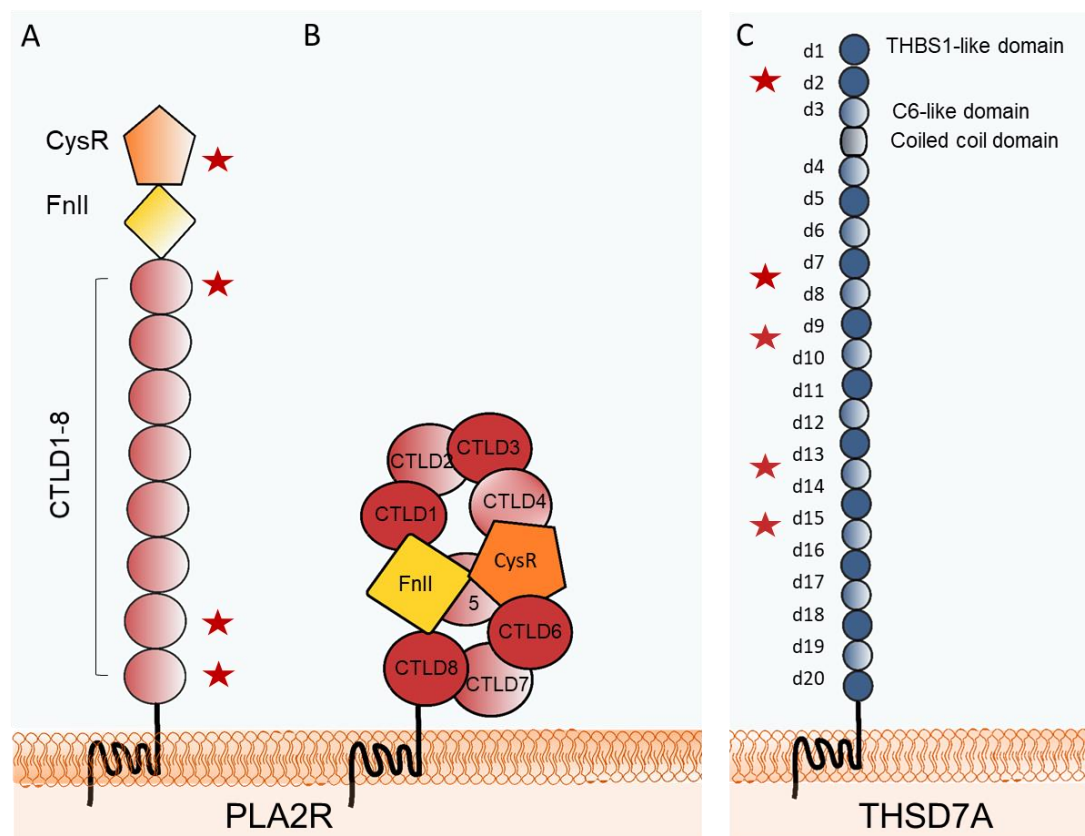


**Figure 2: Antigens of membranous nephropathy.** (A) Schematic structure of the extracellular domains (ECD) of PLA2R. It contains a cysteine-rich domain (CysR), a fibronectin type II (FnII) domain and multiple sequential C-type lectin domains (CTLD1 to CTLD8) [22] (B) Arrangement of domains in PLA2R according to Fresquet and colleagues [23]. The immune-dominant domains (CysR, FnII, CTLD1, CTLD7 and CTLD8) are accessible and exposed. (C) Schematic structure of the ECD of THSD7A. It is made up of 21 extracellular domains containing THBS1-like domains, a coiled coil domain and C6-like domains. The two most N-terminal domains are THBS1-like domains followed by a C6-like domain and one coiled coil domain. Then C6-like domains alternate with THBS1-like domains until the transmembrane domain. Domain numbering as seen in Seifert et al. [24]. Red stars indicate autoantibody-binding sites.

THSD7A is a large (250 kDa), highly glycosylated transmembrane protein. It is expressed in multiple tissues, including lungs, brain, kidney, and soft tissues [2]. THSD7A is made up of 21

extracellular domains containing THBS1-like domains, a coiled coil domain and C6-like domains. The two most N-terminal domains are THBS1-like domains followed by a C6-like domain and one coiled coil domain. Then C6-like domains alternate with THBS1-like domains until the transmembrane domain as depicted in Figure 2C [8; 24]. Seifert et al. [24] did a comprehensive study of the distribution of epitopes along the protein. The autoantibody profile of THSD7A-positive MN patients is more heterogenous compared to PLA2R-positive MN patients. Most patients recognized the most N-terminal domain of THSD7A (87%) but also domains d15\_d16 (61%), d9\_d10 (52%), and d13\_d14 (45%) among others in different combinations. In contrast to PLA2R-positive patients, no correlation between autoantibody titer and disease progression or remission could be found in the patients that have been investigated so far [25].

### 1.3 Current treatments in MN

Conventional treatment plans for MN patients include global immunosuppressants such as calcineurin inhibition with either ciclosporin or tacrolimus in combination with prednisolone for the first 6 to 12 months of therapy. Another treatment strategy involves alkylating agents such as cyclophosphamide or chlorambucil in combination with steroids. These therapies can achieve remission and improve proteinuria but are in some cases toxic and many patients relapse after the treatment is withdrawn. Also, the suppression of the immune system can increase the risk of infections for patients and hamper the response to vaccinations. After the discovery that autoantibodies targeting podocytes are involved in MN, the treatment shifted to B cell specific treatments with monoclonal antibodies. A variety of monoclonal antibodies can interfere in any stage of the B cell development and maturation: anti-CD20 therapeutic antibodies such as rituximab and ofatumumab target CD20 expressing B cells such as pre-B cells, immature, mature and activated B cells [26–29]. Plasma cells can be targeted by anti-CD38 antibodies such as daratumumab and isatuximab [30; 31]. Belimumab stops B cell differentiation into plasma cells by binding the B lymphocyte stimulator BLyS [32]. Even though these treatments are safer than the conventional ones, for some patients they still fail: 25-30% of patients treated with rituximab show no improvement due to CD20 internalization or conformational changes in the epitope of the large loop of CD20 [33]. Memory B cells or plasma cells that do not express CD20 and therefore are resistant to rituximab could be targeted with daratumumab and isatuximab because they express high levels of CD38. Phase 2 studies to test the safety and efficacy of daratumumab in PLA2R-positive MN patients and belimumab for primary MN are still ongoing [34; 35].

All of these treatments interfere with all B cells and not just the autoantibody producing ones and can impede the immune response to all presented antigens including pathogens. Even though they are an improvement for patients there is still a need for more antigen-specific therapeutics.

Therefore, engineered antibodies are explored as an antigen-specific treatment for PLA2R- and THSD7A-MN in this thesis.

## 1.4 Engineered antibodies as a new therapeutic concept

Antibodies have long been used to treat different diseases in a variety of ways. When Chu et al. [36] developed a human antibody with a higher affinity towards the Fc $\gamma$ RIIB paired with the binding of CD19, they opened the door for therapeutics mediating immune complex depletion through Fc gamma receptors (Fc $\gamma$ R). The affinity towards the Fc $\gamma$ RIIB was increased 430-fold with the substitutions of amino acids S267E and L328F (SELF mutations) in the constant heavy chain (C<sub>H2</sub>) of IgG. While they used it to co-engage CD19 and Fc $\gamma$ RIIB on the surface of B cells to induce apoptosis, Desjarlais et al. [37] later used this mutation to sequester IgE to treat allergic asthma. Iwayanagi et al. [38] combined the higher affinity towards Fc $\gamma$ RIIB with pH dependent antigen binding to degrade hIL-6R in mice (Figure 3A). They found that the pH dependent binding was critical to increase the degradation of antigen bound by the engineered antibody inside the serum. Antibodies without pH dependent binding, by contrast, increased the half-life of the immune complex and increased the risk of immune complex disease. After administration, the engineered antibodies bound hIL-6R inside the serum and the resulting immune complex was then taken up by endothelial cells through receptor-mediated endocytosis. In the sorting endosome, the pH shifts from neutral to slightly acidic (pH 6) and the hIL-6R is released from the engineered antibody. While the antibody bound by the Fc $\gamma$ RIIB is shuttled back to the cell surface and released there, the antigen is degraded in the lysosome. Thus, the modified affinity to the Fc $\gamma$ R allows efficient recirculation of the therapeutic antibody from endothelial cells to the plasma, which in turn leads to removal of further antigens from the circulation, creating a “sweeping” effect. This technology was therefore called “sweeping antibody technology” [39] and is depicted in Figure 3B.

The characteristics are enabled by different mutations in the sweeping antibody: i) pH-dependent antigen binding can be achieved by histidine mutagenesis. Random amino acids in the Fab region of the antibody are substituted for histidines. In the sorting endosome, the protonated histidines lead to conformational changes in the Fab region of the sweeping antibody. The binding to the antigen weakens, leading to dissociation of antibody and antigen. ii) Enhanced immune complex uptake is achieved by mutations in the Fc region, affecting the binding to Fc receptors, as described above [40]. We modified this technology to remove antigen-specific antibodies (instead of certain antigens). To this end, we engineered therapeutic antibodies, the antigen Fc fusion constructs (AgFc). Immuno-dominant domains of THSD7A and PLA2R were fused to a mouse IgG2a (mIgG2a) Fc backbone with the mutations discovered by Chu and colleagues [36]

increasing the affinity to Fc $\gamma$ RIIB dramatically. We hypothesized that these AgFc $\gamma$ s would be able to bind autoantibodies against THSD7A and PLA2R in the serum specifically and trap them in an immune complex that can then be taken up and degraded by specialized endothelial cells.

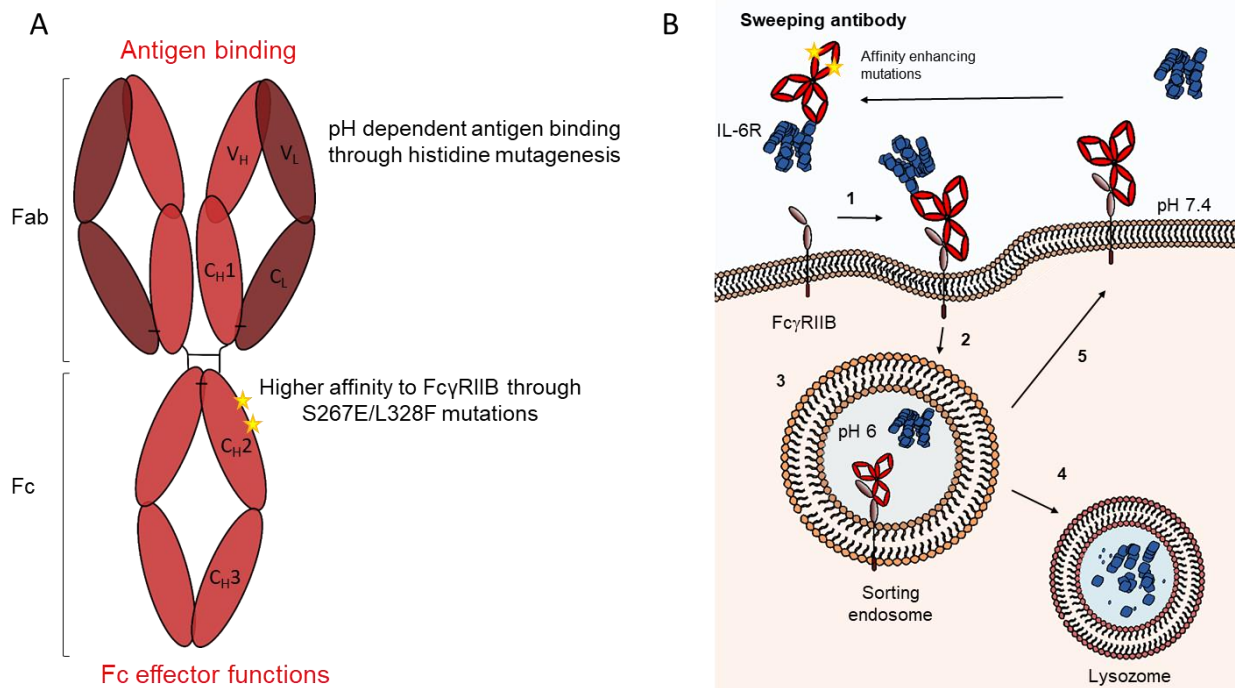


**Figure 3: The sweeping antibody concept.** (A) Schematic of a sweeping antibody. It consists of a heavy ( $V_H$ ,  $C_{H1}$ ,  $C_{H2}$  and  $C_{H3}$ ) and a light chain ( $V_L$  and  $C_L$ ) connected by disulfide bonds. The amino acid sequence has been modified through histidine mutagenesis to bind its antigen pH dependent. The Fc part still has its normal effector function but additionally the amino acids serine (S267) and leucine (L328) were mutated to aspartic acid (E) and phenylalanine (F), respectively, to increase the affinity towards Fc $\gamma$ RIIB. (B) Schematic of the sweeping antibody principle with enhanced Fc $\gamma$ RIIB binding. 1. After injection, the sweeping antibody binds its target interleukin 6-receptor (IL-6R) in the circulation. 2. Scavenger cells like liver sinusoidal endothelial cells (LSECs) that express Fc $\gamma$ RIIB bind the circulating immune complex (IC) and internalize it through receptor-mediated endocytosis. 3. Due to a pH shift from neutral to pH 6 inside the sorting endosome, IL-6R is released from the sweeping antibody-receptor complex. 4. The antigen is degraded inside the lysosome. 5. The Fc receptor-bound sweeping antibody is returned to the surface and can bind new circulating antigens causing the “sweeping” effect [39].

## 1.5 Fc gamma receptors and their role in immunity

The majority of IgG immune functions is mediated by receptors that bind the Fc part: Fc gamma receptors (Fc $\gamma$ R). They are membrane-bound surface receptors, with the exception of the neonatal Fc receptor (FcRn), which is an atypical intracellular receptor.

Fc $\gamma$ RI, Fc $\gamma$ RIII and Fc $\gamma$ RIV are classified as activating receptors as they include an intracellular immune-receptor tyrosine-based activation motif (ITAM) that mobilizes activating tyrosine kinases. The subsequent signaling leads to phagocytosis, cell differentiation, degranulation, secretion of cytokines for cell migration or antibody-dependent cellular cytotoxicity (ADCC). Furthermore, Fc $\gamma$ Rs are classified according to their affinity towards monomeric/free IgG: the only high-affinity interactions are between mFc $\gamma$ RI and IgG2a, mFc $\gamma$ RIV and IgG2a/IgG2b, while

FcRn binds all IgG subclasses with high-affinity [41]. FcγRIII is considered a low-affinity FcγR expressed on multiple immune cells mediating inflammatory processes such as ADCC. While FcγRI is expressed on tissue macrophages and monocyte-derived dendritic cells (DC) and clears antibody-coated pathogens via phagocytosis [42], it is thought to be saturated by monomeric IgG under steady-state conditions. Since the affinity of FcγRI towards IgG2a is high, the binding has only a half-life of  $t_{1/2} \approx 2.6$  min [43], enabling FcγRI to participate in the clearance of immune complexes despite high IgG levels in the serum [44]. FcγRIV is expressed on Ly6C<sup>low</sup> monocytes and neutrophils where it contributes to autoimmunity by binding solely IgG2a and IgG2b [45].

FcγRIIB is the only inhibitory Fc receptor with an immune-receptor tyrosine-based inhibitory motif (ITIM) and normally has a very low affinity towards monomers of IgGs (IgG1 << IgG2a = IgG2b < IgG3) [46]. It has two membrane-bound isoforms: FcγRIIB1 and FcγRIIB2. While FcγRIIB1 is mainly expressed on B cells and regulates their activation, FcγRIIB2 is expressed on myeloid-derived cells and regulates endocytosis through clathrin-coated pits [47].

Usually, inhibitory and activating receptors are co-expressed on the same cells [48], creating a threshold that immune complexes need to overcome for cell activation and mediation of the subsequent response. The single-chain inhibitory receptors are the sole receptors that can signal autonomously, while the activating receptors have to associate with adapter molecules. For instance, to activate FcγRIII on NK cells the ζ-chain must be co-engaged [49]. In the case of a therapeutic antibody against autoantibodies of THSD7A or PLA2R, binding B cells that produce autoantibodies could lead to co-engagement of the BCR on the one hand and the FcγRIIB on the other. This co-engagement might inhibit the production of autoantibodies by these B cells and be another mechanism of action of the developed AgFcs of this thesis.

The FcRn is an atypical FcγR functioning in recycling both albumin and IgG, transporting them bi-directionally across polarized cell barriers [50]. The long half-life of IgG and albumin (19-21 days) is caused by the FcRn rescuing both proteins from endosomes and shuffling them back to the cell surface, while other proteins get degraded inside the lysosome [51; 52]. Interestingly, the FcRn is also expressed in epithelial cells of the kidney, where it prevents the accumulation of IgG at the glomerular filtration barrier [53]. Blood enters the glomerulus through the afferent arteriole and is filtrated through three size- and charge-selective filters: first through the fenestrations of the endothelial cells, next the charged pores of the basement membrane and lastly the slit diaphragms of the podocytes [53]. To prevent clogging of the filter, podocytes express FcRn and transcytose IgG to the glomerular filtrate. Since the pore size of the barrier is between 60-70 kDa, on occasion albumin (66.5 kDa) escapes into the glomerular filtrate. To rescue these molecules,

the proximal tubule also expresses FcRn, which shuffles albumin and IgG into the interstitial space. Through lymph drainage it can re-enter the blood stream, rescuing both IgG and albumin [53–56].

## **1.6 Liver sinusoidal endothelial cells as an endogenous degradation system**

Liver sinusoidal endothelial cells (LSECs) are specialized endothelial cells at the interface between the blood stream on the one hand and hepatocytes and stellate cells on the other. They have a discontinuous architecture creating 'fenestrae' and are organized in sieve plates. Therefore, they can retain blood cells, while smaller molecules like metabolites and proteins can pass through and can be taken up by hepatocytes or stellate cells [57]. The absence of a diaphragm and the lack of a basement membrane make them the most permeable cells in the body [58]. In their capacity as scavenger cells, they specialize to clear blood from small immune complexes (SIC) through receptor-mediated endocytosis mediated by Fc $\gamma$ RIIB [59]. They are part of the 'dual-cell principle' of waste clearance, where large particles (>0.5  $\mu$ m) are eliminated by macrophages through phagocytosis and smaller particles through pinocytosis in LSECs [58]. SIC are called soluble complexes because they do not sediment at low gravity forces, while large complexes are termed insoluble and are taken up through receptor-mediated endocytosis. SIC can be created by either an antigen excess or an antibody excess. At the point of equivalence (POE), the equal molar ratio of antigen and antibody, a lattice structure is formed producing large and insoluble immune complexes [60]. If these insoluble immune complexes persist inside the circulation, it increases the risk of immune complex-mediated disease where deposits can cause inflammation of the kidney and other organs [61; 62].

Pinocytosis, which describes the uptake of extracellular fluids and therein solved small particles, in LSECs is mediated through the Fc $\gamma$ RIIB and clathrin-coated pits [63]. The uptake through clathrin-coated pits is undirected while the uptake through the Fc $\gamma$ RIIB is receptor-mediated endocytosis. Fc $\gamma$ RIIB has two splice variants: Fc $\gamma$ RIIB1 and Fc $\gamma$ RIIB2, which only differ in the first cytoplasmic exon. Here, Fc $\gamma$ RIIB1 has a 47 aa insert. Without this insert, Fc $\gamma$ RIIB2 is able to mediate endocytosis, whereas Fc $\gamma$ RIIB1 is a non-endocytic receptor and regulates inhibition of B cell receptors (BCR) on B cells [63]. LSECs express 90% of the livers Fc $\gamma$ RIIB2 on their surface [64], while the rest is expressed on Kupffer cells. Ganesan et al. [59] showed that small immune complexes are cleared 3-fold more efficiently in mice with Fc $\gamma$ RIIB than in mice lacking Fc $\gamma$ RIIB. More recently, the key role of LSECs in inducing tolerance through suppression of CD8<sup>+</sup> and CD4<sup>+</sup> T cell populations made a therapeutic approach through the Fc $\gamma$ RIIB even more attractive for treatment of an autoimmune disease [65; 66].

Identifying LSECs is a rather complicated matter: while CD31 is only expressed on LSECs during a certain maturation step [67], CD146 is not exclusively expressed on LSECs but also on other endothelial cells and NK cells [68; 69]. CD32b (FcγRIIB) is not expressed on periportal LSECs but also on myeloid dendritic cells [70; 71]. CD45 is highly expressed on periportal LSECs, while low expression is found on midlobular LSECs and no expression on centrilobular LSECs [70]. This made identification through flow cytometry and immune-magnetic purification challenging until Bhandari et al. [72] analyzed liver cell subsets with transcriptome and proteome profiling. They found low expression of CD45 in the LSEC transcriptome and even less in the proteome. They could identify only a small subset of LSECs positive for CD45 (4%). Su et al. [73] discovered with single-cell transcriptomics that all LSEC populations expressed CD31 and also very highly CD32b (FcγRIIB). Based on these findings we identified LSECs as CD45<sup>low</sup>CD31<sup>high</sup>CD32b<sup>+</sup> shown in our FACS panel described in 2.2.8 to analyze the uptake of our therapeutic AgFc with their target autoantibodies.

## 1.7 Experimental MN mouse models

To test the AgFc for their therapeutic efficacy, mouse models that combine the intrinsic production of autoantibodies, defined epitopes targeted by the autoantibodies, a mature immune system as well as an *in vivo* degradation system were needed to analyze the effect on the whole organism. Three different experimental autoimmune membranous nephropathy (EAMN) mouse models have been established by our group: one for THSD7A in WT BALB/c (Seifert et al., unpublished data) and two for PLA2R in transgenic mice, either in chimeric PLA2R-mice (Tomas et al., unpublished data) or in human PLA2R mice [74]. In THSD7A-EAMN, mice are immunized with fragments of the extracellular domains of THSD7A (d1\_d2 and d15\_d16) with complete Freund's adjuvant (first immunization) and then incomplete Freund's adjuvant (three booster immunizations). Chimeric PLA2R-mice express a chimeric PLA2R protein inside the kidneys consisting of the human CysR, FnII and CTLD1 domains and the murine CTLD2-8 domains. For PLA2R-MN, they are immunized with recombinant human PLA2R in Titermax® Gold adjuvant. All mice are monitored over several weeks with blood withdrawals and urine collection. After 5 to 9 weeks, antibody titers increase and proteinuria develops. These mice show positive mIgG staining along the GBM, high proteinuria (>3 g/g), increased serum cholesterol, and in severe cases ascites. In both mouse models, mIgG1 was found to be the most abundant subtype in sera and glomeruli (Seifert et al., unpublished data and Tomas et al., unpublished data). mIgG1 is similar to hIgG4 as it cannot bind C1q to activate the classical complement pathway [74]. They also found the other complement activating subtypes in varying frequencies, closely reflecting the typical findings in MN patients.

The autoimmune human PLA2R mouse model was developed by Tomas et al. [74], where no immunization is needed to induce autoantibody production. This transgenic mouse line expresses human PLA2R in podocytes through a knock-in and mice spontaneously develop anti-PLA2R antibodies and the typical signs of MN: podocyte foot effacement, subepithelial electron-dense deposits, severe albuminuria, and mIgG deposits along the GBM at three weeks of age. Interestingly, the prominent subtype found in these deposits again was mIgG1, which cannot bind the complement factor C1q [74]. Further studies on activated complement pathways showed the involvement of the classical and alternative pathways. This mouse model is rather aggressive as the majority of animals show severe signs of MN by week six of age.

These mouse models develop autoantibodies either after an active immunization in the cases of PLA2R- and THSD7A-EAMN or spontaneously in the case of the transgenic hPLA2R mice as opposed to passive models where antibodies against the antigens PLA2R or THSD7A are directly injected into the animals, causing disease [75; 76]. All models above include immunological processes such as antigen presentation, activation of B cells, production of antibodies which target the antigens in the podocyte, as well as induction of local damage with subsequent proteinuria. Therefore, they are adequate models to test new antigen-specific therapies for MN developed by the student of this thesis and are a platform to perform in-depth analysis of the very same.

## **1.8 Aim of this work**

The objectives of this thesis are: i) to create domain-specific antigen Fc constructs (AgFcs) with higher affinity towards Fc $\gamma$ RIIB through the SELF mutation and verify their binding properties to monoclonal antibodies by different domains of the podocyte proteins THSD7A and PLA2R as well as the binding properties of different Fc $\gamma$ Rs, ii) to test the AgFcs *in vitro* to determine the uptake of immune complexes in primary LSECs, iii) to analyze the ability of AgFcs to induce ADCC in combination with NK cells, iv) to characterize the uptake kinetics of the AgFc-mAb immune complexes and degradation *in vivo* in WT mice, and v) to test the therapeutic efficacy in various stages of the disease in the mouse models of THSD7A and autoimmune hPLA2R.

## 2 Material and Methods

### 2.1 Material

#### 2.1.1 Equipment

All the equipment used in this study is listed in Table 2-1.

*Table 2-1: List of equipment*

<b>Equipment</b>	<b>Model</b>	<b>Manufacturer</b>
<b>Centrifuges</b>	ThermoScientific	
	Multifuge 1S-R	Eppendorf, Hamburg, Germany
	Centrifuge 5417R	Eppendorf, Hamburg, Germany
<b>Confocal Microscope</b>	LSM 800 with airyscan	Carl Zeiss AG, Oberkochen
<b>Electrophoresis chamber</b>	Mini Protean Tetra System for SDS PAGE	Bio-Rad Laboratories, München, Germany
<b>ELISA Reader</b>	MITRAS LB940	Berthold Technologies, Bad Wildbad
	EL808 Ultra Microplate Reader	BIO-TEK Instruments, Inc. Winooski, VT, USA
<b>ELISA Washers</b>	Columbus Pro	Tecan, Crailsheim, Germany
	405 Select	BioTek Germany, Bad Friedrichshall, Germany
<b>Gel Documentation</b>	Amersham Imager 600	GE Healthcare, Chicago, IL, USA
<b>Incubators</b>	Infors HT	Infors, Leipzig, Germany
	BE 400	Memmert. Schwabach, Germany
	Vortemp 56	Labnet International, Edison, NJ, USA
<b>In vivo imaging systems (IVIS)</b>	IVIS 200	Spectral Instruments Imaging, Texas USA
<b>Laminar flow benches</b>	HERAsafe	Heraeus Instruments, Hanau, Germany
<b>Light microscopes</b>	Axio Scope. A1	Carl Zeiss AG, Oberkochen
<b>Photometers</b>	NanoDrop ND1000	PeqLab, Erlangen, Germany
	Libra S11	Biochrom, Holliston, USA
<b>Pipettes</b>	Research	Eppendorf, Hamburg, Germany
	Accu-jet	Brand
<b>Power Supplies</b>	Electrophoresis Power Supply 601	Amersham Bioscience, Freiburg, Germany

<b>Rocker</b>	GFL 3013	Omnilab Laborzentrum, Bremen, Germany
<b>Steam cooker</b>	FS10	Braun GmbH, Kronberg im Taunus
<b>Thermocycler</b>	S1000 ThermalCycler	Biometra GmbH, Göttingen
<b>Ultrasound sonication</b>	Bioruptor® Plus Sonication System	Diagenode s.a, Seraing, Belgium
<b>Vortexer</b>	Vortex-Gene 2	Scientific Industries Inc., NY, USA
<b>Water Installation</b>	Arium pro	Sartorius, Göttingen, Germany
<b>Western Blot system</b>	Trans-Blot Turbo Transfer System	BioRad Laboratories, Inc. Hercules, USA

### 2.1.2 Consumables

Table 2-2 lists all the consumables that were used throughout this study.

*Table 2-2: List of consumables*

<b>Material</b>	<b>Manufacturer</b>
<b>96 well plates</b> High-bind, conical or flat	Sarstedt, Nürnberg, Germany
<b>BD Micro-Fine 0.3ml U-100 Insulin syringe</b>	Becton Dickinson GmbH, Germany
<b>Black 96 well plates, F-Bottom</b>	Greiner Bio-One, Germany
<b>CD146 Beads</b>	Miltenyi, Germany
<b>Corning 250 ml Erlenmeyer flask</b>	Corning Incorporated, USA
<b>Disposable serological pipettes</b> (2 mL/5 mL/10 mL/25 mL)	Sarstedt, Nürnberg, Germany
<b>Injekt-F 1ml syringe</b>	B. Braun SE, Germany
<b>Mini-PROTEAN TGX Gels</b> 10-well, 12-well, 15-well, 4-15 %	BioRad Laboratories, Inc. USA
<b>Multiply-<math>\mu</math>Strip Pro 8-strip</b>	Sarstedt, Nürnberg, Germany
<b>Omnifix 1 ml syringe</b>	B. Braun SE, Germany
<b>Petri dishes (10 cm)</b>	Greiner-Bio-One, Frickenhausen, Germany
<b>Pipette tips</b>	Sarstedt, Nürnberg, Germany
<b>Pipette tips, filtered, TipOne</b>	Starlab International Inc., Germany
<b>Reaction tube</b> 1.5 mL, 2 mL	Sarstedt, Nürnberg, Germany
<b>Reaction tube</b> 15 mL, 50 mL	Sarstedt, Nürnberg, Germany
<b>Screw-top micro caps, 2 mL, PP</b>	Sarstedt, Nürnberg, Germany

<b>Sealing Tape optically clear</b>	Sarstedt, Nürnberg, Germany
<b>Sterile filter</b> 0.2 µm, 0.45 µm	Sarstedt, Nürnberg, Germany
<b>TC-Flask ventilated cap</b> T25, T75, T175	Sarstedt, Nürnberg, Germany
<b>White 96 well plates, Cellstar, F-Bottom</b>	Greiner Bio-One, Germany
<b>Zeba™ Spin Desalting Columns</b> 40K, 10 ml, 2 ml	ThermoScientific, USA

### 2.1.3 Chemicals

All chemicals were bought from Carl Roth GmbH (Karlsruhe, Germany), Sigma-Aldrich Chemie GmbH (Steinheim, Germany), Merck KGaA (Darmstadt, Germany) or Roche Diagnostics GmbH (Penzberg, Germany) if not clearly stated otherwise.

### 2.1.4 Enzymes and buffers

The enzymes and their buffers used in this study are listed in Table 2-3.

Table 2-3: List of enzymes

<b>Enzyme</b>	<b>Manufacturer</b>
DNA Polymerases	
<b>GoTaq® G2 DNA polymerase</b>	Promega, Madison, WI, USA
<b>5x green GoTaq® Flexi Buffer</b>	Promega, Madison, WI, USA
<b>MgCl<sub>2</sub> (25 mM)</b>	Promega, Madison, WI, USA
<b>Phusion® High-Fidelity DNA Polymerase</b>	Thermo Scientific, Dreieich, Germany
<b>5x Phusion® HF Buffer</b>	Thermo Scientific, Dreieich, Germany
Endonucleases	
<b>EspI</b>	New England BioLabs, Frankfurt a. M., Germany
<b>NcoI</b>	New England BioLabs, Frankfurt a. M., Germany
<b>NotI-HF</b>	New England BioLabs, Frankfurt a. M., Germany
<b>CutSmart® Buffer</b>	New England BioLabs, Frankfurt a. M., Germany
Phosphatase	
<b>Alkaline Phosphatase, Calf intestinal (CIP)</b>	New England BioLabs, Frankfurt a. M., Germany
DNA Ligases	
<b>T4 DNA ligase</b>	Promega, Madison, WI, USA
<b>10x T4 DNA ligase buffer</b>	Promega, Madison, WI, USA
Proteases	

<b>Trypsin</b>	Sigma-Aldrich Chemie GmbH, Steinheim, Germany
----------------	--------------------------------------------------

### 2.1.5 Antibodies

The commercial antibodies listed in Table 2-4 were used in ELISAs or Western Blots that were conducted. The antibodies conjugated with horseradish peroxidase (HRP) were used as detection antibodies, the mouse anti-Strep tag II antibody was used intermediary to bind the TwinStrep tag of the produced soluble peptides.

*Table 2-4: List of commercial antibodies*

<b>Antibody</b>	<b>Conjugate</b>	<b>Dilution (ELISA)</b>	<b>Manufacturer</b>
<b>Donkey anti-mouse IgG</b>	HRP	1:10.000 (detection)	Jackson Laboratories
<b>Mouse anti-Strep tag II</b>		1:2.000	iba
<b>Rabbit anti-mouse IgG2a</b>	HRP	1:20.000 (detection)	Invitrogen
<b>Goat anti-mouse IgG1</b>	HRP	1:20.000 (detection)	Southern Biotech
<b>Goat anti-rabbit IgG</b>	HRP	1:20.000 (detection)	Sigma, A0545

The antibodies in Table 2-5 were cloned, produced, and/or purified by the student of this thesis.

*Table 2-5: List of used Antibodies*

<b>Antibodies</b>	<b>Format</b>	<b>Manufacturer</b>
<b>B64</b>	IgG	III. Department of Medicine, UKE, Germany
<b>B4</b>	IgG	III. Department of Medicine, UKE, Germany
<b>A146</b>	IgG	III. Department of Medicine, UKE, Germany
<b>A11/10</b>	IgG	III. Department of Medicine, UKE, Germany
<b>A19/30</b>	IgG	III. Department of Medicine, UKE, Germany
<b>A121/8</b>	IgG	III. Department of Medicine, UKE, Germany
<b>A113/4</b>	IgG	III. Department of Medicine, UKE, Germany
<b>d1d2 WT</b>	AgFc	III. Department of Medicine, UKE, Germany
<b>d1d2 SELF</b>	AgFc	III. Department of Medicine, UKE, Germany
<b>d1d2 LALAPG</b>	AgFc	III. Department of Medicine, UKE, Germany
<b>d15 WT</b>	AgFc	III. Department of Medicine, UKE, Germany
<b>d15 SELF</b>	AgFc	III. Department of Medicine, UKE, Germany
<b>d15 LALAPG</b>	AgFc	III. Department of Medicine, UKE, Germany
<b>hCysFnII WT</b>	AgFc	III. Department of Medicine, UKE, Germany
<b>hCTLD1/2 WT</b>	AgFc	III. Department of Medicine, UKE, Germany
<b>hCTLD7/8 WT</b>	AgFc	III. Department of Medicine, UKE, Germany

Antibodies	Format	Manufacturer
hCysFnII SELF	AgFc	III. Department of Medicine, UKE, Germany

### 2.1.6 Commercial kits and markers

The commercial kits listed in Table 2-6 were used to purify DNA after PCR or digestion and extract DNA from bacterial cells.

Table 2-6: List of commercial kits

Kit	Manufacturer
NucleoSpin Gel and PCR Clean-Up	Macherey-Nagel, Düren, Germany
NucleoSpin Plasmid EasyPure	Macherey-Nagel, Düren, Germany
NucleoBond Maxi Prep	Macherey-Nagel, Düren, Germany

The markers listed in Table 2-7 were used as a reference on an agarose gel for DNA and in SDS-PAGE as reference for proteins.

Table 2-7: List of markers

Marker	Manufacturer
GeneRuler 1 kb Plus DNA Ladder	Thermo Scientific, Dreieich, Germany
Precision plus Protein unstained	Bio-Rad, München, Germany

### 2.1.7 Bacterial strains

The bacterial strains mentioned in Table 2-8 were used to transform DNA into and extract it to transfect HEK293-6E cells or continue cloning different constructs.

Table 2-8: Used bacterial strains

Strain	Genotype	Application	Source
<i>E. coli</i> DH5 $\alpha$	fhuA2 lac(del)U169 phoA glnV44 $\Phi$ 80' lacZ(del)M15 gyrA96 recA1 relA1 endA1 thi-1 hsdR17	Cloning	ThermoFischer Scientific

### 2.1.8 Cell lines

The cell lines used in this study are described in Table 2-9. Mouse hybridomas express a BCR on their surface and secrete the corresponding mIgG into the supernatant. Fc $\gamma$ R-HEK cells express the different mouse Fc $\gamma$ R on their surface and were used for binding studies including AgFc. HEK cells were used to produce multiple recombinant proteins e.g. AgFc or md1d21-TwinStrep.

Table 2-9: Used cell lines

Cell line	Type	Description	Manufacturer
<b>B64, anti-d1_d2</b>	mHybridoma	produces B64-mIgG1 monoclonal, binding domain 2 of THSD7A, Luciferase positive	Larissa Seifert
<b>B4, anti-d15</b>	mHybridoma	produces B4-mIgG2b monoclonal, binding domain 15 of THSD7A, Luciferase positive	Larissa Seifert
<b>A121/8, anti-CysR</b>	mHybridoma	produces A121/8-mIgG1 monoclonal, binding domain CysR of PLA2R, Luciferase positive	Fritz Nolte
<b>A19/30</b>	mHybridoma	produces A19/30-mIgG1 monoclonal, binding domain CysR of PLA2R, Luciferase positive	Fritz Nolte
<b>FcγRI</b>	HEK	HEK cell line stably transfected with mFcγRI	Björn Rissiek
<b>FcγRIIB</b>	HEK	HEK cell line stably transfected with mFcγRIIB	Björn Rissiek
<b>FcγRIII</b>	HEK	HEK cell line stably transfected with mFcγRIII	Björn Rissiek
<b>FcγRIV</b>	HEK	HEK cell line stably transfected with mFcγRIV	Björn Rissiek
<b>HEK293</b>	6E	Human embryonic kidney cells	Invitrogen

### 2.1.9 Plasmids and oligonucleotides

The plasmids used for building the AgFc constructs are described in Table 2-10. The oligonucleotides used for gene amplification and sequencing are listed in Table 2-11.

Table 2-10: Used plasmids

Plasmid	Description	Reference
<b>pCSE2.5</b>	Expression vector for HIS-tagged and Fc-tagged proteins	[77]
<b>pDSG-IBA102</b>	Mammalian expression vector for secretion of C-terminal Twin-Strep-tag fusion proteins	IBA Lifesciences, Germany

Table 2-11: Used oligonucleotides

<b>ID</b>	<b>DNA sequence (5'→3')</b>	<b>Fwd. /rev.</b>	<b>Description</b>
<b>CMV5</b>	GGGAGGTCTATATAAGCAGAG	Fwd.	Sequenzierprimer pCSE2.6
<b>BgH3</b>	TAGAAGGCACAGTCGAGG	Rev.	Sequenzierprimer pCSE2.6
<b>FcγRI</b>	AGGGCTGCTCTGGCAGCAATGGAAGTGGTTAATGCCACC AAG	Fwd.	FcγRI TwinStrep
<b>FcγRI</b>	GTGGCTCCAAGCGCTCCCAGGAGCTGATGACTGGGGACC	Rev.	FcγRI TwinStrep
<b>FcγRIIB</b>	AGGGCTGCTCTGGCAGCAATGACTCATGATCTTCCAAAG GCTAAA	Fwd.	FcγRIIB TwinStrep
<b>FcγRIIB</b>	GTGGCTCCAAGCGCTCCCTAAAGACCTGCT GGACTTGGG	Rev.	FcγRIIB TwinStrep
<b>FcγRIII</b>	AGGGCTGCTCTGGCAGCAATGTTGCCAAAAGCAGTTGTG AAACTT	Fwd.	FcγRIII TwinStrep
<b>FcγRIII</b>	GTGGCTCCAAGCGCTCCCGAGTGAAATACTGCTGCTGGT	Rev.	FcγRIII TwinStrep
<b>FcγRIV</b>	AGGGCTGCTCTGGCAGCAATGGGACTCCAGAAGGCAGT TGTC	Fwd.	FcγRIV TwinStrep
<b>FcγRIV</b>	GTGGCTCCAAGCGCTCCCTTGGTGCCAGGGAGGAAACAT	Rev.	FcγRIV TwinStrep
<b>hd1d20</b>	AGGGCTCTGGCAGCAATGGCGGCGCAGGGCGAGGCGG AG	Fwd.	Human d1d20 THSD7A
<b>hd1d20</b>	GTGGCTCCAAGCGCTCCCATGGCATGTTTTTGTCTCGCT	Rev.	Human d1d20 THSD7A
<b>md1d20</b>	AGGGCTCTGGCAGCAATGGCGGCGCAGGGAGACACCGA G	Fwd.	mouse d1d20 THSD7A
<b>md1d20</b>	GTGGCTCCAAGCGCTCCCGGCGCAGGTCTTCATCTCACT	Rev.	mouse d1d20 THSD7A

### 2.1.10 Proteins

The recombinant proteins listed in Table 2-12 were used in this study.

Table 2-12: Used proteins

<b>Proteins</b>	<b>Description</b>	<b>Source</b>	<b>Predicted Size [kDa]</b>
<b>Md1d21</b>	TwinStrep-tagged extracellular domain of THSD7A used for ELISA	Larissa Seifert	174
<b>hCysC8</b>	TwinStrep-tagged extracellular domain of PLA2R used for ELISA	Gunther Zahner	159

<b>Md1_d2</b>	HIS-tagged domains of THSD7A used for immunization	Larissa Seifert	20
<b>Md15_d16</b>	HIS-tagged domains of THSD7A used for immunization	Larissa Seifert	20
<b>FcγRI</b>	TwinStrep-tagged extracellular domain of mFcγRI used for affinity measurement	Larissa Seifert	30.7
<b>FcγRIIB</b>	TwinStrep-tagged extracellular domain of mFcγRIIB used for affinity measurement	Larissa Seifert	20.9
<b>FcγRIII</b>	TwinStrep-tagged extracellular domain of mFcγRIII used for affinity measurement	Sarah Köllner	20.6
<b>FcγRIV</b>	TwinStrep-tagged extracellular domain of mFcγRIV used for affinity measurement	Sarah Köllner	21.2

### 2.1.11 Media and supplements

Liquid media were sterilized by autoclaving at 121°C for 20 min and excess pressure of 1 bar. Supplements were sterilized separately and mixed with the medium under sterile conditions. For solid media, 12 g/L of Agar-Agar was added prior to sterilization. The used media is listed in Table 2-13 through 2-14.

*Table 2-13: Recipe for LB medium*

<b>LB medium</b>	<b>(w/v)</b>
<b>Bacto-Yeast Extract</b>	1.0 %
<b>Bacto-Tryptone</b>	0.5 %
<b>NaCl</b>	1 %

*Table 2-14: Recipe of SOC medium*

<b>SOC medium</b>	<b>(w/v)</b>
<b>Bacto-Yeast Extract</b>	0.5 %
<b>Bacto-Tryptone</b>	2.0 %
<b>NaCl</b>	0.05 %
<b>Glucose</b>	1.8 %

Supplements, listed in Table 2-15, were prepared highly concentrated and sterile filtered with a

0.2  $\mu\text{m}$  filter and added to the medium (Table 2-13) after reaching below 55 °C past sterilization.

Table 2-15: Medium supplements used

Supplement	Stock solution	Final concentration
<b>Ampicillin</b>	100 mg/mL	100 $\mu\text{g/mL}$
<b>Kanamycin</b>	50 mg/mL	50 $\mu\text{g/mL}$

### 2.1.12 Buffers and solutions

All buffers and solutions are listed in Table 2-16.

Table 2-16: List of buffers and solutions

Buffer/solution				
<b>Agarose Gel</b>				In TAE Buffer
Agarose	1.0	%	(w/v)	
<b>CHO Media</b>				
DMEM (high glucose)	450	ml		Gibco, LifeTechnologies
FCS	10	%	(v/v)	
Sodium pyruvate	5	ml		
L-Glutamine	5	ml		
Nonessential AS	5	ml		
HEPES buffer	5	ml		
<b>Coomassie Blue Staining</b>				
<b>DPBS (1x)</b>				Gibco, Life technologies, USA
(-) $\text{CaCl}_2$				
(-) $\text{MgCl}_2$				
<b>Elution Buffer</b>				
<b>Ethanol</b>	20	%		In $\text{H}_2\text{O}$
<b>Ethidium Bromide solution</b>				
Ethidium Bromide	0.1	%	(w/v)	
<b>Glycerole</b>	50	%	(v/v)	In $\text{H}_2\text{O}$
<b>Hybridoma Media</b>				
RPMI (1640, 1x)	450	ml		Gibco, LifeTechnologies
FCS	10	%	(v/v)	
L-Glutamine	5	ml		
$\beta$ -Mercaptoethanol	1	ml		
Sodium pyruvate	5	ml		
<b>MPBS-T</b>				
Skim Milk Powder	2	%	(w/v)	In PBST (0.05 %)

<b>Buffer/solution</b>				
<b>NK cell media</b>				
$\alpha$ -MEM				Gibco, LifeTechnologies
FCS	10	%	(v/v)	
Horse serum	10	%	(v/v)	
L-Glutamine	2	mM		
IL-2	5	ng/ml		
<b>Nycodenz AG</b>				
	30	%	(w/v)	Alere Technologies In H <sub>2</sub> O
<b>PBS-T (0.05 %)</b>				
Tween20	0.05	%	(v/v)	In DPBS
<b>PEI, MW 40.000</b>	40	$\mu$ g	(w/transf ection)	Polysciences, Inc.
<b>Procaine Hydrochloride</b>	1	%	(w/v)	Sigma, in DPBS
<b>SDS sample (Laemmli) buffer (5x)</b>				
SDS	10	%	(w/v)	
Glycerol	50	%	(w/v)	
Bromophenol Blue	0.02	%	(w/v)	
$\beta$ -Mercaptoethanol	15	%	(v/v)	
SDS	10	%	(w/v)	
<b>SDS-PAGE running buffer</b>				
Tris	25	mM		
Glycine	192	mM		
SDS	0.1	%	(w/v)	
<b>TAE buffer</b>				
Tris-HCl	4	mM		
Acetic acid	2	mM		
EDTA	1	mM		
<b>TMB Solution</b>				
<b>1 M Tris-HCl, pH 9.0</b>				
Trisbase	12.1	g		
Hydrochlorid Acid	11.65	ml		
<b>Trypsin/EDTA</b>				PAA, Austria

### 2.1.13 Software and Databases

The software or databases listed in Table 2-17 were used to either process data or analyze it. Inkscape was used to illustrate the figures shown in this study, if not stated otherwise.

Table 2-17: List of software and databases

Software/database	Application	Manufacturer/Source
<b>Graphpad Prism 8.3</b>	Data presentation and statistical analysis	GraphPad Software, Inc.
<b>SnapGene 6.1</b>	Vector maps, DNA & Protein alignments, DNA sequence processing	Dotmatics, San Diego, USA
<b>Inkscape 0.92.3</b>	Figure illustration	GPL (free software)
<b>NCBI</b>	Literature research, Sequence comparisons (BLAST), Gene and protein sequence information	
<b>FIJI</b>	Image processing program	ImageJ
<b>FlowJo</b>	Enables single-cell flow cytometry analysis	BD Biosciences

## 2.2 Methods

### 2.2.1 Cloning of AgFc constructs

To insert the already existing domains of THSD7A or PLA2R into the expression vector pCSE2.5 with the different mIgG2a-Fc backbones (WT, SELF, LALAPG), first vector and inserts had to be digested with *NcoI* and *NotI*. The composition of a digestion mix is listed in Table 2-18.

Table 2-18: Composition of digestion mix

Reagent	Amount ( $\mu\text{L}$ )
<b>Vector (4 <math>\mu\text{g}</math>)</b>	3.5
<b>10 x Buffer CutSmart (NEB)</b>	5
<b><i>NcoI</i> (10 U/<math>\mu\text{L}</math>, NEB)</b>	1
<b><i>NotI</i> (10 U/<math>\mu\text{L}</math>, NEB)</b>	1
<b>ddH<sub>2</sub>O</b>	Up to 50

The reaction was incubated at 37 °C overnight and 10  $\mu\text{L}$  of calf-intestinal alkaline phosphatase mix (10 U/ $\mu\text{L}$ , NEB) was added to dephosphorylate the vector and prohibit re-ligation without an insert the next day. The reaction was purified with the NucleoSpin Gel and PCR clean-up kit (Macherey-Nagel) according to the manufacturer's instructions. The concentration was measured with a spectrophotometer. To determine which amount of insert to use in a ratio of 1:3 to the linearized vector DNA, Equation 1 was utilized.

$$\text{insert (ng)} = \frac{\text{vector (ng)} \times \text{insert size (kb)}}{\text{vector size (kb)}} \times \frac{\text{insert}}{\text{vector}}$$

Equation 1

With an average insert size of 0.2 kb, the vector size of 5.5 kb, and 100 ng of vector, 10.9 ng of the different inserts had to be used. The ligation was carried out according to Table 2-19 (16 °C, o/N).

*Table 2-19: Composition of ligation mix*

<b>Reagent</b>	<b>Amount (μL)</b>
<b>Vector (100 ng)</b>	x
<b>10x Ligase Buffer (NEB)</b>	1
<b>Insert (10.9 ng)</b>	y
<b>T4 Ligase</b>	0.8
<b>ddH<sub>2</sub>O</b>	Up to 10

The next day, the DNA was transformed into *E. coli* via heat shock. In short, 5 μl of the ligation mix was added to 10 beta competent cells and incubated on ice for 30 min. Heat shock was performed for 30 s at 42°C and the cells cooled for 5 min on ice thereafter. 250 μl of pre-warmed SOC medium was added and the cells outgrown for 1 h at 37°C, 300 rpm. Half of the cells were plated onto a LB-Amp 10 cm plate and grown overnight at 37°C. The next day, 10 colonies per ligation were picked to perform a colony PCR to check for positive clones. For this colonies were picked into 50 μl of TE buffer and then 5 μl of that solution was added to the PCR mix. The colony PCR protocol is listed in tables 2-20 and 2-21.

*Table 2-20: Reagents for the colony PCR*

<b>Reagent</b>	<b>Amount (μL)</b>
<b>Colony (Dilution 1:50 in TE Buffer)</b>	5
<b>dNTP mix</b>	0.4
<b>DreamTaq DNA polymerase (5 U/μL)</b>	0.2
<b>5x DreamTag Buffer</b>	2
<b>Primer forward + primer reverse (10 mM each)</b>	0.2 + 0.2
<b>ddH<sub>2</sub>O</b>	12.2
<b>Total volume</b>	20

Table 2-21: Colony PCR protocol

Temperature (°C)	Time	
95	5 min	
95	30 s	40 cycles
64	30 s	
72	6 min	
72	6 min	
10	∞	

Positive results were confirmed on a 1% agarose gel in 1xTAE buffer and corresponding clones were used to inoculate 50 ml LB-A medium overnight (37°C) at 180 rpm. DNA was extracted via a NucleoBond MAXI Kit (Macherey-Nagel) according to the manufacturer's instructions. Glycerol stocks were made with 750 µl *E. coli* overnight culture and 250 µl 80% glycerol. These were frozen and stored at -80°C for further use.

### 2.2.1.1 Seamless Ligation Cloning Extract (SLiCE)

For cloning of md1d20 TwinStrep and hd1d20 TwinStrep constructs, we used the SLiCE cloning extract. Therefore, slightly different primers had to be designed to create short homologous ends for recombination (see table 2-11). The pDSG-IBA102 vector was linearized with *Esp3I* overnight at 37°C and alkaline phosphatase mix (10 U/µL, NEB) was added for 1 h the next day. To amplify the desired inserts, a PCR reaction described in table 2-23 and 2-24 was performed.

Table 2-22: PCR amplification for md1d20 and hd1d20

Reagent	Amount (µL)
Phusion Polymerase	0.2
Phusion Buffer	4
Template (5ng)	x
dNTPs (10 mM)	0.4
Primer forward + primer reverse (10 mM each)	1 + 1
ddH <sub>2</sub> O	y
Total volume	20

Table 2-23: PCR protocol

Temperature (°C)	Time	
98	5 min	
98	30 s	35 cycles
66	30 s	
72	5 min	
72	5 min	
10	∞	

Inserts were purified from an agarose gel with the PCR clean-up kit (Macherey-Nagel) and SLiCE cloning reaction was performed at a 1:1 vector-insert ratio for 45 min at 37°C. After that, transformation in *E. coli* and quality control with colony PCR was done as described in 2.2.1.

## 2.2.2 Production of AgFc

### 2.2.2.1 Plasmid extraction

For this, the *E. coli* cells containing the plasmids were picked from their glycerol stocks with pipette tips and inoculated in 50 mL of LB-A media in 200 ml flasks with a vented cap. The cultures were incubated overnight at 37°C and 180 rpm. The DNA was purified with a NucleoBond Plasmid MAXI extraction kit (Macherey-Nagel) according to the manufacturer's instructions. The DNA was quantified via Spectrophotometer (Denovix) and stored at -20 °C until use.

### 2.2.2.2 Transfection of HEK293-6E cells

The cells were cultivated and passaged to 94 % confluency and a concentration of  $5 * 10^5$  cells/mL. AgFc constructs were produced in 35 mL serum-free medium (Freestyle 293, Gibco). For transfection, 248 µL (80 µg) of PEI was mixed with 252 µL of water and 500 µL of NaCl (300 mM). 35 µg plasmid DNA in 500 µL water was mixed with the same amount of NaCl in a separate tube. Solutions were mixed slowly, vortexed and incubated for 30 min. PEI: DNA mix was then added to the cells and after 24 hours, the cells were fed with 250 µL feeding medium (Freestyle 293 medium supplemented with 20% tryptone). The cells were incubated at 37 °C, 5 % CO<sub>2</sub>, 120 rpm and harvested at day 6 by centrifugation (300 g, 10 min). The supernatant was used for purification described in 2.2.2.3.

### 2.2.2.3 Purification via Protein A

The supernatant of the production was mixed with 1 mL of MabSelect SuRe (rProtein A; GE 17-

5438-01) and incubated overnight on a rocker. On the next day, the large-scale productions were centrifuged at 300 g for 10 min, and approximately 10 mL of the supernatant was left to suspend the sepharose prior to immobilization onto a column. The protein A matrix was washed with 10x CV PBS. For elution, 100 mM citrate buffer (pH 3) was used, which was neutralized with 1 M Tris-HCl (pH 9).

To exchange the elution buffer for PBS, Zeba® Spin Desalting Columns (Thermo Fisher Scientific, Waltham) were used according to the manufacturer's instructions. To determine the protein concentration after purification, the absorbance at 280 nm was measured with a spectrophotometer (Denovix). The molecular weight and molar extinction coefficient of the proteins were used to calculate the actual concentration.

#### **2.2.2.4 Coupling of antibodies and Fc fusion proteins to AF647 and AF488**

Purified monoclonal mAbs and AgFc<sub>s</sub> were coupled to either AF647 or AF488 depending on the assays according to the manufacturer's instructions. In short, the fluorochromes were solved in 100 µl DMF and added to 500 µl of antibodies with a concentration of at least 2 mg/ml. The solution was incubated for 1h protected from light on a rocker. Subsequently, uncoupled fluorochrome and uncoupled mAbs were separated by gravity flow with Sepharose G50 columns (ThermoScientific). Quality controls were done by coomassie blue staining and IVIS analysis. Degree of labelling was calculated according to the manufacturer's instructions. Monoclonal antibodies and AgFc<sub>s</sub> were stored protected from light at 4 °C until further use.

#### **2.2.3 Antibody-mediated cellular cytotoxicity assay (ADCC)**

Hybridomas were transduced with luciferase. Therefore, luciferin can be oxidized into oxyluciferin emitting light that can be measured through a spectrophotometer. After centrifugation (500 g, 5 min, RT), the supernatant of luciferase positive (Luc<sup>+</sup>) hybridomas was discarded and cells were washed with PBS to remove secreted antibodies. The cells were centrifuged again (500 g, 5 min, RT) and resuspended in 1 ml of PBS to quantify. The cells were adjusted to a concentration of  $1 \times 10^5$  cells/ml. NK cells were centrifuged and counted to adjust them to a final concentration of  $3 \times 10^5$  cells/ml. The assay was performed at a 1:3 target effector ratio. Hybridomas were incubated 10 min with 0.5µg of the to be tested AgFc in white 96 well plates prior to adding the NK cells to the wells. After an incubation time of 3 h (37°C, 5% CO<sub>2</sub>), cells were spun down (1000 g, 5 min, RT) and 100 µl supernatant was carefully removed. 100 µl of luciferin solution (150 µg/ml in PBS) was added and the plate incubated in the dark for 20 min before measuring the luciferase activity in a spectrophotometer (MITRAS). The luciferase activity

was divided by the baseline activity of hybridomas only to determine the percentage of dead cells and the effectiveness of induced ADCC.

## 2.2.4 Enzyme-linked immunosorbent assay (ELISA)

The ELISA experiments were performed in 96-well Polystyrene plates (Sarstedt). Different assay setups were used throughout this study, which are described in the following sections.

### 2.2.4.1 Titer ELISA

Titer ELISA was used to determine and compare the titer of animals with the same immunization in different cohorts. To analyze serum from chimeric PLA2R mice and autoimmune hPLA2R, we used human anti-PLA2R1-containing reference serum (diluted in postcoat buffer with 0.05% Tween 20, ranging from 4, 20, 75, 150, 500, 1500 and 3000 relative units [RU]) to develop a standard curve (described in detail in [74]). Plates were coated with 75 ng/well hCysC8-TwinStrep in coating buffer (C3041, Sigma) o/N at 4 °C. Plates were blocked with 300 µl/well postcoat (T6789, Sigma) for 30 min at RT the next day. Serum samples were diluted in dilution buffer 1:200 (autoimmune hPLA2R-mice) or 1:1000 (chim. PLA2R-mice) in dilution buffer (postcoat buffer with 10% Tween-20, E108, Sigma) and incubated in duplets for 2 hours at RT. The detection antibody (mIgG-HRP, 1:10.000) was incubated for 1 h at RT. The ELISA was developed for 3 mins in the dark with 100 µl TMB solution (OORA01684, Aviva/Biozol) before being stopped with 100 µl of 1 M H<sub>3</sub>PO<sub>4</sub>. Between each step, we washed the plates with 3 x 300 µl TBST. The plates were measured with a EL808 Ultraphotometer (BIO-TEK Instruments) to calculate the serum titers.

For analysis of mice immunized with THSD7A variants, a mixture of highly positive sera, derived from THSD7A knockout (THSD7A<sup>-/-</sup>) mice immunized with murine THSD7A was used to generate a standard curve consisting of five calibrators (4, 20, 100, 500, and 1500 relative units [RU] per mL). All samples with an absorption value lower than the lowest calibrator (4) were set as zero (described in detail in Seifert et al., unpublished data). Plates were coated with 100 ng/well md1d21-TwinStrep in coating buffer (C3041, Sigma) o/N at 4 °C. Plates were blocked with 300 µl/well postcoat (T6789, Sigma) for 30 min at RT the next day. Serum samples were diluted in dilution buffer (postcoat buffer with 10% Tween-20, E108, Sigma) 1:100 and incubated in duplets for 2 hours at RT. The detection antibody (dilution and incubation time) as well as the developing time with TMB solution as described for the PLA2R serum titer ELISA.

For double domain ELISAs to determine which domains of THSD7A is bound by certain antibodies, double domains with a HHHHHH-tag were coated with 100 ng/well o/N as described above. The double domains are: d1\_d2, d2\_d3, d3\_d4, d5\_d6, d7\_d8, d9\_d10, d15\_d16 and

d19\_d20. To be tested samples were diluted 1:100 and detected by mIgG-HRP (1:10.000) detection antibody. All other steps were done as described before.

#### **2.2.4.2 Serum blocking ELISA**

To determine how much AgFc is needed to block mouse sera with a specific anti-THSD7A or anti-PLA2R titer, we incubated 10  $\mu$ l of sera with a dilution series of their respective AgFcs ranging from 2  $\mu$ g/well to 0.5 ng/well for 1 h at RT. ELISA plates were coated with 100 ng/well md1d21 TwinStrep or 75 ng/well hCysC8 TwinStrep in coating buffer o/N at 4°C. After blocking the plate with 300 $\mu$ l/well postcoat for 1h at RT, 1  $\mu$ l of the sera/AgFc mix and 99  $\mu$ l of dilution buffer was added to the wells and incubated for 2 h at RT. From this step on, plates were handled as previously described in 2.2.4.1 for the titer ELISA.

#### **2.2.4.3 Titration ELISA**

Titration ELISAs were used to determine the EC<sub>50</sub> of the AgFc on their respective monoclonals. Plates were coated with 100 ng/well of the matching monoclonal in coating buffer o/N at 4°C. The plates were blocked with postcoat with 300  $\mu$ l/well for 1 h at RT. AgFc were added to the wells in a dilution series ranging from 100 nM to 0,1 nM and incubated for 1 h at RT. A specific mIgG2a-HRP (1:10.000) antibody was used for detection and incubated for 1 h at RT. The wells were developed with TMB solution and stopped with 1 M H<sub>3</sub>PO<sub>4</sub> solution with 100  $\mu$ l each. In between each step, the plates were washed with 3 x 300  $\mu$ l TBST and the plates analyzed with a spectrophotometer (MITRAS). The EC<sub>50</sub> was calculated with Graphpad Prism.

#### **2.2.5 Isolation of primary liver sinusoidal endothelial cells**

For liver perfusion, 5 ml per mouse of a collagenase IA (10  $\mu$ g/ml in RPMI) solution was pre-heated to 37°C and infused through the vena cava and portal vein. After discoloration of all liver lobes, the liver was excised and the gallbladder removed. The liver was cut into small pieces and homogenized with another digestion step with 5 ml of collagenase IA (37°C, 180 rpm in a vertical shaker). Cell clusters were destroyed by filtration through a 100  $\mu$ m filter. The filter was washed with 45 ml of PBS and the cell solution centrifuged (1500 rpm, 10 min, RT). To wash out fat that would disturb the gradient later on, the supernatant was discarded, the pellet was resuspended in 45 ml of PBS and the suspension was centrifuged again (1500 rpm, 10 min, RT). This step was repeated up to 3 times until the supernatant appeared clear. To discard hepatocytes, the suspension was centrifuged at low speed (50 g, 4 min, RT). The supernatant containing LSECs and other lymphocytes was transferred to another 50 ml tube and spun down (1500 rpm, 10 min, RT). The supernatant was discarded and the pellet was resuspended in 3 ml of PBS. To create a gradient 3.7 ml of a 30% Nicodenz/ddH<sub>2</sub>O solution was added to the cell suspension. 1 ml of PBS was added

slowly in a sharp angle to create 2 phases. The solution was centrifuged without brake (1400 g, 20 min, RT). The Interphase containing LSECs, Kupffer cells and macrophages was carefully collected and washed with 14 ml PBS/EDTA (2mM). After centrifugation (1500 rpm, 10 min, RT) the pellet was dissolved in 200  $\mu$ l PBS/EDTA and 24  $\mu$ l mouse CD146 Beads (Miltenyi) were added per liver. The suspension was incubated for 15 min on ice and washed with PBS/EDTA. Meanwhile, the LS columns were equilibrated with 3 ml PBS/EDTA. The pellet was resuspended in 500  $\mu$ l PBS/EDTA and added through a nylon filter to a LS column. Unwanted cells were removed by washing the column 3 times with 3ml PBS/EDTA. To elute the LSECs, the columns were taken out of the magnetic holder and placed in a collection tube. With a plunger the cell suspension was eluted into the tube. Cells were counted with a Neubauer chamber and  $5 \times 10^5$  cells/well were added to a 12 well chamber (ibidi) slide. The cells were cultivated for 3 days at 37°C, 5% CO<sub>2</sub> with a daily change of medium (RPMI + 10% FCS).

### **2.2.6 Uptake assays fluorescence-coupled immune complexes**

On the day of the uptake assay, LSECs were switched from cultivation medium with FCS to medium without FCS 4 hours prior to the start of the assay. To synchronize the cells metabolic cycles, they were placed on ice for 15 min and then the immune complex mixture was added in the assay medium. The immune complexes were formed at a molar 1:4 ratio (monoclonal:AgFc) 1 hour at RT. The monoclonals were coupled to AF647 and the AgFc constructs to AF488 to distinguish the two. To stop the uptake, the cells were washed with ice cold PBS and fixed with 4% PFA for 8 min on ice. For confocal microscopy, cells were stained with rabbit anti-EEA antibody (1:400) to visualize the early endosomes and Hoechst (1:1.500) to stain the nuclei. For quantification of the uptake, 10 cells per well were photographed and analyzed with ImageJ. Uptakes assays were performed at least 2 separate times with triplicates of each set up.

### **2.2.7 Immunofluorescence**

Paraffin sections (3-4  $\mu$ m) of formalin fixed paraffin embedded mouse kidneys were deparaffinized and rehydrated to water. Antigen retrieval was obtained by boiling in Dako Target Retrieval pH 9 (Dako, Carpinteria) for 30 min in a steamer at constant 98°C, or by digestion with protease XXIV (5  $\mu$ g/mL; Sigma-Aldrich) for 15 min at 37°C. For cryo sections (5  $\mu$ m) no antigen retrieval was required. Unspecific binding was blocked with 5% horse serum (Vector Laboratories) with 0.05% Triton X-100 (Sigma-Aldrich) in PBS for 30 min at room temperature before incubation at 4°C overnight with primary antibodies in blocking buffer. Staining was visualized with affinity purified, fluorochrome-conjugated secondary antibodies (Jackson ImmunoResearch Laboratories or Invitrogen; 1:200) for 30 min at RT in blocking buffer. Nuclei were counterstained with DRAQ5 (1:1.000; Cell Signaling 40482) or Hoechst33342 (1:1.500; Sigma-Aldrich).

Sections were mounted with Fluoromount-G (Invitrogen). Optical images were obtained using the inverted laser confocal microscope LSM800 from Zeiss. Representative images were obtained with 4-line averages and stored in 1024x1024 or 2048x2048 pixel frames with 16-bit color depth.

For immunofluorescent staining in mice, the following antibodies were used: nephrin (guinea pig, 1:200; Acris Antibodies BP5030), laminin (rabbit, 1:400; Sigma-Aldrich L9393), WGA-rhodamin (1:400; Vector-Laboratories), THSD7A (goat, 1:200; Santa Cruz Biotechnology sc163455 or rabbit, 1:200; Sigma-Aldrich HPA000923), PLA2R (rabbit, 1:200, Atlas Antibodies), and murine IgG (donkey anti-mouse IgG H+L, 1:100; Jackson ImmunoResearch Laboratories).

### 2.2.8 Flow cytometry

To identify the B cell receptor (BCR) and Fc gamma receptor II B (FcγRIIB) on the surface of the different hybridoma cells, the cells were stained with either anti-kappa IgG (1:200, FITC, ThermoFischer) or anti-CD32b (1:200, APC, ThermoFischer) for 20 min at 4°C, respectively. The cells were washed 3x with 250 μl PBS (360g, 3 min). Single cells were identified with FSC-H and alive cells with the Near infrared live dead stain (NIR, 1:2000, 2 min at RT, ThermoFischer). These cells were then checked for their BCR or FcγRIIB expression. The gating strategy is shown in Figure 4A on unstained anti-d1\_d2 hybridoma cells.

To test the binding between the different mFcγR-HEK cells and the AgFc<sub>s</sub>, the HEK cells were stained with the coupled-AgFc<sub>s</sub> for 20 min at 4°C and then washed 3x with 250 μl PBS (360g, 3 min). Duplet cells were excluded using the FSC-H and alive cells were identified with the Near infrared live dead stain (NIR, 1:2000, 2 min at RT, ThermoFischer). The AgFc<sub>s</sub> were coupled to AF488. A representative gating strategy is shown in Figure 4B on unstained FcγRIIB-HEKs.

To identify FcγRIIB<sup>+</sup> LSECs, we developed the panel shown in Figure 4C. After the Nicodenz gradient described in 2.2.5. the interphase was transferred into a new 15 ml falcon and washed with 14 ml of PBS to eliminate the residual Nicodenz (1500 rpm, 10 min, RT). The pellet was resuspended in 100 μl PBS and transferred to a 96 well conical plate for staining. The cells were blocked with CD32b/CD16 specific antibody (Biolegend) for 10 min at 4°C prior to adding the staining antibodies F4/80 (1:200, BV450, ThermoFischer), CD45 (1:200, PerCP, ThermoFischer), CD31 (1:200, PE-Cy7, ThermoFischer), and CD32b (1:200, PE, ThermoFischer). We stained the cells for 20 min at 4°C before centrifuging the plate (360 g, 3 min) and discarding the supernatant. Near infrared live dead stain (1:2000, 2 min at RT, ThermoFischer) was used to exclude dead cells. Cells were washed 3 x with 250 μl PBS before analyzing in the Symphony AIII (BD). The gating strategy excluded cells smaller than 50 K as debris and only single cells were used for analysis. Dead cells were excluded next, followed by Kupffer cells identified with F4/80. LSECs were separated from macrophages using CD31 and CD45. LSECs characterized as CD31<sup>high</sup>

CD45<sup>low/medium</sup>, while macrophages are CD31<sup>low</sup> CD45<sup>high</sup>. Cells that were low stained for either marker were left as unidentified cells. LSECs were then divided into CD32b positive and negative cells, while the majority of LSECs were positive for CD32b (88 %), the majority of macrophages were negative for this marker (90 %). FcγRIIB<sup>+</sup> LSECs took up the majority of immune complexes made of mAb-AF647 and AgFc-AF488.

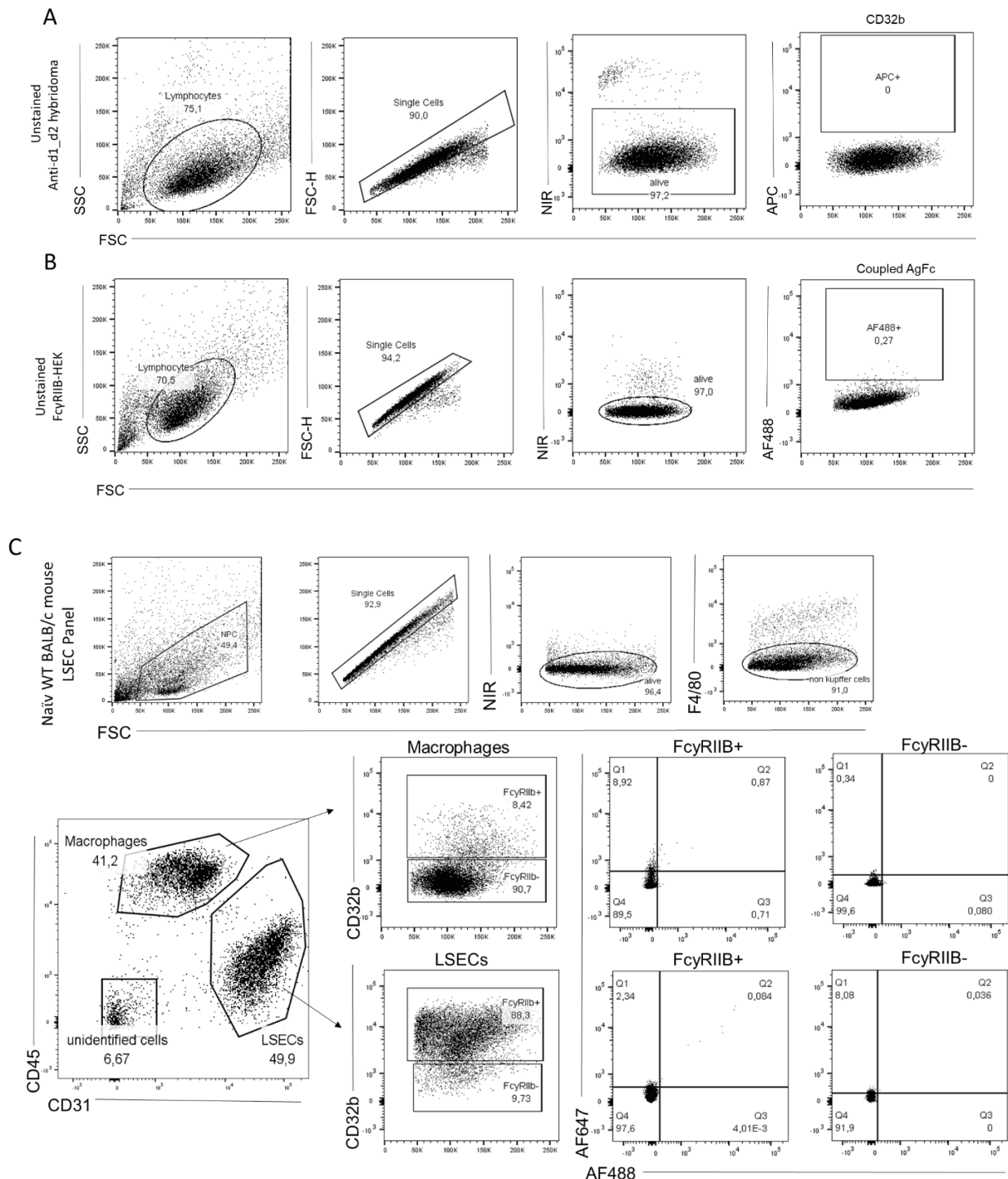


**Figure 4: Gating strategies for flow cytometry.** (A) Gating strategy for hybridoma cells, the unstained anti-d1\_d2 hybridoma is shown as an example. Hybridomas were identified between 50 and 150 k in size. Duplets were excluded using the FSC-H. Alive cells were identified using the live:dead staining near infrared (NIR). The anti-kappa IgG (FITC) and anti-CD32b (APC) antibodies were used to check the surface expression of the BCR and FcγRIIB, respectively. (B) Gating strategy for mFcγR-HEKs, the unstained mFcγRIIB-HEK is shown as an example. HEKs were identified between 50 and 150 k in size. Duplets were excluded using the FSC-H. Alive cells were identified

using the live:dead staining near infrared (NIR). The coupled-AgFcs (AF488) were used to characterize the binding of the different IgG backbones to the four Fc $\gamma$ R subtypes: Fc $\gamma$ RI, Fc $\gamma$ RIIB, Fc $\gamma$ RIII and Fc $\gamma$ RIV. (C) Gating strategy on a naïve mouse for defining LSECs. The non-parenchymal cells (NPC) were defined as cells larger than 50 K in the forward scatter (FSC). Doublets were excluded using the FSC-H. Dead cells or transitioning cells were excluded using the live:dead staining near infrared (NIR). Kupffer cells were excluded using F4/80. LSECs were defined as CD31<sup>high</sup> CD45<sup>low/medium</sup>, while monocyte-derived macrophages (MoM $\phi$ s) were defined CD31<sup>low</sup> CD45<sup>high</sup>, cells that did not fit in either gate were labeled as unidentified cells. Macrophages and LSECs were then stained for Fc $\gamma$ RIIB (CD32b). Most macrophages (90%) were CD32b<sup>-</sup>, while the majority of LSECs were CD32b<sup>+</sup> (88%). In uptake experiments with AF647-labeled monoclonal antibody and AF488-labeled AgFcs, both CD32b<sup>+</sup> and CD32b<sup>-</sup> were observed for double positive cells, which means the immune complex made up of monoclonal antibody and AgFc was taken up into the cells creating double positive populations (AF647<sup>+</sup>AF488<sup>+</sup>).

### 2.2.9 Analysis of fluorescence in organs and blood samples with *in vivo* imaging systems (IVIS)

Blood samples containing AF647-coupled mAbs or AgFcs were added either pure or diluted 1:1 in PBS into black 96 well plates and measured in comparison to a coupled mAb with definite concentration to determine the amount left inside the serum (Figure 5A). For analysis of the organs, mice were perfused with 25 ml of PBS/Procain (1%) through the heart while sacrificing them. Organs were taken out, weighed, and arranged on a black tray (Figure 5B) to measure the total radiant efficiency (TRE). Tested organs included heart (1), lungs (2), kidneys (3), testis (4), spleen (5), and liver (6). The TRE was divided by the organ weight to account for size differences between the mice to acquire TRE/ g organ.

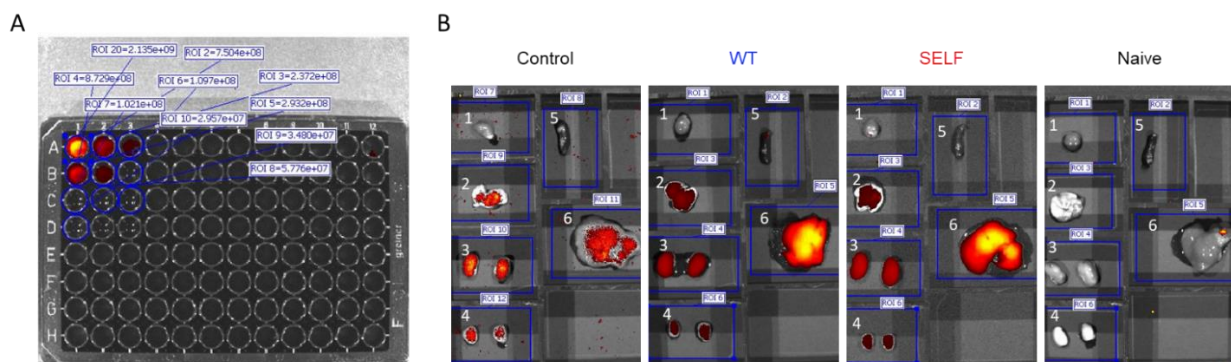


**Figure 5: Analyzing blood and organ samples with IVIS.** (A) Serum samples were analyzed inside a black 96-well plate to minimize background fluorescence. A AF647-coupled mAb with a defined concentration was used as a standard (row A, well 1 to 3), samples were measured on the same plate and the amount of AF647-labeled antibody left in the serum calculated using the ROI of every well (rows B to D, wells 1 to 3). (B) Organs were extracted and analyzed inside the IVIS. Tested organs include heart (1), lungs (2), kidneys (3), testis (4), spleen (5), and liver (6). A template was used to divide the organs and prevent fluorescence spilling from one organ to the next. Total radiant efficiency (TRE) was calculated using ROIs and organ weight in g. While the naïve control shows no TRE in all organs, depending on the mixture of mAb and AgFc the TRE of e.g. the liver is highest in mice with d1d2-WT-AgFc or d1d2-SELF-AgFc, while it is lower in the control mice (mAb + CysFnII-SELF-AgFc).

### 2.2.10 Animal experiments

Wild-type male BALB/c mice, *THSD7A*<sup>-/-</sup> mice, transgenic hPLA2R mice, chimeric PLA2R mice, *FcRn*<sup>-/-</sup> mice, and C57BL/6 mice (12-14 weeks old) were bred in the animal facility of the University Medical Center Hamburg-Eppendorf or acquired from Charles River (France).

Animals had access to water and standard animal chow ad libitum. Animal experiments were performed according to national and institutional animal care and ethical guidelines and were approved by the Veterinarian Agency of Hamburg and the local animal care committee (registration numbers 037/22 and 020/19).

#### **2.2.10.1 Blocking of rabbit anti-THSD7A polyclonal serum in *THSD7A*<sup>-/-</sup> mice**

Complete *THSD7A*<sup>-/-</sup> mice were generated using the knockout-first strategy [78]. Since *Thsd7a*<sup>tm1a</sup> mice showed a residual renal THSD7A expression of approximately 10 %, (Tomas et al., unpublished data) two further breeding steps were necessary to obtain a *THSD7A*<sup>-/-</sup> mouse line. First, *Thsd7atm1a* mice were bred with Flip-deleter mice, constitutively express the Flip-recombinase, leading to *Thsd7a*<sup>tm1c</sup> mice with an almost reconstituted THSD7A expression. Second, *Thsd7a*<sup>tm1c</sup> were bred with complete Cre-deleter mice [79], constitutively expressing the Cre recombinase, leading to *Thsd7a*<sup>tm1d</sup> mice with an efficient removal of exon 4 of THSD7A. In contrast to *Thsd7a*<sup>tm1a</sup> mice, *Thsd7a*<sup>tm1d</sup> (Tomas et al., unpublished data) mice had no detectable renal THSD7A expression. These mice (n=2) were used to inhibit any binding of the purified rabbit anti-THSD7A IgG to THSD7A inside the animals. The IgG was purified from rabbits immunized with THSD7A resulting in polyclonal sera that bound almost all domains of THSD7A, apart from md11\_d12, md13\_d14, and md17\_d18. 50 µg of purified rabbit IgG were incubated with 6.2 µg of d1d2-WT or d1d2-SELF 1 h prior to injecting i.p. into the animals. Control animals were injected with rabbit IgG only. 1 day later the animals were sacrificed to analyze the blocking of rabbit anti-d1\_d2 antibodies in the serum und localization of rabbit IgG inside cryo-sections of the liver that indicate uptake and degradation of formed complexes.

#### **2.2.10.2 Analysis of *in vivo* formed complexes after 6 hours in WT BALB/c mice**

WT BALB/c mice (n=3) were injected i.p. with 25 µg anti-d1\_d2 mAb coupled to AF647, followed by 33 µg i.v. of d1d2-WT-, d1d2-SELF- or 15-SELF-AgFc coupled to AF488 24 hours later. After 6 hours, these animals were sacrificed under Isoflurane anaesthesia. Serum was collected and organs were taken out, weighed, and analysed for their fluorescent intensity using the IVIS. Kidneys and livers were processed even further: kidneys were fixated for 1 h at 4 °C with 4% PFA and then stored in 30% sucrose/PBS for about 4 hours until frozen in Tissuetek™ and stored at -80°C for immunohistochemistry. Livers were digested with collagenase 1A and LSECs isolated for FACS analysis as described before.

#### **2.2.10.3 Time course of degradation in LSECs**

For the degradation of *in vitro* pre-formed complexes 10 µg each of anti-d1\_d2 mAb coupled to

AF647 and d1d2-WT- or d1d2-SELF-AgFc coupled to AF488 were mixed and incubated 1 h at RT prior to i.v. injection into WT BALB/c mice (n=3). Control animals were injected with 10 µg of anti-d1\_d2 mAb coupled to AF647 only. Mice were sacrificed under Isoflurane anaesthesia after 10 min, 1 h, 6 hours, 1 d, and 7 days post injection to analyse the remaining amount of anti-d1\_d2 mAb inside the serum as well as the uptake in LSECs through Flow cytometry. Cryosections of the kidneys were made to determine binding to THSD7A on podocytes. For the degradation of *in vivo* formed complexes, 25 µg of anti-d1\_d2 mAb coupled to AF647 was injected i.p. into WT BALB/c (n=3), followed by 33 µg i.v. of d1d2-WT-, d1d2-SELF- or d1d2-LALAPG-AgFc coupled to AF488 24 hours later. Control animals were injected with anti-d1\_d2 mAb only. Mice were sacrificed after 60 min, 3 days, and 7 days. The same analyses were performed as for the degradation of *in vitro* formed complexes.

#### **2.2.10.4 FcRn involvement in degradation of immune complexes**

FcRn knock out mice (*FcRn*<sup>-/-</sup>; B6.129X1-Fcgrt<sup>tm1Dcr</sup>/DcrJ) were purchased from Charles River (France) and bred in the animal facility for experiments. Mice (n=3) were injected with 25 µg anti-d1\_d2 mAb coupled to AF647 i.p. and 22 hours later, a small amount of blood was collected. 24 hpi, 33 µg of AF488-coupled d1d2-SELF-AgFc or d15-SELF-AgFc was injected i.v. retrobulbar as the start of the *in vivo* uptake assays. Control animals were injected with 25 µg anti-d1\_d2 mAb coupled to AF647 i.p. only. WT C57BL/6 mice with normal FcRn expression were used as a control group in all experiments. Mice were sacrificed under Isoflurane anesthesia after 1 hour and 3 days. Serum was collected again. Organs were taken out, weighed, and analyzed for their fluorescent intensity using the IVIS. Kidneys were fixated for 1 h at 4 °C with 4% PFA and then stored in 30% sucrose/PBS for about 4 hours until frozen in Tissuetek™ and stored at -80°C for immunohistochemistry. Livers were cut and digested with Col1A following the protocol described previously to analyze the LSECs with flow cytometry.

#### **2.2.10.5 Safety assessment of AgFcs in healthy WT BALB/c or chimeric PLA2R-mice**

To assess the safety of the AgFc constructs for healthy mice, we injected WT BALB/c mice (n=10) with 10 µg of d1d2-SELF-AgFc i.p. over 7 consecutive weeks. To determine the same for the PLA2R-constructs, chimeric PLA2R (chPLA2R1) mice were used. Chimeric PLA2R mice were generated as described previously [79]. In short, Rosa26/CAG/Stop/chPLA2R/eGFP mice without chPLA2R expression were crossed with podocin promoter carrying Cre<sup>+</sup> mice, resulting in Rosa26/CAG/chPLA2R/eGFP Cre<sup>+</sup> mice with a chPLA2R expression in podocytes. These mice express a chimeric PLA2R molecule on podocytes consisting of human cysteine-rich domain (CysR), fibronectin domain II (FnII) and C-type lectin domain 1 (CTLD1) and murine CTLD 2

to 8. Under basal conditions these mice are healthy and do not develop proteinuria against the chimeric protein on their podocytes (data not published). We injected chim. PLA2R mice (n=10) with 10 µg of CysFnII-SELF-AgFc in the same manner. To exclude effects from the repeated injections we included animals (n=4) that were injected i.p. with 100 µl of saline. Animals were weighed weekly and urine was collected to detect increasing albumin output. At the end of the experiment, animals were sacrificed under anesthesia. Serum samples were analyzed for liver function (AST and ALT) and kidney function (BUN and ACR) as well as cholesterol and triglyceride levels. Paraffin slices of the kidneys were stained with anti-mIgG and counterstained with laminin and Hoechst to determine binding of mIgG along the glomeruli.

#### **2.2.10.6 *In vivo* blocking of polyclonal autoantibodies**

Mice lacking THSD7A (*THSD7A*<sup>-/-</sup> mice) were immunized with the N-terminal domains of THSD7A d1\_d2 and received three shots with 20 µg: first an immunization with complete Freund's adjuvant (CFA), and two boosters with incomplete Freund's adjuvant (IFA) three and five weeks later subcutaneously. Blood samples were taken 1 week after the first and second boost. One week after the second boost, mice were injected with d1d2-SELF-AgFc-AF647 or CysFnII-SELF-AgFc-AF647 (300 µg i.p.) to either block the anti-THSD7A titer *in vivo* (d1d2-AgFc-AF647) or act as a control (CysFnII-AgFc-AF647). Mice were sacrificed 24 hours later, serum was collected for analysis of anti-THSD7A titer and remaining fluorescence (IVIS), kidneys were taken for cryo-sections and livers for LSECs analysis in FACS.

#### **2.2.10.7 Experimental autoimmune THSD7A-membranous nephropathy (THSD7A-EAMN)**

For immunizations of WT BALB/c mice, a mixture of murine THSD7A fragments was used: d1\_d2 only for pre-treatment or d1\_d2 and d15\_d16 for treatment after >3 g/g proteinuria was exceeded. Mice received a total of four immunizations: 20 µg of protein per fragment were mixed with an equal volume of complete Freund's adjuvant and injected subcutaneously, followed by three boost immunizations of 20 µg per fragment in an equal volume of incomplete Freund's adjuvant after three, five and seven weeks. Control mice received the equal amounts of adjuvant diluted in PBS. A total of 21 BALB/c mice (1 with PBS and 20 with THSD7A domains) were experimented. Serum was taken before the first immunization and after 4, 8 and 14 weeks. Urine was collected using metabolic cages and mice were weighed weekly. Albumin content in the urine was quantified using a commercially available ELISA system (Bethyl) according to the manufacturer's instructions. The urine albumin values were standardized against urinary creatinine values (as determined according to Jaffé) of the same sample. Blood urea nitrogen

(BUN), triglycerides, alanine aminotransferase (ALT), aspartate aminotransferase (AST), and cholesterol levels were measured by standard procedures using the cobas system (Roche Diagnostic). Mice were euthanized after the predefined observation period for the final collection of blood, urine, and organs. For pre-treatment experiments in THSD7A-immunized mice, the animals received 100 µg AgFc twice a week i.p. starting after the second boost. Every week two animals per group were taken out of the experiment to observe the mIgG binding inside the glomerulus over the treatment time.

For treatment experiments in THSD7A-immunized mice, mice received 200 µg of AgFc twice a week i.p. for a total of four weeks, starting when proteinuria exceeded 3 g/g albumin-to-creatinine, which was defined as week 0. Two THSD7A-immunized mice were sacrificed at week 0 to assess glomerular mIgG deposition at the time of treatment initiation. Mice were sacrificed for histological and serum analysis after a predefined observation period of four weeks from the first AgFc administration.

#### **2.2.10.8 Treatment of transgenic human PLA2R mice**

To obtain transgenic human PLA2R (hPLA2R) mice on the BALB/c background the same breeding method was performed as described in [74]. Mice start developing autoantibodies very early, therefore, mice were weaned off from their mothers at 21 days of age and blood was taken. Urine was collected twice a week to detect rapid decline of kidney function. Mice were injected twice a week with 10 µg/g of CysFnII-WT-AgFc, CTLD1/2-WT-AgFc and CTLD7/8-WT-AgFc i.p. to block all autoantibodies circulating the system. Blood was collected once a week to determine the anti-PLA2R titer and success of injections. Mice were sacrificed after 3 weeks of treatment, blood collected to analyze BUN, triglycerides, ALT, AST, blood creatinine and cholesterol, as well as kidneys for immunohistochemistry.

Criteria to determine whether animals needed to be removed from the experiments prematurely included, amongst others, development of visible ascites, respiratory distress due to fluid accumulation, and a weight gain of >20% in one week. A nephrotic syndrome clinical score was calculated for each mouse. This score involved proteinuria of >10 g/g (1 point), proteinuria >100 g/g (1 point), a serum albumin level > 20% below control level (1 point), a serum cholesterol or triglyceride level of >50% above control level (1 point), and a weight gain of >20% in comparison to the weight at week 0 (1 point), thus allowing a maximum score of 5 points.

#### **2.2.11 Statistics**

For the determination of the half maximal effective concentration (EC<sub>50</sub>) the nonlinear regression tool of GraphPad Prism 8.3.0 was used. All data sets were tested if they follow a Gaussian

distribution under the null hypothesis. If so, a Student's t-test was used to compare the data sets. If not, a Mann-Whitney test was used. To compare three groups of numerical response data a one-way ANOVA was used. For non-parametric data a Kruskal-Wallis test was used. For the analysis of more than one time point a two-way ANOVA was used and either the Sidak's multiple comparison or the Tukey's multiple comparison was used.

### 3 Results

#### 3.1 Characterization of AgFc constructs

The different domains of murine THSD7A (d1\_d2 and d15) and human PLA2R (CysFnII) were cloned into pCSE2.5 vectors with the corresponding IgG2a backbones: WT, higher affinity towards Fc $\gamma$ RIIB through mutation of S267E and L328F (SELF) and ablated Fc $\gamma$ R binding through mutation of L234A/L235A, P329G (LALAPG). The schematic structure can be seen in Figure 6A. The AgFc constructs were produced in HEK293-6E cells and were checked for correct assembly into dimers with a Coomassie blue staining after purification and coupled to fluorochromes (AF647 or AF488) for further uses. While CysFnII constructs (WT, SELF and LALAPG) are 103 kDa in size, d1d2- and d15-AgFc constructs are smaller, 84 kDa and 71 kDa, respectively (Figure 6B). B cells isolated from mice immunized with various domains of the antigens THSD7A and PLA2R were fused to myeloma cells to create hybridoma cells: endlessly-replicating and monoclonal antibody (mAb) producing cells targeting specific domains of either THSD7A or PLA2R. For determination of the epitope regions of the monoclonal antibodies produced by the hybridoma cells, a subfragment ELISA with domains of THSD7A and PLA2R was performed and showed that the mAbs raised against mouse THSD7A (B64 and B4) bind domains 2 and 15, respectively, while the mAb raised against human PLA2R (A19/30) binds the cysteine-rich domain (CysR) (Figure 6C-E). With these mouse mAbs previously developed by our lab, the binding of the AgFc constructs in ELISA was tested and the mutations appeared to have no influence on the binding between mAb and AgFc (Figure 6F-H) with the exception of d15-LALAPG on the anti-d15 mAb (Figure 6G). The half maximal effective concentration ( $EC_{50}$ ), an indicator of a drug's potency, was determined to be 1.63 nM, 0.52 nM, and 0.78 nM for d1d2-AgFc, d15-AgFc and CysFnII-AgFc, respectively.

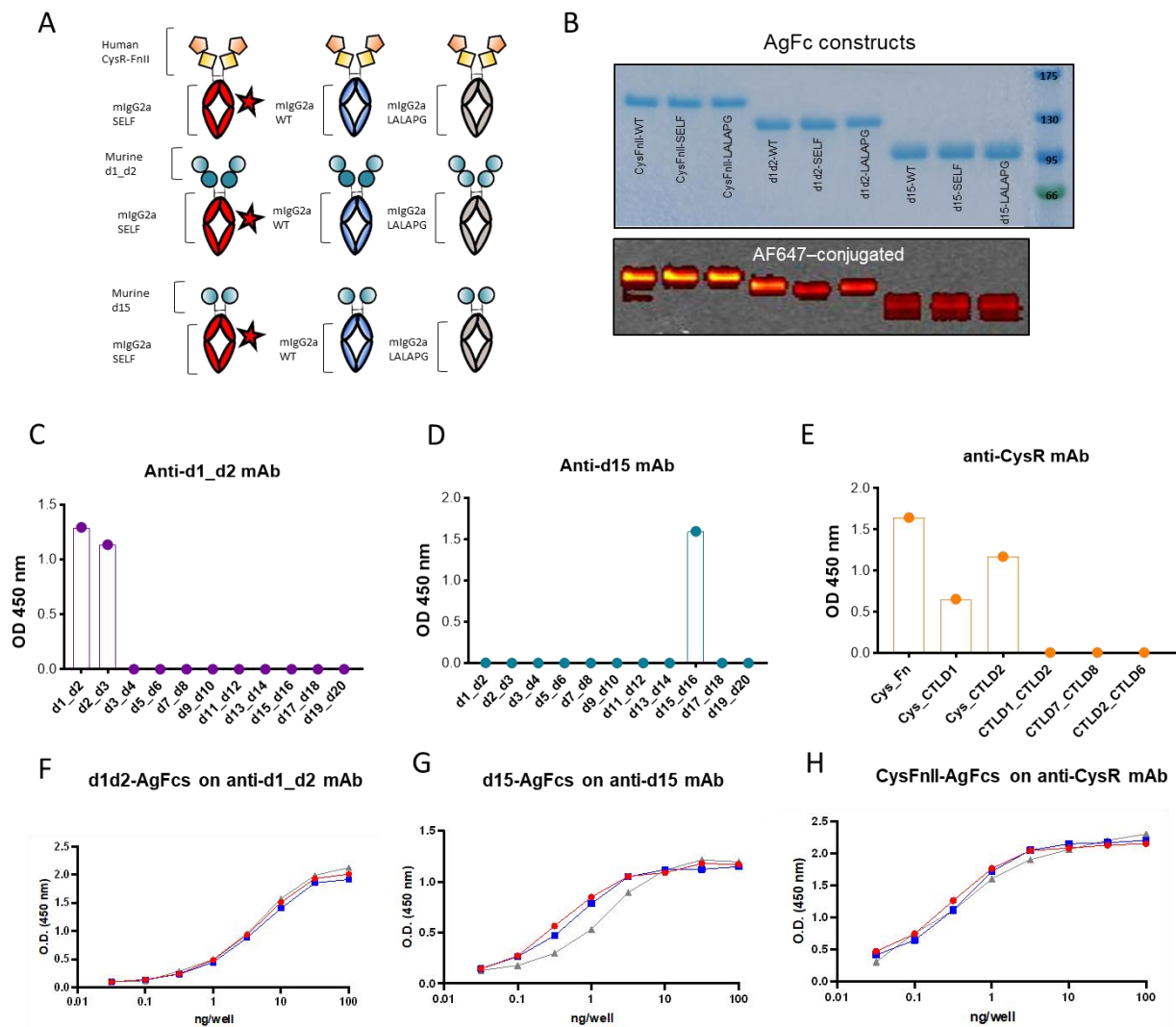


**Figure 6: Creating AgFc constructs.** (A) AgFcs consist of an antigen fragment, which creates specificity towards autoantibodies against PLA2R or THSD7A, e.g. domains 1 and 2 of THSD7A or the most N-terminal region CysFnII (cysteine-rich domain and Fibronectin II domain) of PLA2R and a mIgG2a Fc backbone. We created three different Fc variants: SELF (red) where amino acids S267E and L328F are mutated to increase the affinity towards FcγRIIB, LALAPG (grey) where amino acids L234A/L235A, P329G are mutated to abolish FcγR binding, and WT (blue) with no change to the IgG2a backbone. (B) These constructs were produced in HEK293-6E cells and coupled to either AF488 or AF647 depending on the experimental set up. While CysFnII constructs (WT, SELF and LALAPG) are 103 kDa in size, d1d2-AgFcs and d15-AgFcs are smaller, 84 kDa and 71 kDa, respectively. (C) and (D) show ELISA results to determine the epitope region of the mAbs raised in mice immunized with different double domains of the corresponding antigens. Coated double domains of THSD7A are: d1\_d2, d2\_d3, d3\_d4, d5\_d6, d7\_d8, d9\_d10, d15\_d16 and d19\_d20. Anti-d1\_d2 mAb binds the double domain fragments d1\_d2 and d2\_d3, while anti-THSD7A (d15) mAb binds the double domain fragment d15\_d16. (E) Fragment-ELISA and domains of PLA2R shows the anti-PLA2R (CysR) mAb binds all fragments that include the cysteine-rich domain (CysR). (F) Titration ELISA of d1d2-AgFcs on an anti-d1\_d2 mAb. No difference in binding between WT (blue), SELF (red) or LALAPG (grey) constructs could be observed. (G) Titration ELISA of d15-AgFcs on an anti-d15 mAb. No difference in binding between WT (blue) and SELF (red) constructs and only a slight variation in LALAPG (grey) could be detected. (H) Titration ELISA of CysFnII-AgFcs on an anti-CysR mAb. We observed no difference in binding between WT (blue), SELF (red) or LALAPG (grey) constructs. For all Titration-ELISAs 100 ng/well of the mAb was coated, and a dilution series ranging from 100 ng to 0.03 ng/well AgFc was added.

The hybridomas not only secrete the mAb into the supernatant, but also express a membrane-bound B cell receptor (the equivalent to the secreted monoclonal) on their surface. Once the AgFcs were purified and coupled to fluorochromes, the binding to the corresponding hybridomas was tested

with flow cytometry. The anti-d1\_d2 hybridoma was found to bind d1d2-AgFc (WT and SELF) but not a not fitting AgFc like CysFnII-WT (Figure 7, upper row). The anti-d15 hybridoma was found to bind d15-AgFc (WT and SELF) while a non-fitting AgFc produced no positive cells (Figure 7, middle row). The anti-CysR hybridoma bound CysFnII-AgFc constructs (WT and SELF) but no other constructs like d1d2-WT-AgFc (Figure 7, lower row). Also, the expression of the FcγRIIB and the BCR (anti-kappa heavy chain) was confirmed with commercial antibodies. All hybridomas expressed FcγRIIB and a BCR on their surface (Figure 7, 1<sup>st</sup> and 3<sup>rd</sup> column). The binding was specific since the isotype control did not stain the cells (Figure 7, 2<sup>nd</sup> column).

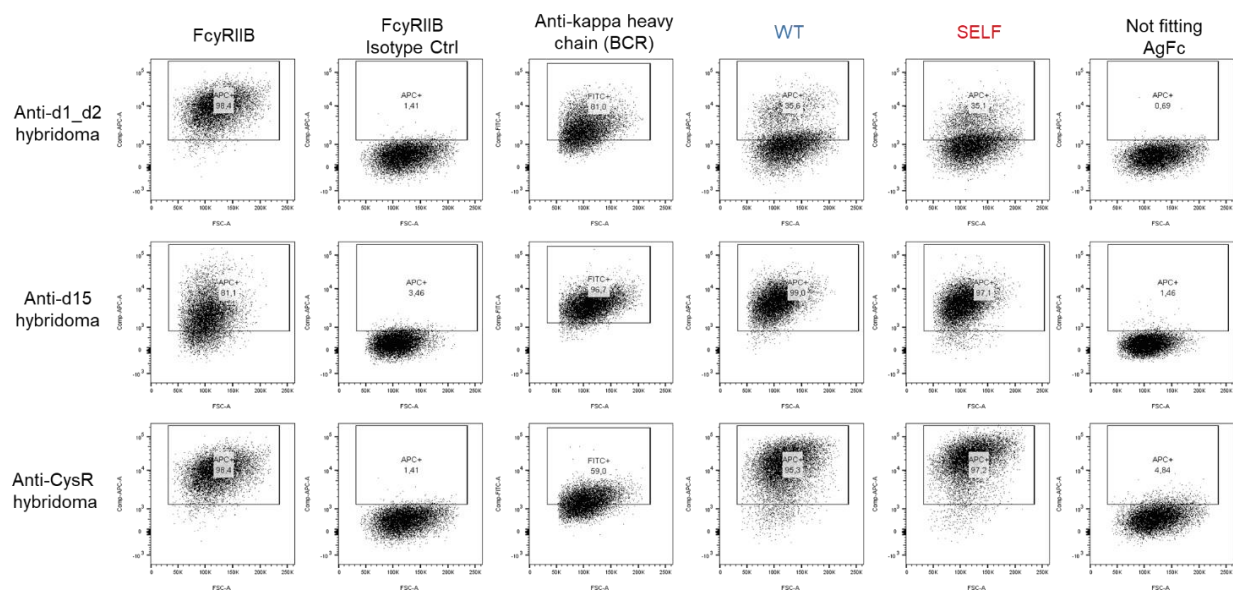


**Figure 7: Characterization of anti-THSD7A and anti-PLA2R hybridomas.** Most of the anti-d1\_d2 hybridoma cells expressed FcγRIIB (98%) but did not stain with the corresponding isotype Ctrl. The staining with the anti-kappa heavy chain mAb showed 81% of cells expressed a BCR on their surface. When stained with the fitting AgFcs like d1d2-WT-AgFc-AF647 and d1d2-SELF-AgFc-AF647 a clear positive population was found (35%), which was not observed in combination with a non-fitting construct like CysFnII-WT-AgFc-AF647. 81% of the anti-d15 hybridoma expressed the FcγRIIB and did not stain with the isotype Ctrl. This hybridoma also expressed a BCR on its surface (96%) and was stained well with the corresponding AgFcs (d15-WT-AgFc-AF647 and d15-SELF-AgFc-AF647), while a non-fitting AgFc did not stain the cells (CysFnII-WT-AgFc-AF647). The anti-CysR hybridoma expressed FcγRIIB specifically (98%) but showed the lowest expression of the BCR (59%) compared to all other hybridoma cell lines. The specific staining with CysFnII-WT-AgFc-AF647 and CysFnII-SELF-AgFc-AF647 was very good (95% and 97%, respectively), while d1d2-WT-AgFc-AF647 (not fitting AgFc) did not stain the cells.

To determine if the different IgG backbones influence the binding to a membrane-bound BCR, we used the hybridoma cell lines and detected binding of our fluorescently labeled constructs with flow cytometry (Figure 8, upper panel). We found no unspecific binding of constructs that should not bind certain BCRs and that the different Fc backbones did not have a significant influence on the binding of the domains to their respective BCRs (Figure 8B-D). To confirm binding to a membrane-bound FcγR, we used HEK cells stably transfected with mFcγRI, mFcγRIIB, mFcγRIII and mFcγRIV. The binding was dependent on the receptor and also the Fc-part of the AgFc constructs. The AgFcs with the LALAPG mutation in the Fc part showed no detectable binding

to any receptor, while WT and SELF constructs showed significantly higher binding to the FcγRI and FcγRIIB. The binding to FcγRIII of all constructs was weak, as expected for a low affinity receptor (Figure 8, F-H).

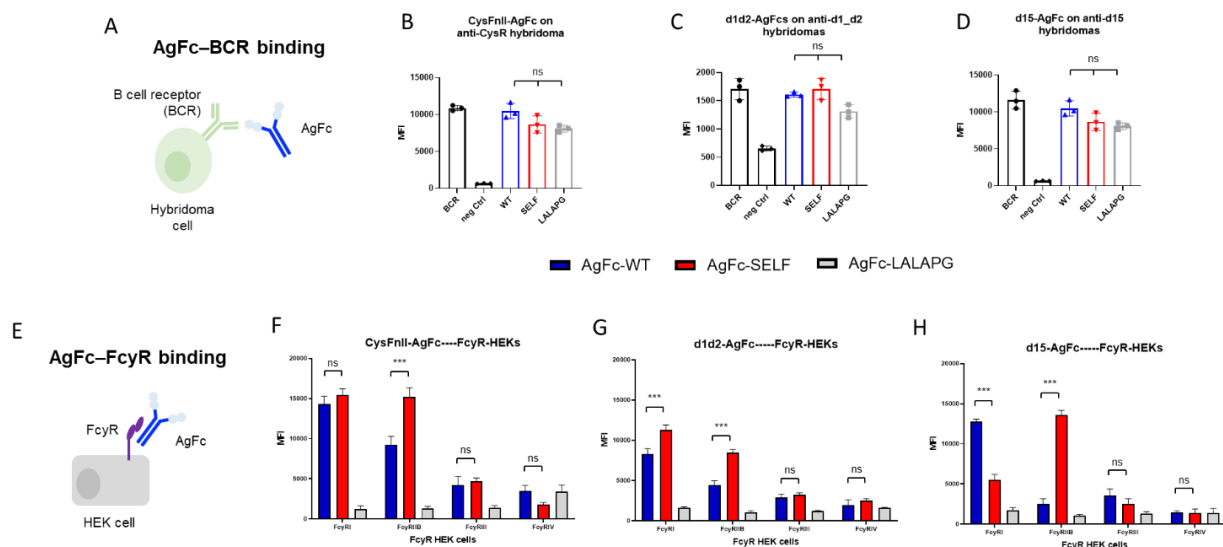


**Figure 8: Binding characterization of AgFc constructs.** (A) Binding of fluorochrome coupled AgFc to their corresponding hybridomas. A specific CD16/32b blocking antibody was used to exclude unspecific binding to FcγRs (B-D) Comparing the mean fluorescent intensity (MFI) of fluorochrome-coupled AgFc to hybridoma cells expressing different BCRs on their surface. Specific binding was observed between the domains of the AgFc and the BCR. The BCR was stained with an anti-kappa FITC antibody to confirm BCR expression on the surface of the cells. Different mIgG backbones were used: WT (blue), SELF (red) and LALAPG (grey). Ctrl conditions include an AgFc which should not be able to bind to the respective BCR e.g., CysFnII-WT-AgFc with anti-d1\_d2 hybridoma. All cells express a BCR on their surface and do not bind the Ctrl AgFc. All AgFc bind to their respective hybridoma and no significant difference could be found for the different mIgG backbones. (B) CysFnII-AgFc on their fitting hybridoma. (C) d1d2-AgFc on their fitting hybridoma. (D) d15-AgFc on their fitting hybridoma. (E) Comparing the MFI of fluorochrome coupled AgFc bound to HEK cells expressing different FcγRs on their surface. No specific CD16/32b blocking antibody was used. (F-H) Throughout the set ups, AgFc with a LALAPG mIgG backbone did not bind any FcγR expressing HEK cells. While no significant difference between WT- and SELF-AgFc could be observed on FcγRIII and FcγRIV, binding of SELF-AgFc was increased significantly on FcγRIIB compared to WT-AgFc. (F) CysFnII-AgFc on all four FcγR-HEKs. (G) d1d2-AgFc on all four FcγR-HEKs. (H) d15-AgFc on all four FcγR-HEKs. In conclusion, all AgFc bound to their corresponding BCRs independent of a mutated Fc part. By contrast, the SELF mutations increased the binding of all AgFc to FcγRIIB, while the LALAPG mutations completely abrogated binding to FcγRs. All Statistics: Two-way ANOVA, Tukey's multiple comparison test,  $p^{***}=0,0001$ .

In summary, we successfully generated AgFc containing different immuno-dominant domains of the antigens THSD7A and PLA2R to create specific binding to their target mAbs, confirmed the functional SELF-mutation on FcγR-HEKs and the ability to bind membrane bound BCRs.

### 3.2 Antibody-dependent cellular cytotoxicity mediated through AgFc

Next, we wanted to investigate, whether AgFc can induce ADCC through the specificity of the BCR of the hybridomas in combination with murine NK cells. Therefore, we used murine NK cells stably transfected with mFcγRIII and added them to AgFc pre-incubated hybridomas in a target:effector ratio of 1:3 (Figure 9A). After 3 h, viability was measured through the hybridomas' ability to convert luciferase. In all set ups, killing was most efficiently induced through SELF-

AgFcs, though WT constructs were also able to mediate ADCC on the fitting hybridomas (Figure 9B-D). We saw only slight unspecific killing of our constructs on the non-fitting hybridomas, for example CysFnII-SELF-AgFc induced ADCC of 10 % on the anti-d1\_d2 hybridoma (Figure 9A). While wells with only hybridomas were set as 100 % viability, wells incubated with LALAPG-AgFcs showed increased luciferase activity so that in all tested set ups the viability of hybridomas pre-incubated with LALAPG was higher than 100 %.

The low ADCC activity on the anti-PLA2R hybridoma cells might be explained through the lower expression of BCR (59%) on its surface (as seen in Figure 8, bottom row). With fewer BCR expressed on the cell surface, the AgFcs cannot induce killing through the NK cells as efficiently.

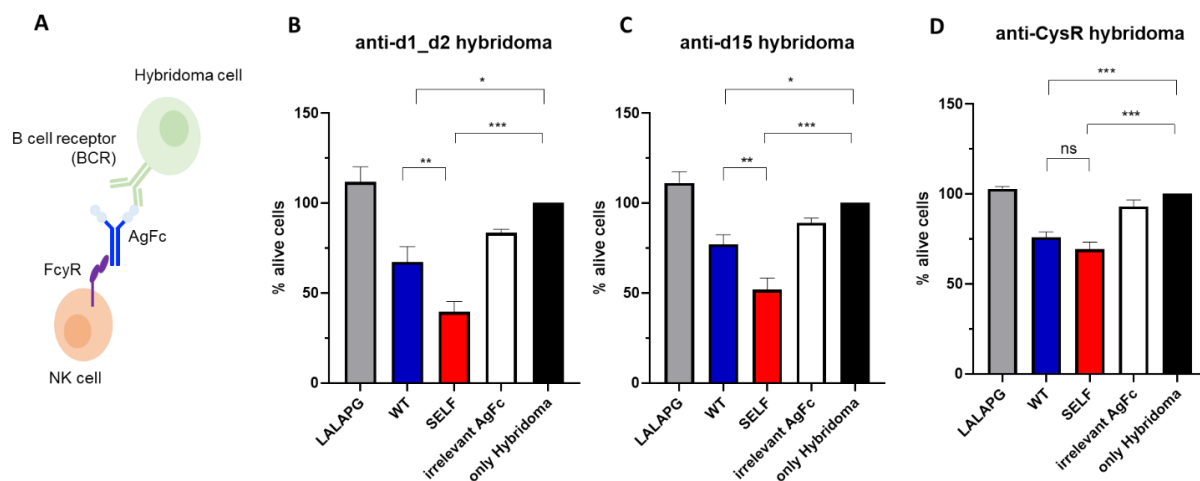


**Figure 9: ADCC through AgFcs.** (A) ADCC mediated through binding of AgFcs on their target  $luc^+$  hybridomas. (B) Anti-d1\_d2 hybridomas were incubated with either d1d2-SELF-AgFc (red), d1d2-WT-AgFc (blue), d1d2-LALAPG-AgFc (grey) or an irrelevant AgFc (CysFnII-SELF, white) before murine NK cells were added. Hybridomas only (black) were used to display 100 % viability. Significantly more target cells died when they were incubated with WT- or SELF-AgFcs ( $p^*$  and  $p^{***}$ , respectively). SELF-AgFcs were more potent than WT-AgFcs in mediating ADCC ( $p^{**}$ ). Wells incubated with LALAPG-AgFcs showed slightly higher viability than the wells with only hybridomas. (C) shows ADCC mediated through d15-AgFc on anti-d15 hybridomas. Again, killing was more efficient with WT and SELF-AgFcs ( $p^*$  and  $p^{***}$ , respectively), while LALAPG did not mediate any ADCC. When comparing efficiency of WT-AgFc and SELF-AgFc, we found SELF-AgFcs to be a better mediator for ADCC ( $p^{**}$ ). (D) CysFnII-AgFc mediated ADCC on anti-CysR hybridomas was not as successful as on the other tested cells. The highest killing rate only achieved to kill 32 % of cells (CysFnII-SELF-AgFc,  $p^{***}$ ). The difference between WT- and SELF-AgFcs was non-significant. LALAPG-AgFcs again yielded more than 100 % viability of hybridomas. Statistical analysis: One-way ANOVA,  $p < 0.0001$ , Tukey's multiple comparison test,  $p^* < 0.05$ ,  $p^{**} < 0.001$ ,  $p^{***} < 0.001$ .

These results suggest, that the mutations we added to the mIgG2a backbone are functional. LALAPG backbones did not induce ADCC independent of the antigen part of the construct. Even though a higher affinity towards FcγRIII is not described in the literature, we saw that the SELF mutation is most efficient in inducing ADCC through the FcγRIII. However, if our AgFcs are also be capable of inducing ADCC of antigen-specific B cells *in vivo* remains unclear at this point.

### 3.3 *In vitro* immune complex uptake by primary LSECs

Before testing the clearance of specific antibodies *in vivo*, we aimed to explore the uptake of the immune complexes consisting of mAbs and AgFcs in an *in vitro* system. Therefore, primary LSECs from murine livers were isolated and plated on cover slides. After adhesion, cells were incubated with pre-formed immune complexes containing a mAb coupled to AF647 and an AgFc coupled to AF488 in a 1:4 molar ratio. AgFc excess creates smaller immune complexes and decreases the risk of precipitation by avoiding the point of equivalence (POE) where the complexes are no longer soluble and precipitate [60].

Co-localization of WT- and SELF-AgFc and fitting mAb could be observed with the early endosome marker EEA, which is present on early sorting endosomes [80]. In the control setup with AgFcs that cannot bind the respective mAb, less to no co-localization with EEA was observed (Figure 10B, D and F). When a specific anti-Fc $\gamma$ RIIB blocking antibody was used before adding the immune complexes to the cells, no uptake was detected. The immune complexes containing mAb and AgFc-SELF constructs were taken up more efficiently compared to the complexes containing AgFc-WT (Figure 10A, C and E,  $p$  \*\*\* or  $p$  \*\*). This was true for all three combinations tested: anti-d1\_d2 mAb + d1d2-AgFc, anti-d15 mAb + d15-AgFc and anti-CysR mAb + CysFnII-AgFc.

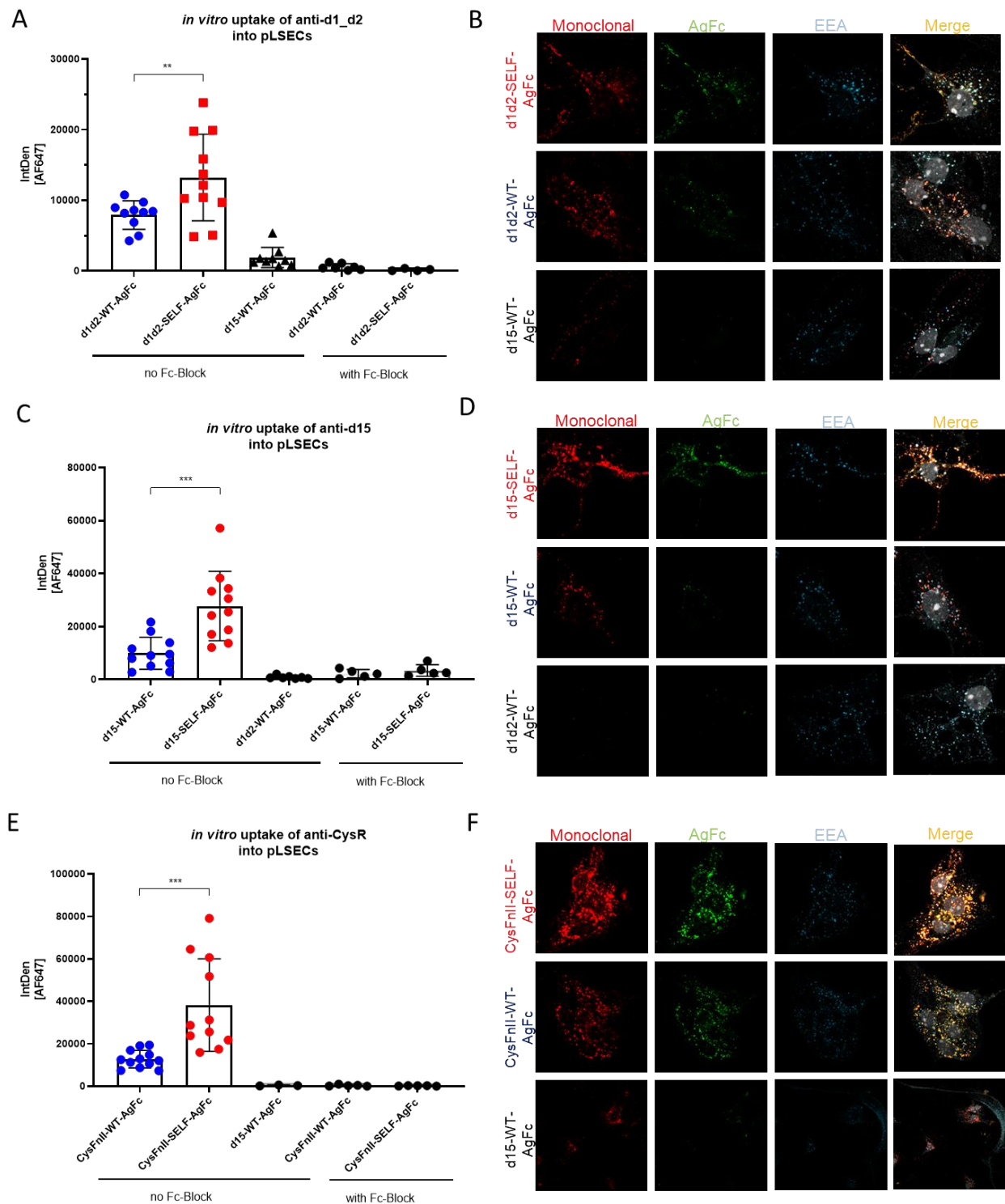


**Figure 10: Immune complex uptake in primary LSECs.** (A) and (B) show the uptake of immune complexes made of anti-d1<sub>d2</sub>-AF647 mAb and d1d2-WT-AgFc-AF488, or d1d2-SELF-AgFc-AF488 or d15-WT-AgFc-AF488 into primary LSECs after a 60 min chase with Fc-block and without. (A) shows the integrated density analysis made with ImageJ, while (B) shows the confocal microscopy images with co-staining of EEA and Hoechst. The blocking antibody inhibits almost all of the binding/uptake of the immune complexes compared to set ups without an Fc-block. Mixtures of anti-d1<sub>d2</sub>-AF647 mAb and d15-WT-AgFc-AF488, which cannot form an immune complex, are only minimally taken up by the cells. Immune complexes with SELF-AgFcs are taken up significantly more than the combination with WT-AgFcs (One-way ANOVA, Tukey's multiple comparison test,  $p^{**}=0.0098$ ). The immune complexes co-localize with the endosome marker EEA more often compared to the set up with anti-d1<sub>d2</sub> mAb together with d15-WT-AgFc. (C) and (D) show the *in vitro* uptake of immune complexes made up of anti-d15-AF647 mAb and d15-WT-AgFc-AF488, or d15-SELF-AgFc-AF488 or d1d2-WT-AgFc-AF488 into primary LSECs after a 60 min chase with Fc-block and without. While a specific Fc $\gamma$ RIIB blocking antibody inhibits the uptake of all

complexes, without it complexes with d15-SELF-AgFc are taken up more efficiently compared to the ones consisting of d15-WT-AgFc (Tukey's multiple comparison test,  $p^{***}<0.001$ ). That can also be observed in the confocal microscopy images with co-staining of EEA and Hoechst. (E) and (F) show the same for complexes made up of anti-CysR-AF647 mAb and CysFnII-WT—AgFc-AF488, or CysFnII-SELF-AgFc-AF488 or d15-WT-AgFc-AF488. Again no uptake could be detected when Fc $\gamma$ RIIB is blocked by a specific commercial antibody, while without it complexes made up of CysFnII-SELF-AgFc is taken up more efficiently than the ones with CysFnII-WT-AgFc (Tukey's multiple comparison test,  $p^{***}<0.001$ ). IF: Monoclonal antibody (red), AgFc (blue), EEA (light blue), merged images (orange).

To sum up, we detected Fc $\gamma$ RIIB-mediated uptake of immune complexes containing WT- and SELF-AgFc and their respective mAb into murine primary LSECs. We could block this uptake with a specific commercial anti-CD16/32 blocking antibody. In combination with AgFc that cannot bind the respective monoclonal, we saw only isolated uptake of monoclonal and AgFc constructs. Immune complexes could be co-localized with the early endosome marker EEA indicating uptake rather than surface binding of the complexes.

### 3.4 *In vivo* blocking of rabbit anti-THSD7A IgG with AgFc

Next, we wanted to test if rabbit anti-THSD7A IgG could be blocked through a specific AgFc *in vivo*. In these proof-of-concept experiments, we only focused on one antigen/AgFc pair (THSD7A and d1d2-AgFc, respectively). Therefore, we used purified rabbit IgG (rbIgG) that was raised in rabbits that were immunized with the complete extracellular domain of THSD7A. Every animal displays different binding profiles and has to be characterized before usage. The IgG mixture used for this experiment recognized domains d1\_d2, d2\_d3, d3\_d4, d5\_d6, d7\_d8, d9\_d10, d15\_d16, and d19\_d20 of THSD7A but not d11\_d12, d13\_d14 or d17\_d18 when tested in a THSD7A domain ELISA as described in 2.2.4. *THSD7A*<sup>-/-</sup> mice were used to circumvent binding of the anti-THSD7A rbIgG inside the kidney. *THSD7A*<sup>-/-</sup> mice were injected with 50  $\mu$ g of rabbit anti-THSD7A IgG i.p., previously incubated with 6.2  $\mu$ g of either d1d2-SELF-AgFc or d1d2-WT-AgFc. The control animal was injected with 50  $\mu$ g rabbit anti-THSD7A IgG without added AgFc. After 24 hours, we sacrificed the animals and analyzed their serum and livers (Figure 11A). In a THSD7A-domain ELISA with the domains d1\_d2, d2\_d3, d3\_d4, d5\_d6, d7\_d8, d9\_d10, d15\_d16, and d19\_d20, we found that animals injected with complexed rbIgG with either d1d2-SELF-AgFc or d1d2-WT-AgFc constructs did not react with the domains d1\_d2 of THSD7A anymore. The mouse that was injected with only rbIgG could clearly still bind d1\_d2. Binding to all other domains of THSD7A was unaffected (Figure 11B). In cryo-sections of the liver, we detected rbIgG inside LSECs shown by white arrowheads in the zoomed in confocal images (1.3x) in the bottom row of Figure 11C. This could not be seen in the mouse injected with rbIgG only (Figure 11C, top row).

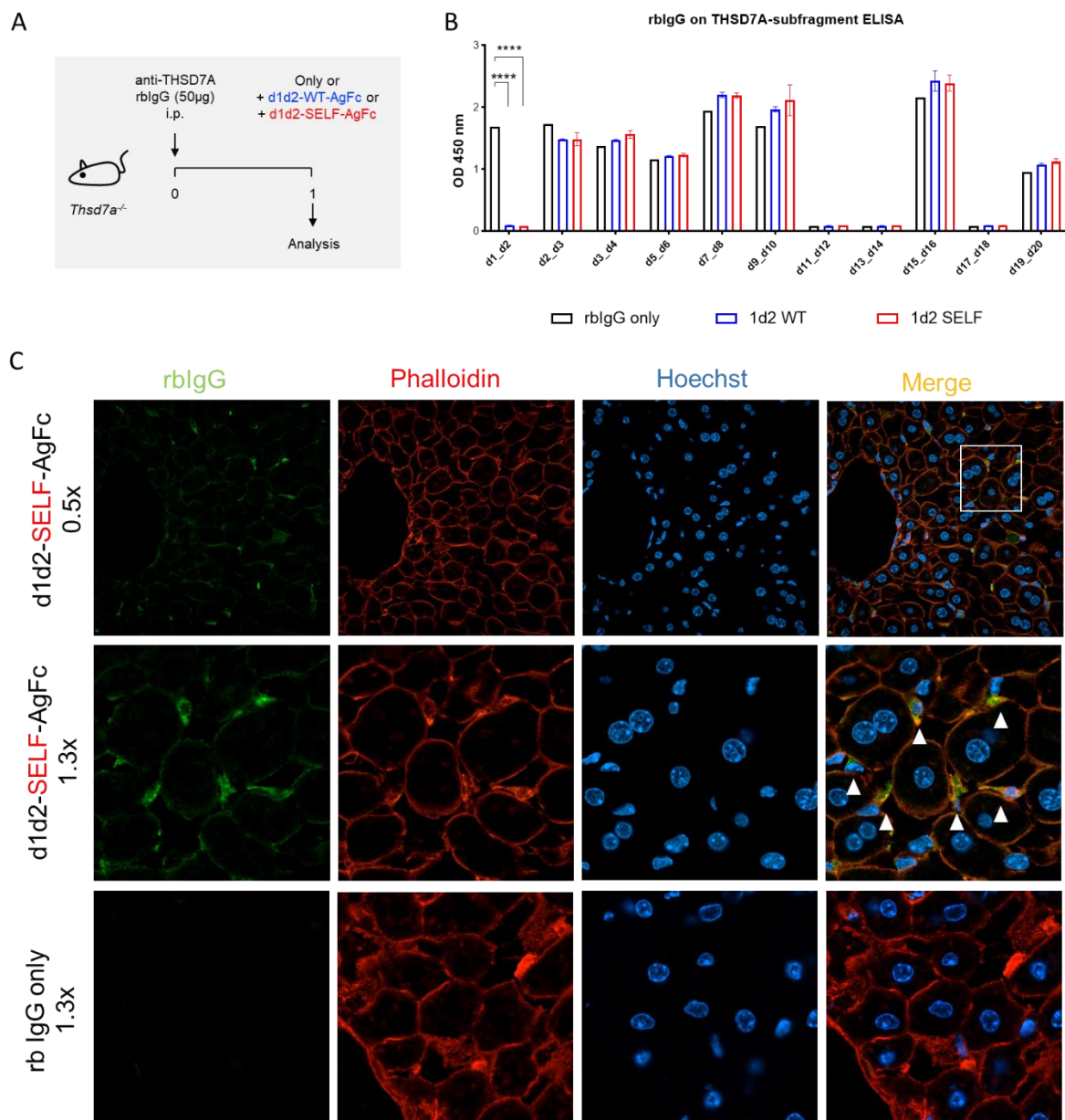


**Figure 11: Blocking of rbgG with d1d2-AgFc in *THSD7A*<sup>-/-</sup> mice.** (A) shows the experimental setup. *THSD7A*<sup>-/-</sup> mice were injected with 50 µg of purified rabbit anti-THSD7A IgG that reacts against multiple domains of THSD7A in combination with d1d2-WT-AgFc or d1d2-SELF-AgFc. The control mouse was injected i.p. with 50 µg of rbgG only. One-day post injection animals were analyzed. (B) Serum samples of all mice were diluted 1:100 and tested for their domain reactivity in ELISA. Binding occurred on domains d1\_d2, d2\_d3, d3\_d4, d5\_d6, d7\_d8, d9\_d10, d15\_d16 and d19\_d20. Animals that were injected with either d1d2-WT-AgFc or d1d2-SELF-AgFc showed no binding to the domains d1\_d2 of THSD7A anymore, while the control mouse that was injected with sole rbgG reacted to these domains. Binding to all other domains remained unaffected (Two-way ANOVA, Tukey's multiple comparison test,  $p^{****} < 0.0001$ ). (C) Frozen liver sections of mice injected with rbgG and d1d2-SELF-AgFc were stained with anti-rbgG-Cy2 to detect rbgG that might be degraded in LSECs. Counterstaining was done with phalloidin (actin) and Hoechst (nuclei). The upper row shows of a liver section (1.3x) of the animal injected with rbgG only. No rbgG staining could be detected here. The middle row shows a liver section of an animal injected with d1d2-SELF-AgFc and rbgG. LSECs that took up rbgG are indicated by white arrowheads in the zoomed in confocal images (1.3x) in the bottom row. LSECs are lean, elongated cells that are found in the space between larger hepatocytes.

In this proof-of-concept experiment, we could specifically block only the rbgG antibodies that bind domains d1 and d2 of THSD7A *in vivo*. All other anti-THSD7A antibodies were unaffected

by our AgFc. The rIgG that was complexed through our AgFc was found inside LSECs in the liver for we could not detect any rIgG in the animal injected with rIgG only.

### **3.5 *In vivo* time course of immune complex degradation**

Next, we wanted to understand how the immune complexes are degraded in LSECs over time. For the uptake experiments *in vivo*, we used d1d2-AgFc constructs and their corresponding anti-d1\_d2 mAb. Results from these experiments were used to determine a time interval between treatments. Therefore, we first injected *in vitro* pre-formed complexes into WT BALB/c animals and observed the uptake into LSECs at 10 min, 60 min, 6 hours, 1 day and 7 days post injection. Later, we injected anti-d1\_d2 mAb and AgFc sequentially (24 h apart) to observe the turnover of *in vivo* formed complexes at 60 min, 3 days, and 7 days after AgFc injection. PLA2R-AgFc were excluded for these proof-of-concept experiments except as irrelevant AgFc controls (Chapter 3.5 to 3.9). For the treatment experiments in 3.13 with transgenic hPLA2R mice, results from this chapter were translated to the PLA2R-AgFc constructs.

#### **3.5.1 Time course of *in vitro* pre-formed immune complexes**

To understand the uptake of pre-formed immune complexes, 10 µg of AF647-coupled anti-d1\_d2 mAb and 10 µg of AF488-coupled d1d2-AgFc (SELF or WT) were incubated for 1 h at RT *in vitro* to form immune complexes. After that, complexes were injected i.v. into WT BALB/c mice. Animals were analysed after 10 min, 60 min, 6 hours, 1 day and 7 days (n=3). Serum was analysed in ELISA to detect unbound anti-d1\_d2 mAb and an *in vivo* imaging system (IVIS) to detect all anti-d1\_d2-AF647 mAb still in circulation. LSECs were extracted from whole livers and stained with the LSEC FACS-panel described above. Kidneys were frozen and cut in 5 µm slices for IF stainings. Counterstaining was done with laminin (basement membrane) and Hoechst (nuclei).

We saw that no anti-d1\_d2 mAb could bind in the ELISA in set ups with d1d2-WT-AgFc or d1d2-SELF-AgFc (Figure 12A). For animals injected with anti-d1\_d2 mAb only, a decreasing signal from 10 min to 7 days could be observed, which indicates the natural turnover of IgG. Through the IVIS all remaining anti-d1\_d2 mAb could be detected and revealed a fast decline in AF647 fluorescence whenever it was injected with d1d2-WT-AgFc or d1d2-SELF-AgFc in the first hour after injection. Sera from animals with anti-d1\_d2 mAb only showed a slower, less rapid decline (Figure 12B). The mean fluorescent intensity (MFI) was used to compare all AF647<sup>+</sup> LSECs and indicates the amount of mAb that has been taken up into these cells. The analysis of the MFI of AF647 showed an increasing amount of fluorescence in FcγRIIB<sup>+</sup> LSECs in early time points (10 min and 60 min), reaching its peak at until 6 hours after injection and decreasing on the later time points (day 1 and 7). For animals injected only with anti-d1\_d2 mAb, the course was slightly different for they reached their peak earlier compared to the immune complex injected mice, at

60 min after injection (Figure 12C). A similar time course could be observed in the amount of double positive cells inside  $Fc\gamma RIIB^+$  LSECs (Figure 12D). In cryo-sections of the kidneys we could not detect any anti-d1\_d2-AF647 mAb signal at any time point when it was injected in complex with d1d2-WT- or d1d2-SELF-AgFcs. In animals that were only injected with anti-d1\_d2 mAb a signal could be found along the GBM, which increased until 1-day post injection and then stagnated (Figure 12E).

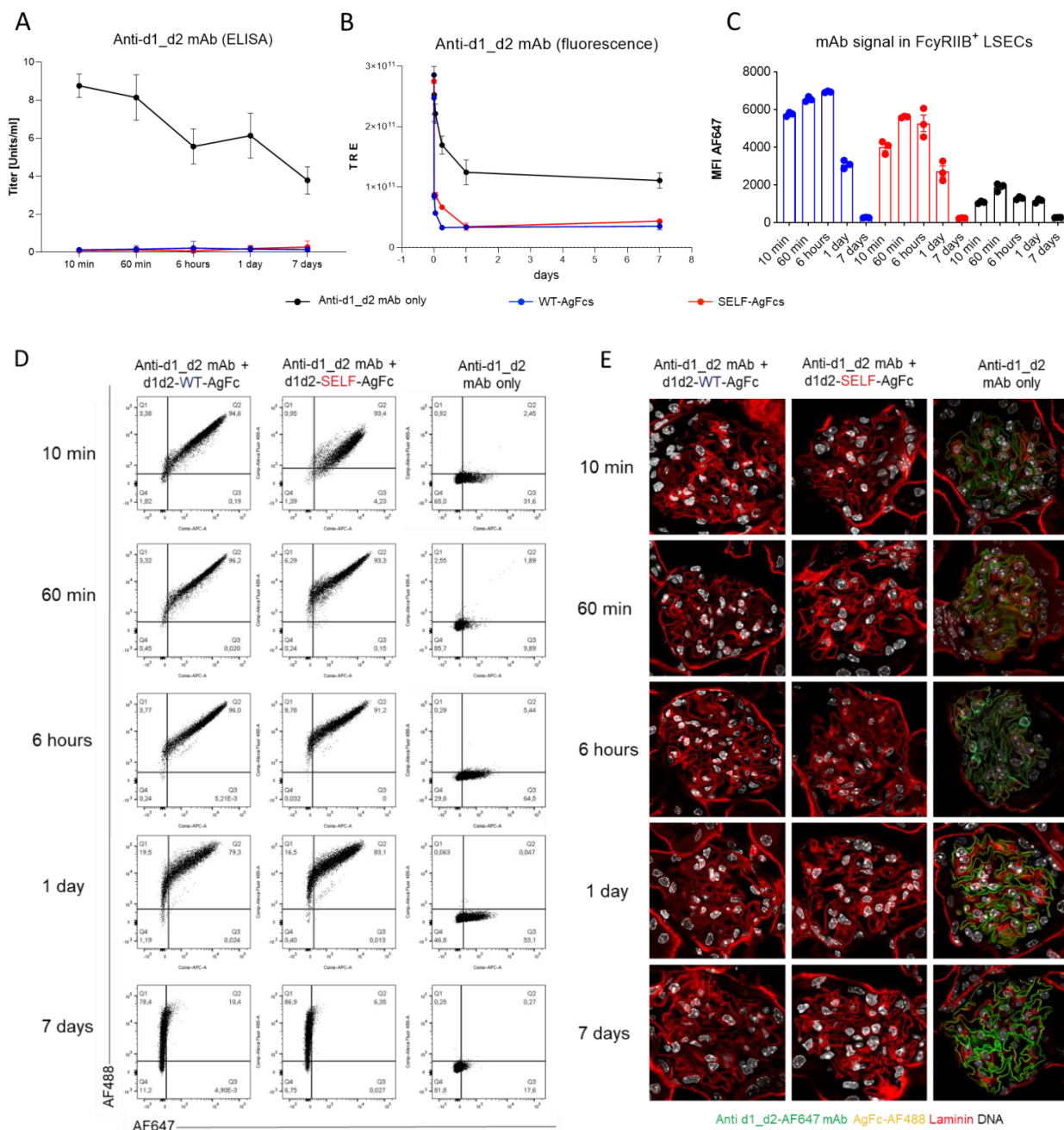


**Figure 12: Time course of *in vitro* formed immune complexes *in vivo*.** (A) The amount of unbound anti-d1\_d2 mAb in ELISA and (B) total amount in IVIS detected by its fluorescence. In ELISA no free mAb was detectable in any of the time points measured. All mAb seems to be bound to its fitting AgFcs. For animals that were injected with anti-d1\_d2 mAb only, a decrease over time can be observed with both ELISA and IVIS. The IVIS shows that in the earlier time points (10 mins to 6 hours) all monoclonal is cleared from the circulation and the amount stays stable between time points day 1 and day 7. (C) Mean fluorescent intensity (MFI) of anti-d1\_d2-AF647 mAb in  $Fc\gamma RIIB^+$  LSECs. (D) Dot plots of  $Fc\gamma RIIB^+$  LSECs. The y-axis shows the AgFcs that are coupled to AF488, while the x-axis

shows the anti-d1\_d2 mAb which is coupled to AF647. Double positive cells took up both antibodies whereas the controls took up only the mAb (anti-d1\_d2). The most antibody can be detected 60 min and 6 hours after i.v. injection, after that the amount in the LSECs decreases until 7 days' post injection when there is hardly any anti-d1d2 monoclonal left to detect. (E) Cryo-sections of the kidneys. Anti-d1\_d2 mAb is coupled to AF647 and can be observed over time. While the amount of monoclonal in animals injected with mAb only (anti-d1\_d2) increases until 1-day post injection and then stagnates, animals injected with the *in vitro* formed complexes show no staining inside the kidneys.

### 3.5.2 Time course of *in vivo* formed immune complexes

To investigate *in vivo* degradation of immune complexes formed *in situ*, WT BALB/c mice were injected with 25  $\mu$ g of AF647-coupled anti-d1\_d2 mAb i.p. and then, 24 hours later, 33  $\mu$ g of AF488-coupled d1d2-AgFc i.v. The LALAPG-backbone was included in these experiments: the L234A/L235A, P329G (LALAPG) mutation abolishes binding to all Fc $\gamma$ Rs and was used to investigate the effect of the mutation in an immune complex and *in vivo*. Immune complexes with LALAPG should be degraded slower because the LALAPG-Fc parts, in contrast to the Fc part of the anti-d1\_d2 mAb, cannot bind the Fc $\gamma$ RIIB of the LSECs. To study the uptake kinetics, we looked at three different time points after injecting the AgFc constructs: an early time point (60 min), an intermediary time point (3 days) and a late time point (7 days). Per time point investigated, three mice were injected (n=3). We tested different combinations of immune complexes: anti-d1\_d2 mAb + d1d2-WT-AgFc, anti-d1\_d2 mAb + d1d2-SELF-AgFc and anti-d1\_d2 mAb + d1d2-LALAPG-AgFc. To analyse the components by themselves, we also included only anti-d1\_d2 mAb and only d1d2-WT-AgFc as controls for uptake and degradation. Since d1d2-WT-AgFc is coupled to AF488, we could not detect it in the d1d2-AgFc only set up with the IVIS. Therefore, it is not included in Figures 13A-C. Unbound anti-d1\_d2 mAb could only be detected in the control group and decreased over time, while the signal was blocked after 60 min in all other samples when tested in a THSD7A-ELISA (Figure 13A). Circulating anti-d1\_d2 antibody, bound or free, could be detected with IVIS analysis of the serum samples. A similar effect could be observed here: the signal of the anti-d1\_d2 antibody slowly decreased over time, while in complex with AgFc it disappeared quickly from circulation - regardless of the type of AgFc it was mixed with. Only with LALAPG-AgFc the degradation was slowed compared to WT or SELF-AgFcs (Figure 13B). When we looked at the MFI of anti-d1\_d2-AF647 mAb inside Fc $\gamma$ RIIB<sup>+</sup> LSECs, we found the strongest signals after 60 min and it decreasing over time (Figure 13C). Some turnover inside these cells could be detected in samples where only anti-d1\_d2 mAb was injected. The dot plots in Figure 13D show AF647<sup>+</sup>AF488<sup>+</sup> double positive Fc $\gamma$ RIIB<sup>+</sup> LSECs in all setups except for the controls with only anti-d1\_d2 mAb or only d1d2-AgFc. Here, as expected, we could observe only AF488<sup>+</sup> cells in the d1d2-AgFc injected mice and only AF647<sup>+</sup> cells in mice injected with only anti-d1\_d2 mAb. Immune complexes with anti-d1\_d2 mAb and d1d2-LALAPG-AgFc showed less AF647<sup>+</sup>AF488<sup>+</sup> positive cells compared to set ups with d1d2-

WT or d1d2-SELF-AgFc. In cryo-sections of the kidneys, we saw strong signals of AF647-coupled anti-d1\_d2 mAb in all samples after 60 min (Figure 13E). Over time there was a decrease in signal in samples in combination with AgFc constructs, while the control group (anti-d1\_d2 mAb alone) showed an increase in signal. The anti-d1\_d2 mAb signal decreased slower in the set up with d1d2-LALAPG-AgFc compared to the set ups with WT-AgFc or SELF-AgFc (3 days; Figure 13E). Although after 7 days all set ups with AgFc looked the same. The set up with only d1d2-AgFc-WT showed no signal inside the kidney. Of note, we could observe less AF647<sup>+</sup>AF488<sup>+</sup> positive cells in the set up with LALAPG-AgFc inside the liver (Figure 13D) but still the AF647 signal in the kidneys decreased overtime (Figure 13E) which indicates immune complex removal even though LALAPG abolished FcγRIIB binding.

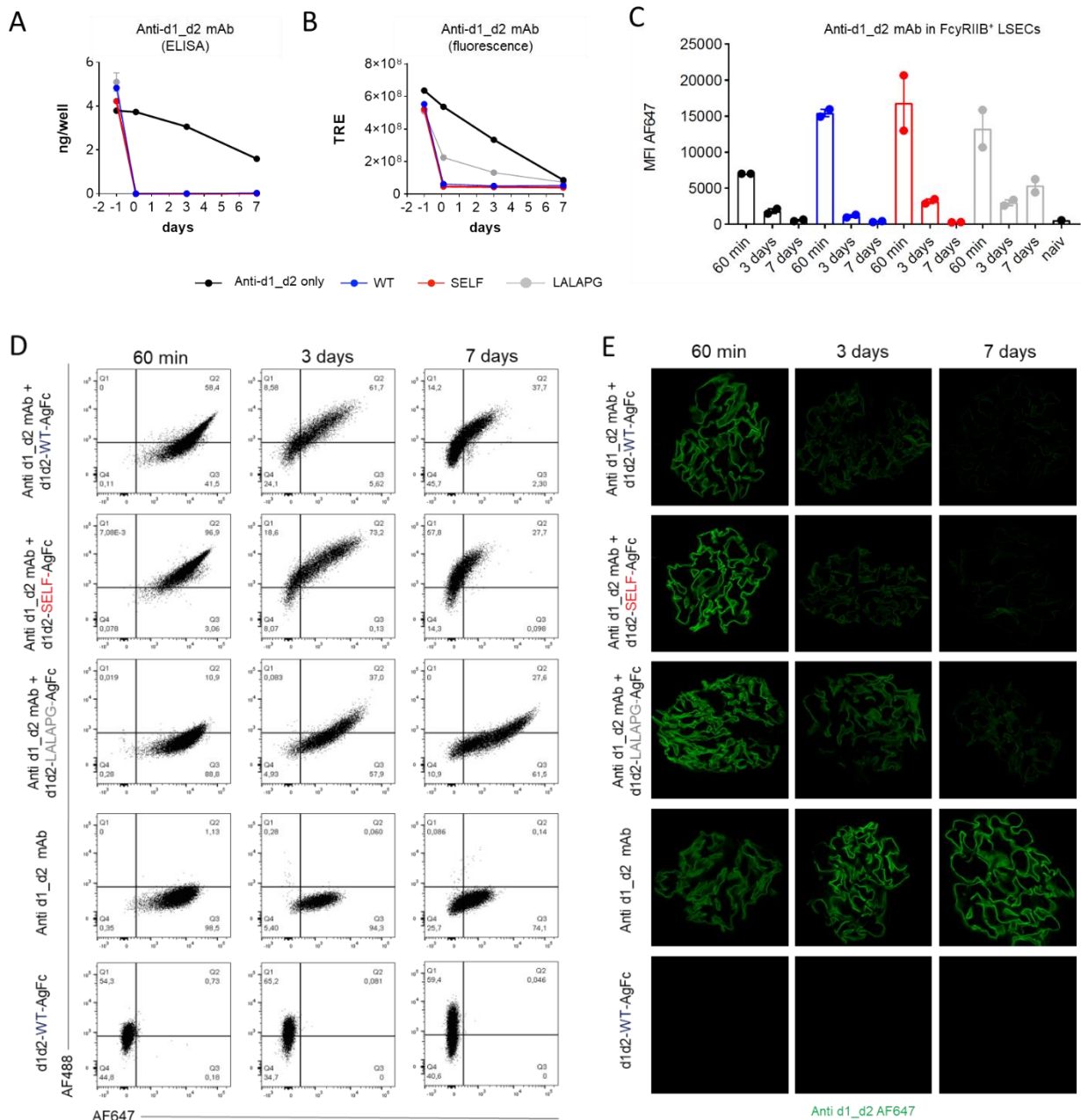


**Figure 13: Time course of *in vivo* degradation.** (A) The amount of unbound anti-d1\_d2 mAb in ELISA and (B) total amount in IVIS. The mAb is not only bound by the AgFcs 10 min after injection but also gone from circulation. The ELISA can only detect unbound anti-d1\_d2 mAb while the IVIS detects the fluorescence of total amount of mAb still remaining in circulation. The normal turnover of the anti-d1\_d2 mAb (Control) could be observed over time. (C) MFI analysis of anti-d1\_d2-AF647 mAb in Fc $\gamma$ RIIB<sup>+</sup> LSECs over the time course of 7 days. The highest MFI could be detected after 60 min, while 3 days and 7 days only show MFIs below 5000. (D) Dot plots of Fc $\gamma$ RIIB<sup>+</sup> LSECs. The y-axis shows the AgFcs that are coupled to AF488, while the x-axis shows the anti-d1\_d2 mAb which is coupled to AF647. Double positive cells took up both antibodies whereas the controls took up only either mAb (anti-d1\_d2) or AgFc (d1d2-WT). (E) Cryo-sections of the kidneys. Anti-d1\_d2 mAb is coupled to AF647 and can be observed over time. While the amount of mAb in animals injected with mAb only (anti-d1\_d2) does not decrease over time, animals injected with AgFcs (not depending on the IgG backbone) decrease over the time course of 7 days. The animals that were injected with d1d2-AgFc only showed no staining whatsoever.

With these results we concluded, that the uptake into LSECs is very rapid: 10 min after AgFc injection complexes can be found inside Fc $\gamma$ RIIB<sup>+</sup> LSECs. If no additional amount of immune complexes is added to the system, it takes the LSECs roughly 6 hours to degrade most of the

injected immune complexes. We saw that the backbone (WT or SELF) does not affect the uptake into LSECs, at least not at the time points that we investigated. We also discovered that complexes with LALAPG backbone are still degraded but prolong the progress compared to the other backbones. Lastly, already bound anti-d1\_d2 mAb was removed from the glomerulus over time through clearance by the AgFc constructs.

### 3.6 *In vivo* distribution of immune complexes 6 hours post injection

To assess the distribution of *in vivo* formed complexes throughout multiple organs, we injected WT BALB/c mice (n=3) with AF647-coupled anti-d1\_d2 mAb i.p. followed by i.v. injection of AF488-coupled d1d2-AgFc (WT or SELF) 24 hours later. As a control set up, we injected an irrelevant AgFc i.v. (d15-SELF-AgFc; Control). Naïve mice were used as a baseline for fluorescent signal in the IVIS. 6 hours post i.v. injection, we analysed the organs of the respective animals as well as blood samples and kidney sections (Figure 14A). The organs (heart, lungs, kidneys, testes, spleen and liver) were weighed and analysed with IVIS to see the distribution of AF647-coupled anti-d1\_d2 mAb in these organs (Figure 14B). The highest total radiant efficiency (TRE) was found in the liver whereas animals that were injected with anti-d1\_d2 mAb in combination with d1d2-WT-AgFc or d1d2-SELF-AgFc showed significantly higher fluorescence compared to animals injected with anti-d1\_d2 mAb in combination with the irrelevant AgFc d15-SELF. No fluorescence was detectable inside the heart and spleen. Coinciding with the expression of THSD7A, we found fluorescence to be detectable in lungs, kidneys and testes. More fluorescence could be detected in animals that were injected with anti-d1\_d2 mAb in combination with d15-SELF-AgFc (Control), while animals that were injected with either d1d2-WT-AgFc or d1d2-SELF-AgFc showed significantly lower fluorescence in these organs ( $p^*$ ,  $p^{**}$  and  $p^{***}$ ). Binding inside the testis was not influenced by different AgFc (Figure 14B). In serum samples we found no unbound anti-d1\_d2-AF647 mAb except for in the control group in the ELISA set up ( $p^{****}$ ; Figure 14C). When detecting AF647-coupled antibody with the IVIS, we saw some residual AF647 fluorescence inside the serum of d1d2-WT- and d1d2-SELF-AgFc injected mice, while control mice had a strong signal ( $p^{****}$ ; Figure 14D). When analysing the mean fluorescent intensity (MFI) of Fc $\gamma$ RIIB<sup>+</sup> LSECs in flow cytometry (Figure 14E), we found significantly more AF647 signal in complex groups (d1d2-WT-AgFc and d1d2-SELF-AgFc) compared to the animals with anti-d1\_d2 mAb in combination with d15 SELF-AgFc ( $p^{***}$ ). That correlated to small amounts of double positive cells in the samples of the control group (anti-d1\_d2 mAb + d15-AgFc) and significantly more double positive cells in the groups of d1d2-WT-AgFc and d1d2-SELF-AgFc in LSECs (Figure 14F). The difference between d1d2-WT-AgFc and d1d2-SELF-AgFc was not significant at the investigated time point. Since we injected the mAb and

AgFcS consecutively, we found strong binding of AF647-coupled anti-d1\_d2 mAb in all setups co-localizing with laminin except for the naïve control animal in cryo-sections of the kidneys (Figure 14G).

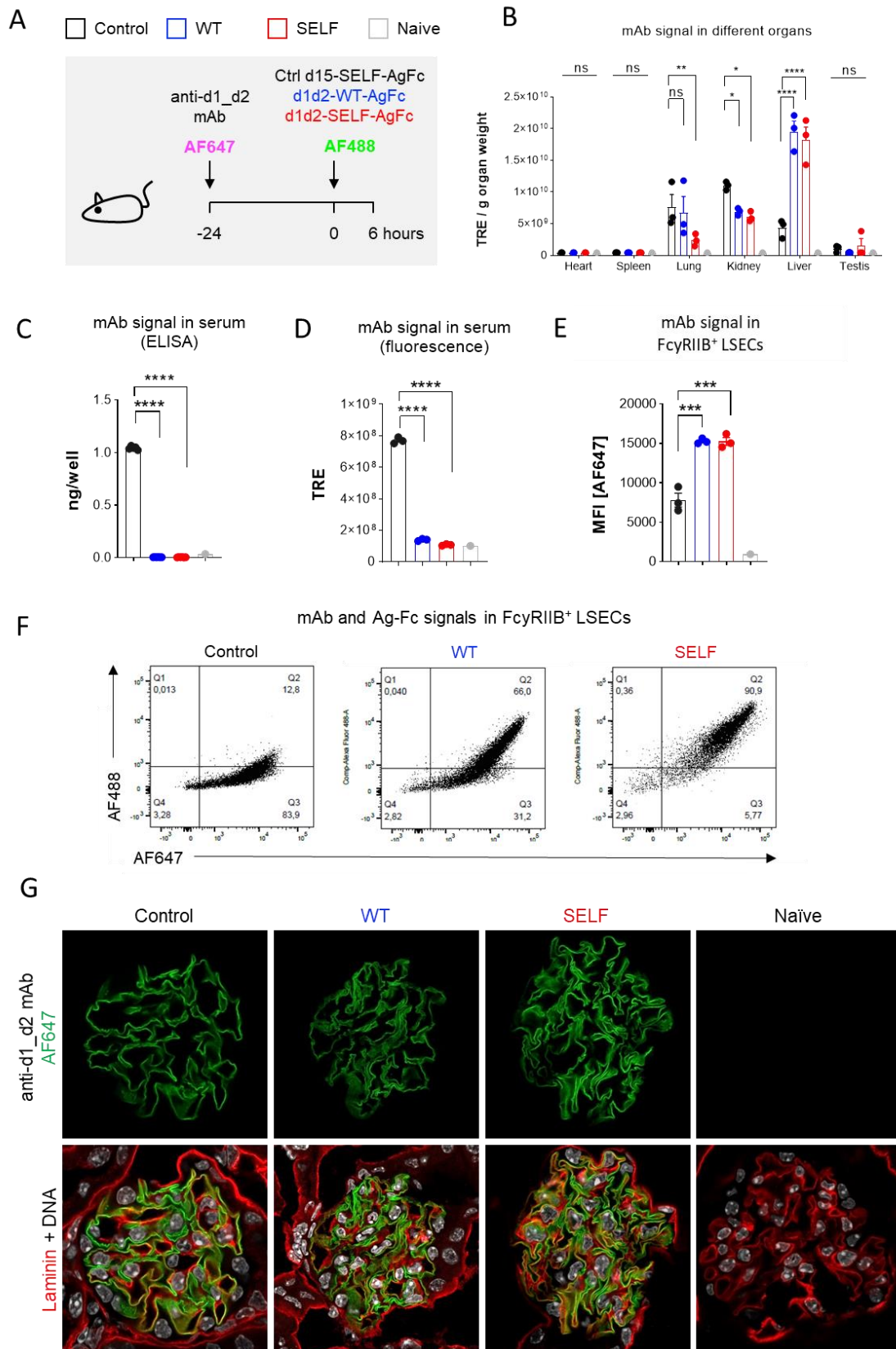


Figure 14: *In vivo* uptake in WT BALB/c mice. (A) shows the experimental set up. Mice were injected with 25  $\mu$ g

of anti-d1\_d2-AF647 mAb i.p. and 24 h later with either 33 µg d1d2-WT-AgFc-AF488 (blue), d1d2-SELF-AgFc-AF488 (red) or d15-SELF-AgFc-AF488 (Ctrl, black) i.v. The naïve animal is shown in grey. 6 h after i.v. injection the animals were analyzed. (B) The organs were extracted, weighed and analyzed in IVIS for their total radiant efficiency (TRE). Lungs, kidneys, testes, heart, spleen and liver were analyzed. Whenever THSD7A is expressed, fluorescence can be detected (lungs, testes, kidneys and lungs). In the kidneys and lungs intensities differ between the set ups: whenever anti-d1\_d2 mAb and d1d2-WT- or d1d2-SELF-AgFc are combined, significantly lower amounts of fluorescence can be detected compared to animals that were injected with anti-d1\_d2 mAb and d15-SELF-AgFc (p\*, p\*\* and p\*\*\*\*). No difference could be detected between the set ups in the testis. In the liver where THSD7A is not expressed, some turnover of the fluorescent antibody can be observed but in combination with d1d2-WT- or d1d2-SELF-AgFc significantly higher amounts of the anti-d1\_d2 mAb can be found (p\*\*\*\*). After 6 hours no anti-d1\_d2 mAb can be detected in the serum in ELISA (C) or IVIS (D), only in animals injected with the d15-SELF-AgFc which cannot form an immune complex with the mAb (black bar) (p\*\*\*\*). (E) MFI analysis of FcγRIIB<sup>+</sup> LSECs in the liver and representative corresponding dot plots in (F). While some turnover can be observed in anti-d1\_d2 mAb + d15-SELF-AgFc set ups (12% double positive cells), significantly more double positive cells can be detected in combination with WT-AgFc or SELF-AgFc (66 % and 90%, respectively; p\*\*\*). (G) Cryo-sections of the kidneys. All animals show co-localization of the anti-d1\_d2-AF647 mAb (green) in combination with the basement membrane marker laminin (red). Hoechst (white) was used to stain the nuclei. The naïve control animal showed no AF647 inside the glomerulus. Statistics: Tukey's multiple comparison, p\* < 0.05, p\*\* < 0.01, p\*\*\* < 0.001, p\*\*\*\* < 0.0001.

In summary, we saw the highest uptake into the liver, coinciding with FcγRIIB expression. Organs that expressed THSD7A were also stained depending on which AgFc was injected in combination with the anti-d1\_d2 mAb. In combination with d15-SELF-AgFc, which cannot form an immune complex with anti-d1\_d2 mAb, we saw the highest signal in lungs, kidneys, and testes. After 6 hours, all anti-d1\_d2 mAb is bound by AgFc (ELISA) or bound inside other cells but not yet degraded through the LSECs. AgFc increase the degradation inside LSECs but we could detect no significant difference between WT- or SELF-AgFc constructs. Due to the sequential injection of mAb and AgFc we detected mAb binding in all investigated kidneys except for the naïve controls.

### 3.7 The FcRn's involvement in the rescue of immune complexes

The long half-life of serum proteins like albumin and IgG is due to the FcRn. It shuffles both proteins across polarized barriers and rescues them from degradation through lysosomes. Inside the kidney it is expressed in the tubules to rescue escaped proteins from excretion and in podocytes where it prevents the accumulation of IgG at the filtration barrier. To understand the relationship between uptake into LSECs for degradation and rescue of immune complexes through the FcRn, we compared the degradation of *in vivo* formed immune complexes in WT C57BL/6 and *FcRn*<sup>-/-</sup> mice. Therefore, we i.p. injected both mouse strains with 25 µg of anti-d1\_d2 mAb coupled to AF647. 24 hours later, we i.v. injected either 33 µg of d1d2-SELF-AgFc-AF488 or the irrelevant d15-SELF-AgFc coupled to AF488. Anti-d1\_d2 mAb in combination with an irrelevant AgFc (d15-SELF-AgFc) to study the interference another antibody might have on the degradation. Control animals only received 25 µg anti-d1\_d2 mAb coupled to AF647 to assess basic IgG turnover. Three animals were injected per group and time point (n=3). Animals were analyzed 1 h

after i.v. injection for an early time point and 3 days after i.v. injection for a later time point.

Serum samples were analyzed in an anti-THSD7A titer ELISA for unbound circulating mAb, while we detected all remaining mAb, in complex or unbound, through the IVIS (Figure 15A-C). *FcRn*<sup>-/-</sup> mice injected with anti-d1\_d2-AF647 mAb + d1d2-SELF-AgFc-AF488 showed significantly lower serum titers after 3 days compared with WT animals even though this difference could not be seen in the IVIS (Figure 15A). *FcRn*<sup>-/-</sup> mice injected with anti-d1\_d2-AF647 mAb + d15-SELF-AgFc-AF488 showed significantly lower unbound and total mAb after 3 days compared to the WT animals (Figure 15B). The same was true for *FcRn*<sup>-/-</sup> mice injected with anti-d1\_d2 mAb only after 3 days (Figure 15C). All *FcRn*<sup>-/-</sup> mice showed  $3 \times 10^7$  TRE 3 days after injection, no matter the construct (Figure 15A-C). This was not true for WT C57BL/6 mice: they showed higher TREs on day 3 post injection when injected with anti-d1\_d2-AF647 mAb + d15-SELF-AgFc-AF488 and anti-d1\_d2-AF647 mAb only. Only when injected with anti-d1\_d2-AF647 mAb + d1d2-SELF-AgFc-AF488 was the difference between residual anti-d1\_d2 mAb in the two mouse strains non-significant (Figure 15A). The analysis of anti-THSD7A serum titers to detect unbound anti-d1\_d2 mAb reflected the IVIS results (Figure 15A-C).

Total radiant efficiency per organ weight (TRE/g) accounts for the difference in organ weight that occur between mice (Figure 15D). The TRE/g in the livers of tested animals was low in both time points in WT animals that were injected with anti-d1\_d2-AF647 mAb only or with anti-d1\_d2-AF647 mAb + d15-SELF-AgFc-AF488, which indicated no significant uptake into LSECs. For animals that were injected with anti-d1\_d2-AF647 mAb + d1d2-SELF-AgFc-AF488 however, after 1-hour post i.v. injection a significantly higher amount of TRE/g could be detected in the liver (p\*\*\*\*) indicating immune complex uptake in FcγRIIB<sup>+</sup> LSECs. In *FcRn*<sup>-/-</sup> mice no difference could be found between the two time points in animals injected with anti-d1\_d2-AF647 mAb only. While significantly higher amounts of anti-d1\_d2 mAb were found in *FcRn*<sup>-/-</sup> mice injected with d1d2-SELF-AgFc or d15-SELF-AgFc after 1-hour post i.v. injection (p\*\*\*\* and p\*\*, respectively). The combination with d1d2-SELF-AgFc indicates normal activity in LSECs whenever immune complexes were formed in both WT and *FcRn*<sup>-/-</sup> animals. The higher signal in *FcRn*<sup>-/-</sup> mice injected with anti-d1\_d2-AF647 mAb + d15-SELF-AgFc-AF488 could indicate unspecific binding between the anti-d1\_d2 mAb and the irrelevant AgFc (Figure 15D). The analysis of the dot plots of FcγRIIB<sup>+</sup> LSECs revealed immune complex uptake: the double positive cells (AF647<sup>+</sup>AF488<sup>+</sup>) in animals that were injected with anti-d1\_d2-AF647 mAb + d15-SELF-AgFc-AF488 could be clearly distinguished from the double positive cells found in animals injected with anti-d1\_d2-AF647 mAb + d1d2-SELF-AgFc-AF488 (Figure 15E, WT C57BL/6 mice, 60 min). Here, the population was quite narrow although the percentage of positive cells

was similar (94% to 88%, respectively). Apart from that, the dot plots of *FcRn*<sup>-/-</sup> and WT animals did not differ significantly, indicating normal immune complex uptake through the LSECs (Figure 15E).

Through analysis of the AF647 signal inside the glomeruli representing bound mAb on THSD7A (Figure 15F), we found a significant increase in WT animals injected with anti-d1\_d2-AF647 mAb only (black bar; p\*\*\*\*) from 60 min to 3 days, while WT animals injected with anti-d1\_d2-AF647 mAb + d1d2-SELF-AgFc-AF488 showed a significant decrease of anti-d1\_d2-AF647 mAb in that time (red bar; p\*\*\*). The difference between the two time points in WT animals injected with anti-d1\_d2-AF647 mAb + d15-SELF-AgFc-AF488 was not significant (grey bar). For *FcRn*<sup>-/-</sup> mice injected with anti-d1\_d2-AF647 mAb only we saw a slight decrease in signal over time (blank black bar), while the signal in *FcRn*<sup>-/-</sup> mice injected with anti-d1\_d2-AF647 mAb + d1d2-SELF-AgFc- or d15-SELF-AgFc-AF488 showed a significant decrease until day 3 (blank red and grey bars; p\*\*\*\* and p\*\*, respectively). However, the lowest amounts of AF647 signal could be found after 3 days in both WT and *FcRn*<sup>-/-</sup> animals that were injected with anti-d1\_d2-AF647 mAb + d1d2-SELF-AgFc-AF488 (red bar and blank red bar; Figure 15F). Figure 15G shows representative cryo-sections of the kidneys for each time point. Only the AF647 fluorescence is shown for better comparability between the groups.

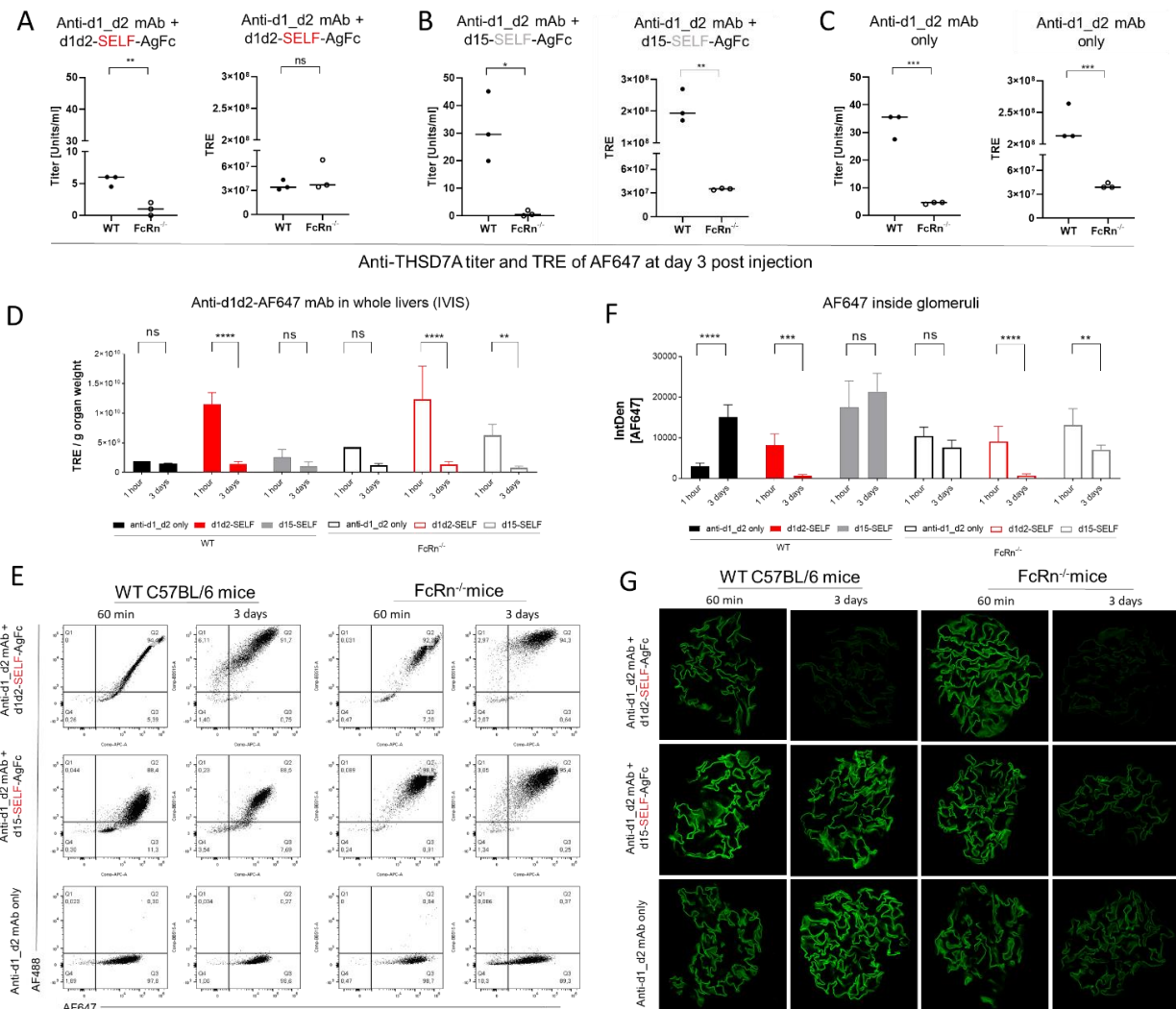


**Figure 15: Immune complex uptake in *FcRn*<sup>-/-</sup> mice.** (A) ELISA (left) and IVIS (right) analysis of serum samples at day 3. WT and *FcRn*<sup>-/-</sup> mice were injected with anti-d1\_d2 mAb + d1d2-SELF. While there was a significant difference to be found in the anti-THSD7A titer between WT and *FcRn*<sup>-/-</sup> animals (p\*\*), the same could not be found in the IVIS analysis of the same samples. This might suggest more unbound anti-d1\_d2 mAb in WT animals or faster degradation inside *FcRn*<sup>-/-</sup> animals. (B) ELISA (left) and IVIS (right) analysis of serum samples at day 3. WT and *FcRn*<sup>-/-</sup> mice were injected with anti-d1\_d2 mAb + d15-SELF-AgFc. Both approaches revealed significantly lower amounts of unbound and total anti-d1\_d2 mAb in *FcRn*<sup>-/-</sup> animals (p\* and p\*\*), which indicates a faster degradation of the mAb in *FcRn*<sup>-/-</sup> animals. The same could be observed in (C), where WT and *FcRn*<sup>-/-</sup> mice were injected with anti-d1\_d2 mAb only (p\*\*\*). ELISA data can be found on the left, IVIS on the right of serum samples at day 3 (Unpaired t-tests, p\* > 0.01, p\*\* > 0.001, p\*\*\* > 0.0001). (D) Total radiant efficiency per g organ weight (TRE/g) in the livers of tested animals showed no significant difference over time in WT animals injected with anti-d1\_d2 mAb only and anti-d1\_d2 mAb + d15-SELF-AgFc. The same was true for *FcRn*<sup>-/-</sup> mice injected with anti-d1\_d2 mAb only. No matter the genetic background, a significant decrease in signal could be found in animals injected with anti-d1\_d2 mAb + d1d2-SELF-AgFc (p\*\*\*\*). For *FcRn*<sup>-/-</sup> mice injected with anti-d1\_d2 mAb + d15-SELF-AgFc, we saw a decrease in signal (p\*\*), even though the amount in livers found at 60 min was not as high compared to animals injected with fitting mAb-AgFc pairs (Two-way ANOVA, Tukey's multiple comparison test, p\*\*\* > 0.001, p\*\*\*\* < 0.0001). (E) Dot plots of double positive FcγRIIB<sup>+</sup> LSECs. The x-axis shows AF647 fluorescence (mAb), while the y-axis shows AF488 signal (AgFc). In animals injected with anti-d1\_d2 mAb only we found only AF647 positive cells no matter the genetic background. (F) ImageJ analysis of integrated density of AF647 signal inside glomeruli. Significant decreases could be observed in WT animals injected with anti-d1\_d2 mAb + d1d2-SELF-AgFc, *FcRn*<sup>-/-</sup> animals with anti-d1\_d2 mAb + d1d2-SELF-AgFc and anti-d1\_d2 mAb + d15-SELF-AgFc (p\*\*, p\*\*\* and p\*\*\*\*). An increase could be found in WT animals injected with anti-d1\_d2 mAb only (p\*\*\*\*), while *FcRn*<sup>-/-</sup> showed no change here (ns). Also, no difference between the time points could be found in WT animals injected with anti-d1\_d2 mAb + d15-SELF-AgFc (Two-way ANOVA, Tukey's multiple comparison test, p\*\* > 0.001, p\*\*\* < 0.001, p\*\*\*\* < 0.0001) (G) Cryo-sections of kidneys. For a better view only the AF647 signal (green) is shown. It decreases in animals injected with anti-d1\_d2 mAb + d1d2-SELF-AgFc over time in both genetic backgrounds, while all *FcRn*<sup>-/-</sup> mice show less signal at day 3. In WT mice this could not be observed, here the signal is stable over time.

Taken together these results suggests an important role for FcRn in the kinetics of immune complex uptake and recycling. While the uptake through LSECs is not influenced, without the FcRn IgG is degraded faster so serum levels deplete quickly over time. This degradation is not dependent on immune complex formation but also occurs to IgG monomers in circulation. That influences the half-life of the AgFcs in the circulation since they are not rescued and recycled back to the cell surface through the FcRn which might ameliorate their function when used as therapeutics.

### 3.8 Clearance of large amounts of polyclonal immune complexes

To investigate if our AgFcs cause immune complex deposition in concurrence with high polyclonal antibody serum titers, we either immunized *THSD7A*<sup>-/-</sup> mice with 20 µg of d1\_d2 of THSD7A or with the vehicle PBS. The first immunization was done in complete Freund's adjuvant (CFA), followed by two booster shots in incomplete Freund's adjuvants (IFA). After 7 weeks blood was taken (time point 0) and mice immunized with d1\_d2 of THSD7A were injected i.v. with 300 µg d1d2-SELF-AgFc coupled to AF647 (or CysFnII-SELF-AgFc-AF647 in the control setup), while the PBS-immunized mice were injected with 300 µg d1d2-SELF-AgFc coupled to AF647. 24 hours post injection mice were sacrificed and analyzed (Figure 16A). Mice that were immunized with d1\_d2 of THSD7A and injected with the control AgFc (CysFnII-SELF) had a similar titer at time point 24 h as at time point 0, before AgFc injection (Figure 16B; black). Mice that were immunized with d1\_d2 of THSD7A and injected with d1d2-SELF-AgFc showed a significant decrease in the titer after 24 h (p\*\*\*\*; red). Mice that were immunized with the vehicle (PBS) showed no titer on either time point (red dots). The serum of all mice was analyzed in IVIS to detect all AF647-coupled AgFc (Figure 16C). Mice immunized with d1\_d2 of THSD7A but injected with the control AgFc (CysFnII-SELF) had a strong signal of AF647 inside the serum samples after injection (p\*; black), while the mice injected with d1d2-SELF showed close to none after 24 hours (non-significant; red). Mice immunized with PBS and injected with d1d2-SELF-AgFc showed AF647 signal after injection (time point 24 h) (p\*). The increase from 0 to 24 h was significant in mice immunized with d1\_d2 of THSD7A and injected with the control AgFc, which cannot form immune complexes, and in mice immunized with PBS and injected with d1d2-SELF, where no autoantibodies can be bound by the AgFc (Figure 16C; p\*). All FcγRIIB<sup>+</sup> LSECs took up AF647 (Figure 16D). When we analyzed the MFI of FcγRIIB<sup>+</sup> LSECs, the setups with control and d1d2-AgFc inside d1\_d2 THSD7A-immunized mice was very similar, while the signal inside PBS-immunized mice was significantly lower (Figure 16E; p\*). Indicating better uptake when immune complexes can form. The high signal in d1\_d2 THSD7A-immunized mice injected with

CysFnII-SELF-AgFc, which should not be able to bind the autoantibodies produced by the mice, can be explained by the higher degree of labelling of CysFnII-SELF-AgFc compared to d1d2-SELF-AgFc (60 moles dye/mole IgG versus 4 moles dye/mole IgG, respectively). When we analyzed cryo-sections of the kidneys from THSD7A<sup>-/-</sup> mice, we found no mIgG deposition along the GBM in any of the setups (Figure 16F). A WT BALB/c mouse from the EAMN model was used as a positive control for mIgG binding at the GBM.

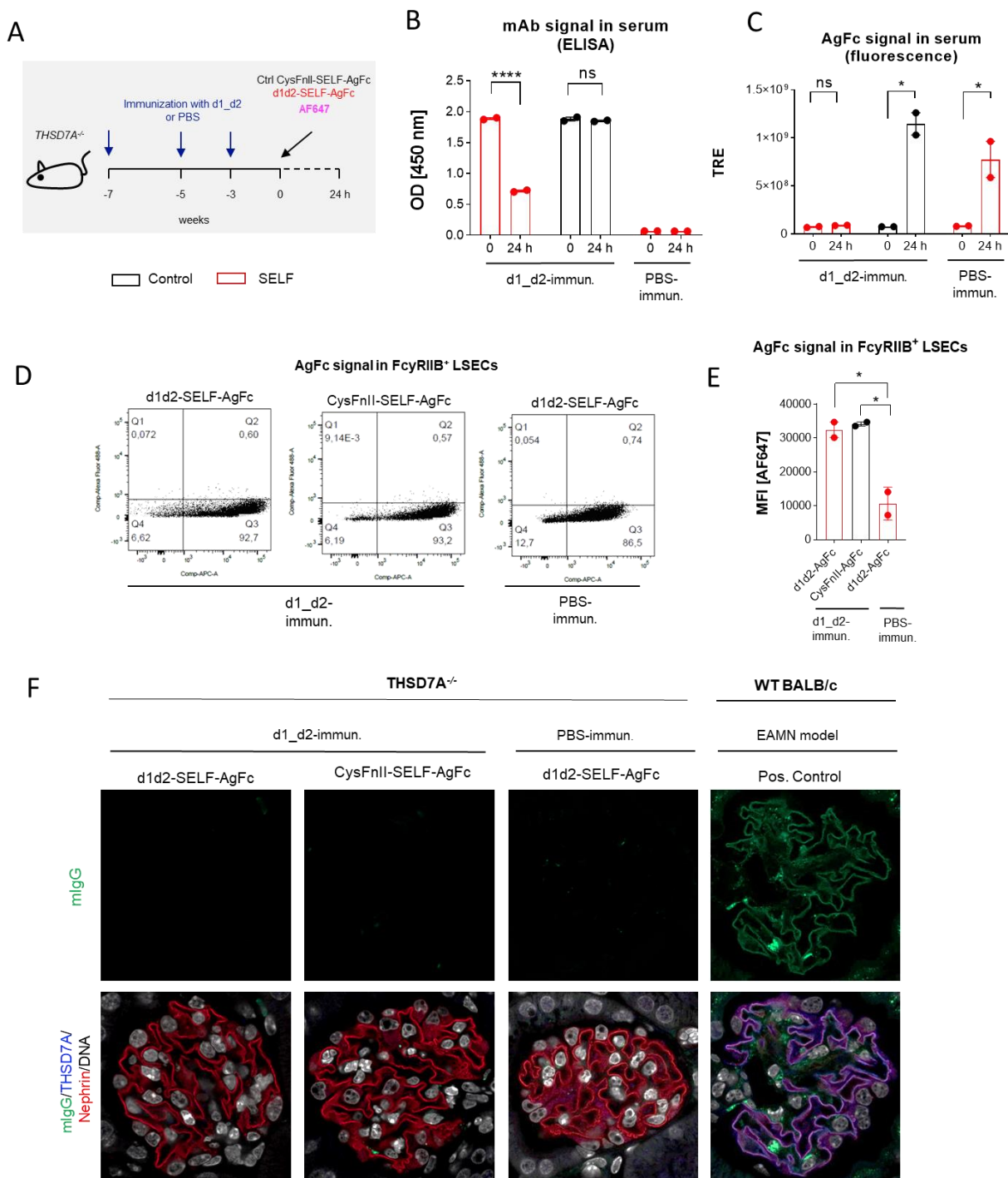


**Figure 16: In vivo clearance of immune complexes.** (A) Experimental setup. THSD7A<sup>-/-</sup> mice were immunized with d1\_d2 domains of THSD7A over several weeks. After two booster injections, mice were injected with AF647-coupled AgFcs. Forming of immune complexes was possible in combination with d1d2-SELF-AgFc, while no immune

complexes should be able to form in combination with the control construct CysFnII-SELF-AgFc. 24 hours post injection the mice were sacrificed and analyzed. Serum contents were analyzed by ELISA (B) and IVIS (C). In ELISA the unbound polyclonal antibodies against d1\_d2 of THSD7A are detected. While the serum titer did not change in combination with ctrl constructs after 24 hours, the titer could be decreased with the fitting AgFc d1d2-SELF. No binding was detected in the PBS-immunized Ctrl mice. With IVIS all coupled AgFc constructs that remain inside the serum after 24 h can be detected. Prior to injection (timepoint 0) no d1d2-AgFc-AF647 could be detected. The ctrl construct in d1\_d2 THSD7A-immunized mice and d1d2-AgFc in PBS-immunized mice could be detected. (D) AgFc-AF647 signal inside FcγRIIB<sup>+</sup> LSECs. All set ups show AF647 signal but more positive cells could be observed in d1\_d2 THSD7A-immunized mice injected with d1d2-SELF-AgFc or CysFnII-SELF-AgFc. (E) Analysis of the MFI (AF647) inside FcγRIIB<sup>+</sup> LSECs. The MFI in d1\_d2 THSD7A-immunized mice injected with d1d2-SELF-AgFc or CysFnII-SELF-AgFc is very similar, while PBS-immunized mice injected with d1d2-SELF-AgFc showed less MFI (One-way ANOVA, Sidak's multiple comparison, p\*). (D) IF of glomeruli. Neither mIgG (green) nor THSD7A were stained in the *THSD7A*<sup>-/-</sup> animals. Nephryn (red) and Hoechst (white) were used as counterstains. A THSD7A-immunized WT BALB/c mouse from the EAMN model was used as a positive control for mIgG and THSD7A staining. Statistics in B and C: Two-way ANOVA, Sidak's multiple comparison test, p\*>0.05, p\*\*\*\*>0.0001.

These results demonstrate that even with high amounts of antibodies and large doses of AgFcs no immune complex deposition could be found inside the kidneys. Also, the AgFcs were able to decrease a high titer by more than half but could not decrease it completely. We suspect that higher amounts of AgFcs are needed for *THSD7A*<sup>-/-</sup> mice to decrease the titer to 0 since they develop extremely high titers compared to WT BALB/c when immunized with the same domains of THSD7A. Therefore, we had to determine a therapeutic dose through other means.

### 3.9 *In vivo* safety assessment of AgFcs

To determine whether our AgFc constructs might cause unwanted side effects in healthy mice, we tested all constructs that would be used in later experiments in MN models: d1d2-AgFcs for THSD7A-EAMN and CysFnII-AgFcs for transgenic hPLA2R mice. WT BALB/c mice were injected with d1d2-SELF-AgFc because they express THSD7A on podocytes inside the kidney. Any antibodies raised against the part of the AgFc construct containing the domains 1 and 2 of THSD7A would also bind THSD7A inside the kidney. Since transgenic hPLA2R progress to nephrotic syndrome within the first 6 weeks and we wanted to observe a longer time period, we choose chimeric PLA2R-mice (hH3mC2C8) for this experiment instead. Chimeric PLA2R mice (hH3mC2C8) express the human head domain of PLA2R (Cystein-rich domain, Fibronectin II domain and CTLD 1) with murine CTLD 2 to 8. Under basal conditions these mice are healthy and do not develop proteinuria nor autoantibodies against the chimeric protein expressed on podocytes. WT BALB/c mice do not express PLA2R on podocytes and would not be suited to assess the safety of the CysFnII-AgFc constructs. WT BALB/c mice and chimeric PLA2R mice were injected with 10 µg AgFc (either d1d2-SELF-AgFc or CysFnII-SELF-AgFc) i.p. over 6 consecutive weeks and analysed one week after the last injection. Body weight was measured and urine samples were collected each week before the AgFc injections to determine overall health and proteinuria development.

Mice did not show significant differences in body weight nor developed an albumin to creatinine ratio (ACR) above 2 g/g during that time (Figure 17A and B). Some animals developed a low serum titer against either THSD7A or PLA2R ranging from 2 to 4 Units at the end of the experiment (week 7, Figure 17C). Compared to actively THSD7A-immunized EAMN animals which show titers around 150 Units, these titers are very low. To exclude liver toxicity of our constructs we analysed the serum parameters alanine transaminase (ALT) and aspartate aminotransferase (AST). Both enzymes are indicators of liver damage. The De-Ritis ratio [81; 82], the ratio of ALT and AST, can be used to detect acute or chronic hepatitis but also chronic kidney disease. In all set ups we found no significant changes in ALT or AST (Figure 17D). Cholesterol and triglyceride levels increase in patients with nephrotic syndrome due to impaired clearance and increased biosynthesis [83]. We found no abnormalities in these parameters (Figure 17E and F). Kidney function was analysed through the serum parameter blood urea nitrogen (BUN). High BUN levels indicate a decline in kidney function for urea nitrogen is a waste product that is normally removed by the kidneys from the blood. No differences could be found in BUN in all compared animals (Figure 17G). The animals injected with either d1d2-SELF-AgFc or CysFnII-SELF-AgFc that developed antibodies against THSD7A or PLA2R also showed mIgG binding along the GBM but with much lower intensity compared to a positive control (Figure 17H). The mIgG co-localized with the expression of THSD7A or PLA2R (blue) as well as nephrin (red).

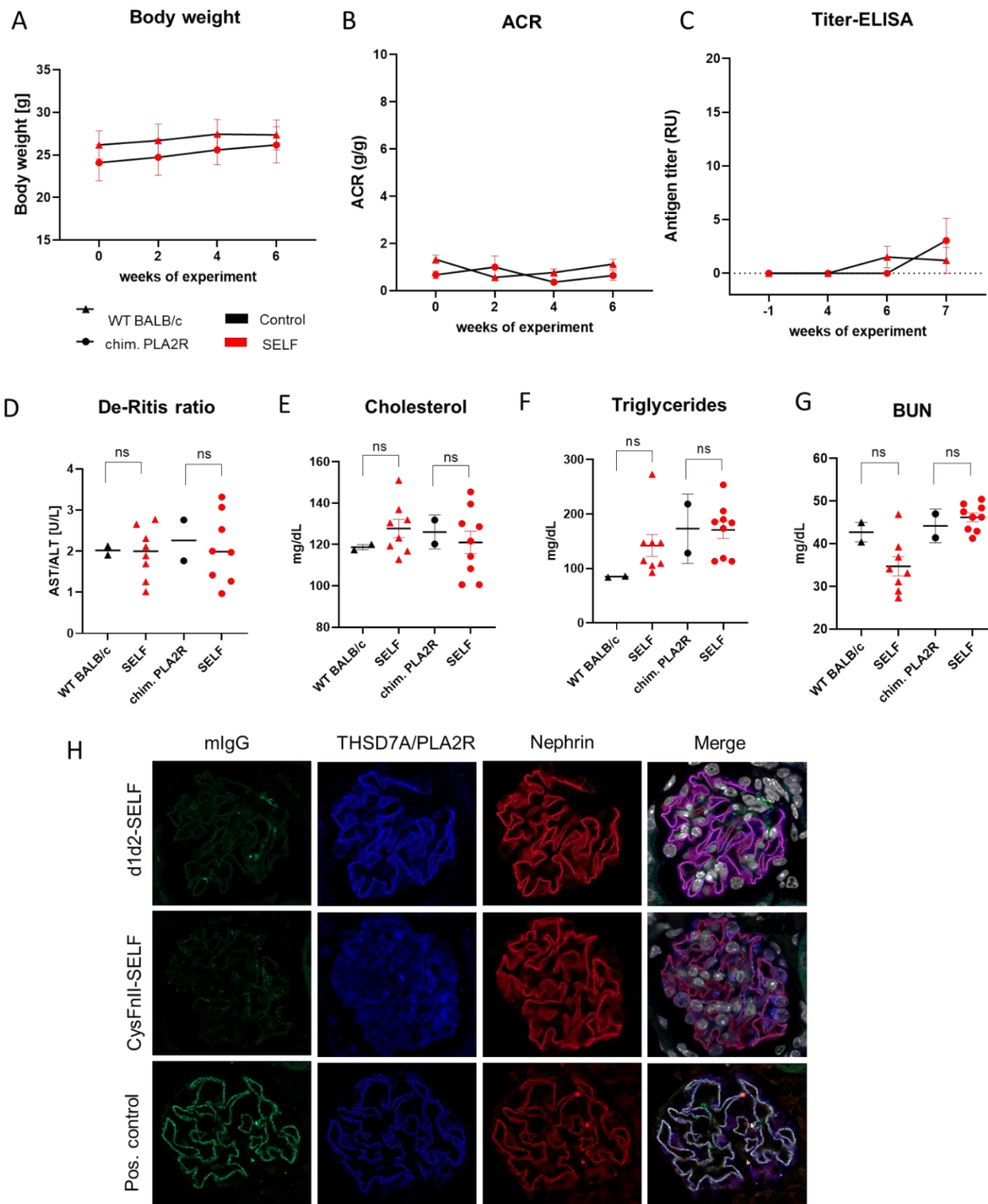


**Figure 17: Safety assessment of AgFcS.** (A) Body weight of mice throughout the experiment. All mice gained weight, no abnormalities could be observed. (B) Albumin/creatinine ratio (ACR) throughout the experiment. ACR of all mice were close to baseline of 0.5 g/g. (C) Anti-THSD7A and anti-PLA2R titers in serum. Some mice reacted with a slight titer, compared to diseased animals (above 150 RU) these titers are rather low with below 5 RU. (D) De-Ritis ratio to determine liver function. No significant change was observed between control animals and animals injected with AgFcS. Cholesterol (E) and triglycerides (F) showed no abnormalities in AgFc injected animals compared to the control animals. (G) Blood urea nitrogen (BUN) was not affected by the injection of AgFcS. (H) IF of glomeruli. mIgG deposits were faint in some animals, counterstaining was done with THSD7A (blue), nephrin (red) and Hoechst (white) or PLA2R, nephrin and Hoechst. Actively THSD7A-immunized EAMN mice with mIgG deposits were used as positive controls. Statistics: One-way ANOVA, Tukey's multiple comparison test).

To summarize, over the time of the experiment we could not find any relevant adverse effects of our AgFc in healthy WT BALB/c or chPLA2R mice. Few mice developed a slight titer against THSD7A (2 out of 10) or PLA2R (4 out of 10) after 5 consecutive weeks of injections but compared to actively THSD7A-immunized mice it was very weak (<100). Since mice neither developed proteinuria nor showed abnormalities in other serum parameters, we concluded that our constructs are relatively safe for healthy mice.

### 3.10 Blocking of actively THSD7A-immunized mice sera to determine a therapeutic dose

To achieve a therapeutic effect in diseased mice, the exact amount of AgFc needed to clear pathogenic autoantibodies from the circulation had to be investigated. Therefore, serum samples from WT BALB/c animals immunized with d1\_d2 and d15\_d16 of THSD7A were used to determine a therapeutic dose for later experiments (3.11 and 3.12). Four previously experimented mice were selected: 4385, 4443, 4414, and 4415 with titers of 96, 204, 113, and 111 Units/ml, respectively. 10  $\mu$ l of each serum with different titers was incubated with either 2  $\mu$ g, 1  $\mu$ g, 0.5  $\mu$ g or 100 ng of d1d2-SELF-AgFc, d15-SELF-AgFc and d16-SELF-AgFc for 1 h at RT. 1  $\mu$ l of this mix was then diluted 1:100 and added to a well with the coated antigen (d1\_d21-Strep) to find the minimal dose that blocks binding to antigen THSD7A effectively. We saw that small amounts like 100 ng or 0.5  $\mu$ g had little effect in blocking the autoantibodies in the mouse sera. Only higher amounts such as 1  $\mu$ g and 2  $\mu$ g could lower the titer significantly (Figure 18).

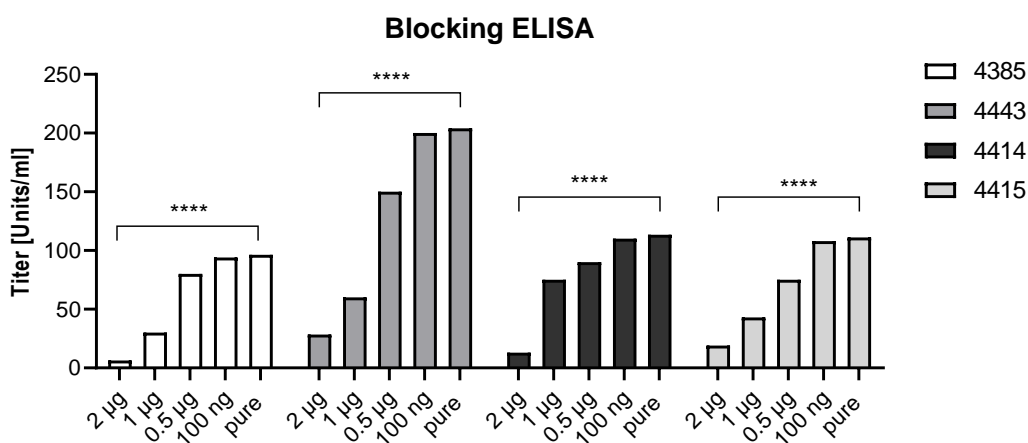


**Figure 18: Blocking of antibodies in sera from actively THSD7A-immunized mice in ELISA.** WT BALB/c mice were immunized with domains d1\_d2 and d15\_d16 of THSD7A. The first immunization included 20  $\mu$ g of each double domain construct mixed with complete Freund's adjuvant (1:1). Three booster immunizations followed in week 3, 5 and 7 with 20  $\mu$ g of each double domain construct mixed with incomplete Freund's adjuvants (1:1). In week 9 serum was collected and the anti-THSD7A titer determined. To test how much AgFc are needed to block certain titers, we selected four mice: 4385, 4443, 4414, and 4415 with titers of 96, 204, 113, and 111 Units/ml, respectively. 10  $\mu$ l of each serum was mixed with either 2  $\mu$ g, 1  $\mu$ g, 0.5  $\mu$ g or 100 ng of d1d2-SELF-AgFc, d15-SELF-AgFc and 16-SELF-AgFc 1 hour prior to adding 1  $\mu$ l to a blocked and d1\_d21-Strep (THSD7A) coated ELISA plate. The standard for the THSD7A-titer ELISA (described in 2.2.4.1) was used to determine Units/ml. 2  $\mu$ g AgFc was most effective in blocking the titers. 2way ANOVA, Tukey's multiple comparison test,  $p^{****}>0.0001$ .

To summarize, with 2  $\mu\text{g}$  we could block almost all signal in all four serum samples with different titers. Based on the body weight (20 g) and the expected serum volume of about 1000  $\mu\text{l}$  per mouse at 15 weeks of age (the time point after the first boost), we determined that we would have to use at least 200  $\mu\text{g}$  of AgFc to block high titers in THSD7A-immunized animals. Combined with the data from the *in vivo* uptake experiments (as seen in 3.6.) where most immune complexes were cleared after 3 days, we decided to treat twice per week through i.p. injections.

### 3.11 Pre-Treatment of actively THSD7A-immunized mice with AgFc

To determine whether the AgFc treatment can delay or even prevent the onset of MN, animals were treated before they showed symptoms like increased proteinuria. Therefore, 22 12-week old WT BALB/c mice were immunized with 20  $\mu\text{g}$  of d1\_d2 (THSD7A). The first immunization was done in complete Freund's adjuvant (CFA), followed by two booster shots in incomplete Freund's adjuvants (IFA). One mouse was immunized with the vehicle (PBS) to be used as a negative control for mIgG deposition in the kidneys. One week after the last boost, two mice were sacrificed as reference before treatment. Since these animals only showed lower titers between 10 and 50 Units/ml and had no symptoms of MN, we either injected with 100  $\mu\text{g}$  d1d2-SELF-AgFc (treated; red) or 100  $\mu\text{g}$  CysFnII-SELF-AgFc (Control; black) twice a week i.p. for the pre-treatment strategy. Every week for five consecutive weeks four mice were sacrificed (two animals per group; treated or control) and blood and kidneys were analyzed. There were no differences in body weight between the two groups (Figure 19A). The albumin loss to the urine by measurement of the urine albumin to creatinine ratio (ACR) showed significantly lower amounts ( $p^{****}$ ) in the treated mice compared to the Control group (Figure 19B) at the end of the experiment (week 10). The serum titer of anti-THSD7A antibodies was also significantly lower ( $p^*$ ) in the treated animals compared to the Control animals (Figure 19C). The De-Ritis ratio [81; 82], the ratio of ALT and AST, was used to determine the liver function. Neither Control nor treated animals had a significantly higher De-Ritis ratio compared to healthy control animals (Figure 19D). Healthy WT BALB/c animals were used as a reference (grey; Figure 19D). No difference in the serum parameters determining kidney function and onset of nephrotic syndrome (cholesterol, triglycerides, BUN) were detectable between the two groups (Figure 19E-G).

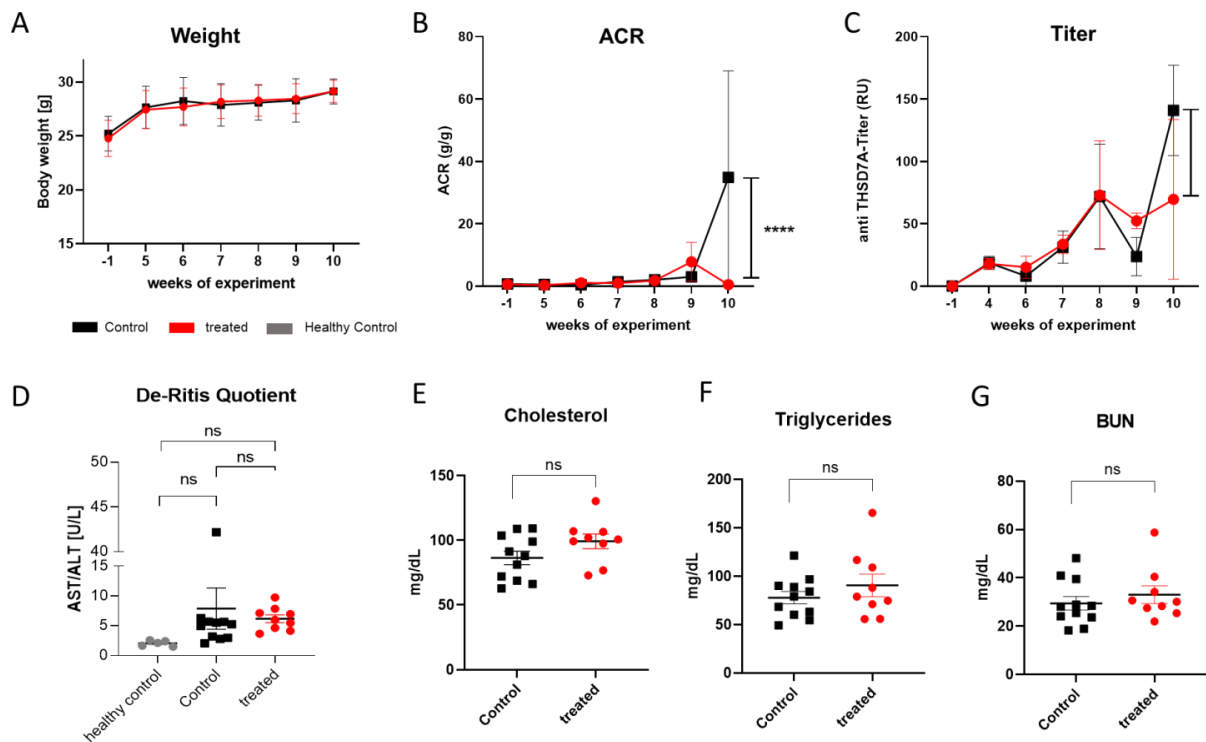


**Figure 19: Pre-Treatment of actively THSD7A-immunized mice.** (A) Body weight between the treated animals (red) and animals treated with an irrelevant AgFc (control; black) showed no abnormalities. (B) Albumin to creatinine ratios (ACR) were stable until week 8 of the experiment. After that both groups increased slightly (week 9). While treated animals fell back to baseline, control animals increased until about 40 g/g with a high variance (week 10). Still, animals injected with d1d2-SELF-AgFc had significantly lower ACR compared to the control group at the end of the experiment ( $p^{****}$ ). (C) The anti-THSD7A titer ELISA revealed a slow increase in titer for all animals until week 8 and while the titer of the treated animals stayed about the same, it was significantly lower compared to the Control animals ( $p^*$ ). The liver function was examined through the serum parameters ALT (D) and AST (E). Both groups remained within a healthy level until the end of the experiment. (F) Cholesterol, (G) triglycerides and (H) blood urea nitrogen (BUN) were also checked after the experiment ended but revealed no difference between the two groups. Statistics: Mann-Whitney test or 2way ANOVA, Sidak's multiple comparison,  $p^* < 0.01$ ,  $p^{****} < 0.0001$ .

The analysis of the mIgG deposition inside the kidney showed slightly less mIgG in the treated group compared to the control animals but was not significant (Figure 20A). The PBS-immunized mice showed no deposition of mIgG, while the animals immunized with d1\_d2 (THSD7A) that were sacrificed before the start of the treatment showed mIgG staining that co-localized with laminin, a basement membrane marker (Figure 20B). Representative IF stainings of mIgG can be seen in Figure 20C through the different weeks of treatment. The AgFc treated animals showed slightly less deposited mIgG starting from week two. While the amount bound in the kidneys of treated animals remained stable after week one, the amount in kidneys of Control animals increased from week one through week four. Overall, the amount of mIgG inside an animals' kidneys was subject to high fluctuations since we selected two animals each week for analysis.

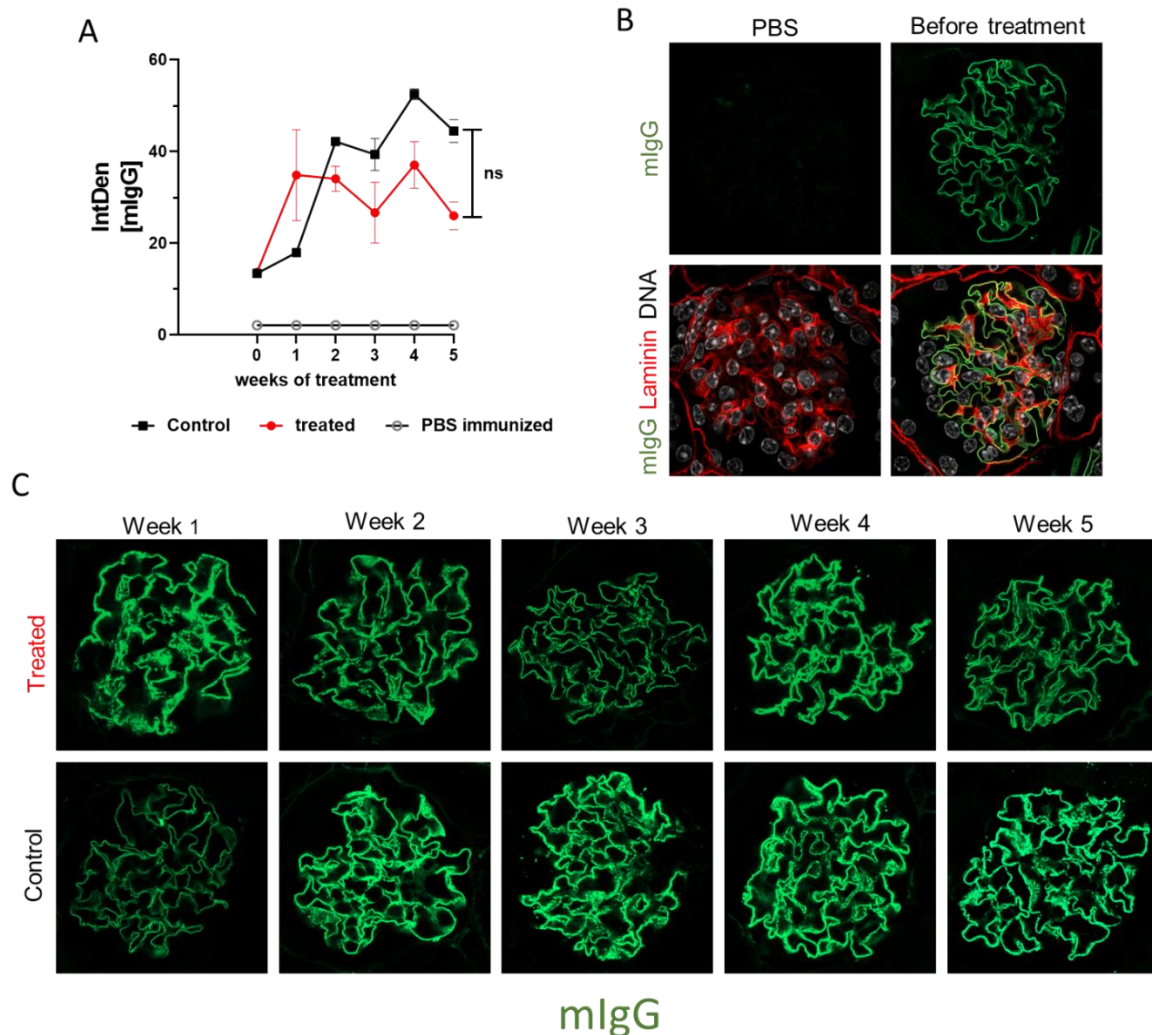


**Figure 20: Analysis of mIgG deposition in pre-treated THSD7A-EAMN mice.** (A) Analysis of the integrated density (IntDen) with ImageJ. 10 gloms of every mouse were photographed and used for this analysis. Overall, the treated (d1d2 SELF-AgFc) animals show less mIgG deposition inside the glomerulus, although not significantly ( $p < 0,0927$ ,  $\alpha = 0,05$ , Sidak's multiple comparison test). (B) Reference glomeruli from PBS-immunized mice that show no mIgG staining along the GBM, while the control animals that were immunized with d1\_d2 (THSD7A) but sacrificed before the start of the pre-treatment, showed a clear mIgG staining along the GBM. Counterstaining was done with laminin for localization and Hoechst (DNA). (C) Kidney sections of the treated (d1d2 SELF-AgFc) or CysFnII-SELF-AgFc (Control) treated animals over 5 weeks stained with mIgG. The mIgG staining in animals injected with CysFnII-SELF-AgFc was slightly stronger compared to the treated animals. However, it varied from week to week and did not show a consistent trend in either group.

In summary, we could decrease the serum titer of anti-THSD7A autoantibodies and the proteinuria (ACR) compared to animals treated with an irrelevant AgFc (Control). Our treatment had no adverse effects on the liver function and animals did not get sick enough for cholesterol and triglyceride levels to be increased. Since we saw a high variance between the individual mice, more animals have to be tested to increase the reliability of these results.

### 3.12 Treatment of actively THSD7A-immunized mice with AgFc

To investigate the potency of our AgFc as therapeutic agents in THSD7A-associated MN, WT BALB/c animals ( $n=20$ ) were immunized with double domains d1\_d2 and d15\_d16 of THSD7A

as described in 2.2.10.7 until the animals developed an albumin/creatinine ratio above 3 g/g. From that time on, the animals were randomly injected with either d1d2-SELF-AgFc and d15-SELF-AgFc (treated; red) with 200 µg each twice per week i.p., or with 200 µg of CysFnII-SELF-AgFc (Control; black) twice a week i.p. for four consecutive weeks. One mouse was immunized with PBS as a negative control for mIgG deposition in the kidneys. After that, animals were sacrificed and analyzed for remaining anti-THSD7A titer in serum, overall liver function (De-Ritis ratio from AST and ALT) and kidney function (BUN, ACR) as well as the amount of mIgG bound inside the glomeruli. Only 8 out of the 20 THSD7A-immunized animals exceeded an ACR of 3 g/g within the 15-week experiment, therefore all results from these animals have to be considered with care. Three animals were injected with CysFnII-SELF-AgFc (control) and five animals with d1d2-SELF-AgFc and d15-SELF-AgFc (treated). The weight did not differ between the two groups and all animals gained weight over the observed time (Figure 21A). Through treatment with the fitting AgFcS the albumin to creatinine ratio (ACR) could be significantly decreased at the end of the treatment period compared to the control mice which increased over time ( $p^*$ ; Figure 21B). The anti-THSD7A serum titer was lower in treated animals than in control animals after the start of the treatment but was not significantly reduced at the end of the observation time ( $p=0.61$ , Figure 21C). Liver enzymes were not elevated compared to healthy animals independent from the AgFcS administered (Figure 21D). Other serum parameters, such as cholesterol, triglycerides, and blood urea nitrogen (BUN), showed no significant increase over the observed time between the two groups (Figure 21E-G). mIgG deposition inside the kidney was significantly increased in both groups, treated and control animals, compared to the PBS-immunized animal that showed no mIgG deposition along the GBM ( $p^{**}$ ; Figure 21H). The treatment had no measureable effect on the amount of mIgG deposited inside the kidneys between treated and control animals (Figure 21H). The IF stainings of mIgG inside the kidney was found along the GBM and co-localized with laminin (red; Figure 21I).

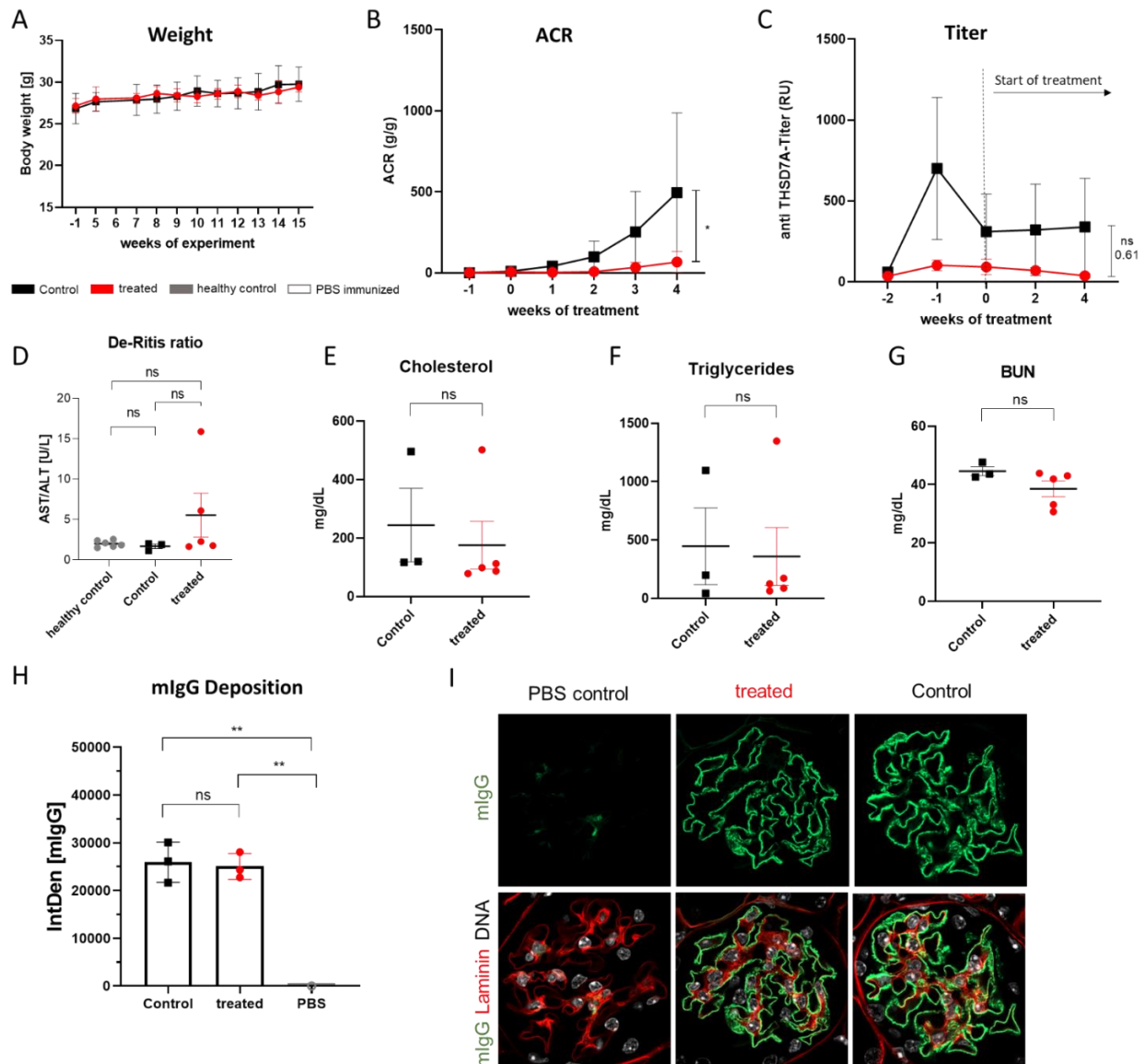


**Figure 21: Treatment of THSD7A-MN mice.** (A) Body weight between the treated animals (red) and animals treated with an irrelevant AgFc (Control; black) showed no abnormalities. (B) Albumin to creatinine ratios increased in both groups over time however significantly less and slower in the treated animals compared to the control animals at the end of the experiment ( $p^*=0.016$ ). (C) The anti-THSD7A titer ELISA revealed lower titers for treated animals (red) compared to the control mice (black) after the start of treatment at week 10. This difference was not significant though ( $p=0.61$ ). One animal in the control group had a serum titer of 1140.2 Units/ml in week 5 which contributes to the high error bar at that time point. (D) The liver function was examined through the serum parameters ALT and AST. Which form the De-Ritis ratio. No significant difference between the groups could be detected. (E) Cholesterol, (F) triglycerides and (G) blood urea nitrogen (BUN) were also checked after the experiment ended but revealed no difference between the two groups. (H) The analysis of mIgG deposition showed no difference between the treated and control group. (I) IF of mIgG (green) in representative glomeruli. Shown are images of the PBS control and the two treatment groups: treated (red) and control (black). Counterstaining was done with laminin (red) and Hoechst (white). Statistics: Student's t-test or 2way ANOVA, Sidak's multiple comparison,  $p^*<0.01$ .

In conclusion, the treatment with fitting AgFc's lowered the ACR and anti-THSD7A serum titer in d1\_d2 and d15\_d16 immunized WT BALB/c mice. Serum parameters were not affected but also no impact could be observed on the mIgG deposition in the kidneys. As aforementioned, the group

size is too small to draw profound conclusions and these results can only be used as a guide. Further cohorts with more animals have to be done to solidify these findings.

### 3.13 Treatment of autoimmune hPLA2R mice

To ascertain if our AgFcs could be used as a treatment strategy for PLA2R-associated MN, transgenic hPLA2R mice were used as a model organism. WT mice do not express PLA2R inside the kidney, therefore transgenic mice were developed which express human PLA2R on podocytes. Starting at 3 weeks of life, hPLA2R-positive mice spontaneously develop anti-PLA2R antibodies against the domains CysR, CTLD1/2 and CTLD7/8 of PLA2R and proteinuria, progressing to full blown nephrotic syndrome from 4 weeks of age onwards [74]. Since we saw no differences between WT and SELF-AgFcs in degradation *in vivo* (Chapter 3.6), we used CysFnII-WT, CTLD1/2 WT and CTLD7/8 WT-AgFc to treat the transgenic hPLA2R mice. Mice were treated with either 100 µg CysFnII-WT, CTLD1/2 WT and CTLD7/8 WT-AgFc (treated; red) each or with 100 µg d15-WT-AgFc (Control; black) twice a week i.p. for 3 consecutive weeks (Figure 22A) starting at week 3 of age. During that time the body weight in both groups increased from 12 g to 20 g and did not differ between the two treatment groups (Figure 22B). Urine was collected twice a week during treatment and ACR was decreased in the treated animals compared to the d15-WT-AgFc treated ones, bordering on significance (Figure 22C,  $p=0.0526$ ). When the anti-PLA2R serum titer was compared, treated animals showed a slightly delayed increase of titer over time compared to the d15-WT-AgFc treated animals (Figure 22D). When analyzing liver function through the serum parameters ALT and AST, we observed a significant increase of the De-Ritis ratio in treated animals compared to d15-WT-AgFc treated ones and healthy control animals ( $p^*$  and  $p^{**}$ ; Figure 22E). d15-WT-AgFc treated animals did not show a significant increase compared to the healthy controls. Since all hemizygous hPLA2R mice develop proteinuria and in later stages nephrotic syndrome, naïve WT BALB/c animals were used as healthy controls to compare the De-Ritis ratio (grey; Figure 22E). When comparing other serum parameters such as blood urea nitrogen (BUN), cholesterol and triglycerides, we found no difference between the two groups (Figure 22F-H). The analysis of mIgG deposition along the GBM inside the kidneys showed no decreased signal in treated animals compared to the d15-WT-AgFc treated ones (Figure 22I). The mIgG staining, co-localizing with the PLA2R staining (blue) and nephrin (red), was subject to variance, depending on the severity of the animal's proteinuria and progression of nephrotic syndrome (Figure 22J).

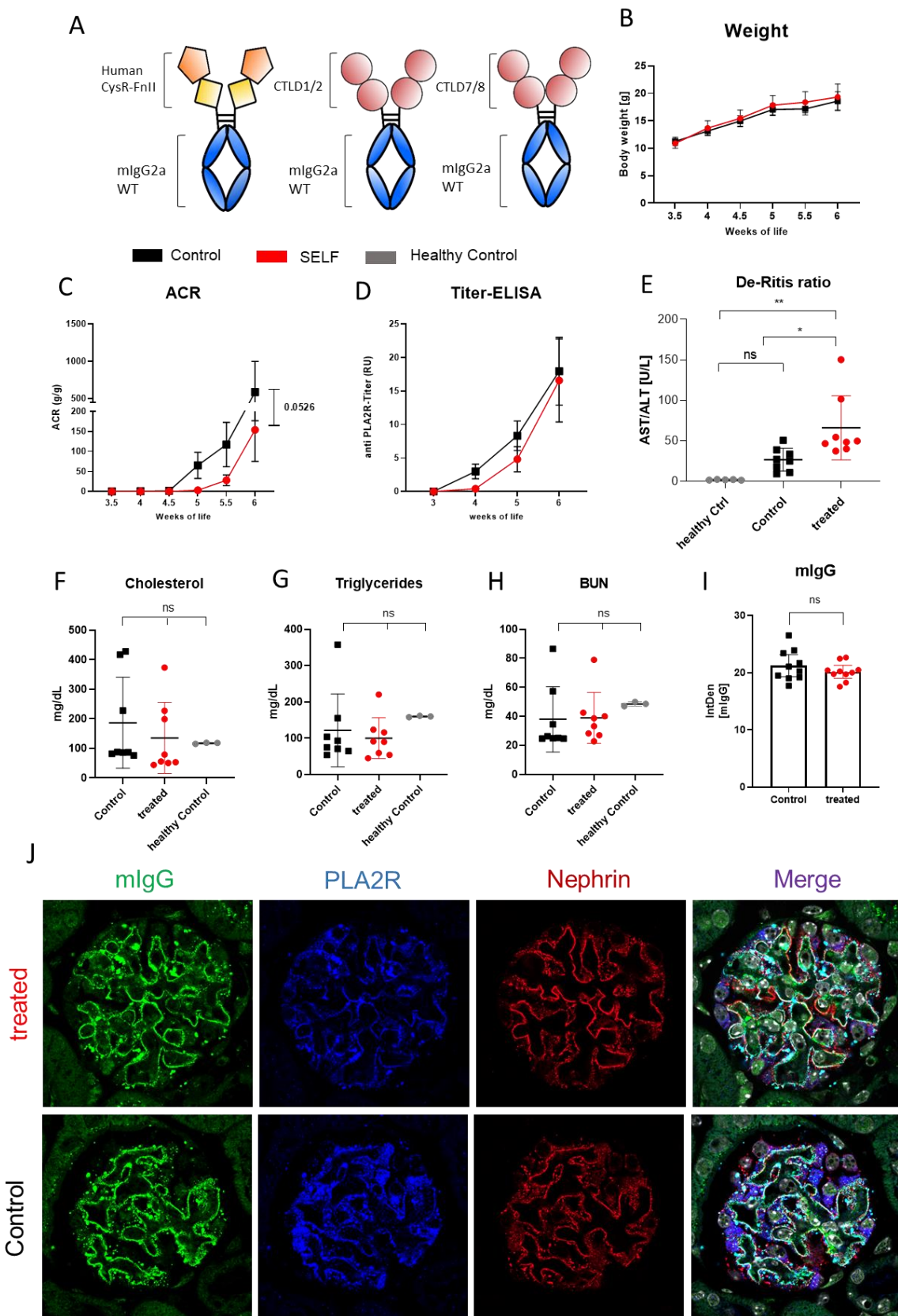


**Figure 22: Treatment of hPLA2R autoimmune mice.** (A) Schematic of newly developed AgFc's to treat the hPLA2R mice: hCysFnII-WT, CTLD1/2-WT, and CTLD7/8-WT. All constructs have a WT mIgG2a backbone. (B) shows the body weight of all animals in the course of the experiment. All animals increased their body weight, whether they received treatment (red) or not (black). No difference could be observed between the groups. (C) The albumin/creatinine ratio was measured twice a week. Both groups ACR (treated and d15-WT treated) increased over time, however the treated animals showed a delay in the onset as well as the severity of the proteinuria (2-way ANOVA mean +/- SEM, Sidak's multiple comparison test,  $p=0.0526$ ). (D) The ELISA revealed increasing anti-PLA2R titers

in both groups over the time of treatment. No significance could be detected between the treated group and d15-WT injected animals. (E) Liver function was determined through the De-Ritis ratio (AST/ALT). Treated animals showed a higher ratio compared to d15-WT-AgFc treated animals and healthy controls of WT BALB/c animals. d15 WT-AgFc treated animals showed no significantly increased ratio compared to healthy mice (One-way ANOVA, Tukey's multiple comparison test,  $p^*>0.05$  and  $p^{**}>0.01$ ). Cholesterol (F), triglyceride (G), and blood urea nitrogen (BUN, H) levels revealed no difference between the groups (ordinary one-way ANOVA). The amount of mIgG bound inside the kidneys (I) Integrated density measured with ImageJ yielded no significant difference (Student's t-test). (J) Representative confocal immunofluorescence images of the kidneys. mIgG staining was influenced by severity of the proteinuria and overall condition of the kidneys. mIgG (green), PLA2R (blue), Nephrin (red) and Merge are shown.

In conclusion, we could not significantly reduce anti-PLA2R autoantibody titers in autoimmune hPLA2R mice with the dosages of AgFc that were used in this experiment. Furthermore, we were not able to decrease the proteinuria albeit we could slow down the onset compared to d15-WT-AgFc treated animals. The De-Ritis ratio in treated animals increased significantly, indicating liver damage in these animals. This could not be observed in animals treated with an irrelevant AgFc (d15-WT; Control).

## 4 Discussion

Membranous nephropathy (MN) is an antibody-mediated autoimmune kidney disease. The autoantibodies developed by patients bind podocyte antigens like PLA2R or THSD7A and damage the filtration barrier of the glomerulus through different mechanisms of action [1; 8; 9]. The disease's hallmarks are proteinuria, podocyte foot process effacement and immune complex deposition along the GBM [3]. The current therapies for MN patients consist of broad immunosuppressants such as cyclosporine or alkylating agents. Steps in the direction of less global therapies have been done by including rituximab in the treatment plans, a mAb which depletes B cells [26], but as of now no antigen-specific therapies exist for MN patients. We tried to improve the treatments options by designing antigen Fc-fusion constructs to capture anti-THSD7A and anti-PLA2R antibodies in the circulation, leading to degradation of these antibodies through specialized cells in the liver.

For specific binding to anti-THSD7A antibodies, d1d2- and d15-AgFc constructs were generated. These domains were selected since they are among the most immunodominant domains recognized by patients' sera [24]. In an active mouse model of THSD7A-associated MN (THSD7A-EAMN), these domains were used for immunization of WT BALB/c mice. After the development of antibody titers against THSD7A, we used these mice to test the AgFcs for their therapeutic potency.

For specific binding to anti-PLA2R antibodies, we created CysFnII-, CTLD1/2- and CTLD7/8-AgFc constructs consisting of the most immunodominant domains recognized by PLA2R-positive patient's [24; 9; 74; 22]. To test these constructs, we used transgenic hPLA2R mice that spontaneously develop signs of MN around 3 weeks after birth [74].

For therapeutic purposes we created two different Fc-parts: one with WT mouse IgG2a backbone and another with mutation of amino acids S267E and L328F (SELF). These mutations are known to enhance the binding to human FcγRIIB 200-fold [39]. We hypothesized that immune complexes consisting of autoantibodies and our therapeutic AgFcs would be taken up and degraded by specialized liver sinusoidal endothelial cells (LSECs) as shown in other models with other antigens [84; 85]. These cells express 90 % of the livers FcγRIIB and use it to clear the blood from circulating small immune complexes (SIC) through FcγR-mediated internalization [59]. We hypothesized that an enhanced binding affinity would speed up the degradation process and increase the beneficial effect of our therapeutic agents. We saw a depleting effect of the AgFcs on the serum titer of anti-THSD7A autoantibodies and a decrease in the proteinuria of THSD7A-

EAMN animals. The results for the transgenic hPLA2R mice were more ambiguous. During the observed time frame, our AgFcS did not show an effect on the deposited mIgG inside the kidneys in either mouse model.

#### 4.1 *In vitro* characterization of AgFcS

Tomas et al. [74] showed that autoantibodies against a podocyte antigen are the source of mIgG deposition along the GBM and initiator of podocyte damage through complement activation. The domain distribution and variation in THSD7A-associated MN patients offers the opportunity for personalized therapeutics [24]. Therefore, we decided to build AgFc constructs, which could be adapted to the patients' needs according to the domain profile determined through ELISAs and are easily produced in different expression systems. Since the crystal protein structure of THSD7A is not yet determined, we do not know the exact epitope inside the immunodominant domains of the autoantibodies causing MN. However, for the generation of therapeutic antibodies against a specific target this information is crucial. We circumvented this by adding the immunodominant domains to a mutated Fc part thereby diverting from the sweeping antibody principle described by Igawa et al. [36]. Through this we forfeited the pH dependent binding and created a construct that could be used for degradation only once, not creating the "sweeping effect" [36], but potentially enabling the clearance of specific pathogenic antibodies. We initially developed several AgFcS but some constructs (as d13d14-WT or d15d16-WT) showed misfolding and multimerization in a non-reducing SDS-Page (Supplementary data, Figure 24A). Since this increases the chance of unwanted side effects and may influence immune complex size, which in turn effects the uptake into LSECs [59], we decided to use only d1d2-AgFcS and d15-AgFcS for depleting anti-THSD7A autoantibodies and CysFnII-, CTLD1/2- and CTLD7/8-AgFcS to deplete anti-PLA2R autoantibodies. The constructs bound to mAbs raised against domains 2 and 15 of THSD7A and CysR of PLA2R, respectively. The median effective concentration ( $EC_{50}$ ) is a commonly used measurement of a drug's potency and ranged from 0.5 to 1.6 nM for our constructs (Figure 6). This is slightly better compared to other approved therapeutic antibodies like rituximab (17.4 nM) [86]. Since this measurement is done with mAbs from murine hybridomas, they do not display values for autoantibodies found in patients. It can only be used as a guide because the germline repertoires of immunoglobulin heavy chain variable (IGHGV) in humans and mice are rather different, resulting in more diverse antibodies in humans [19; 87; 88]. Binding of membrane-bound BCR was confirmed with fluorescently labeled AgFcS in Flow cytometry (Figure 8, upper row). We found that the binding was specific to the BCR and dependent on the BCR expression on the surface. Binding to different Fc $\gamma$ Rs was tested on stably transfected HEK cells and revealed lower MFIs for WT-AgFcS than SELF-AgFcS binding to the

low affinity receptor Fc $\gamma$ RIIB (Figure 8, lower row). For Fc $\gamma$ RIII and Fc $\gamma$ RIV very low values could be detected and the difference between WT and SELF-AgFcs was negligible. Consequently, the SELF mutation appears not to increase affinity to these two receptors in monomeric IgG *in vitro*. The results for the high affinity receptor Fc $\gamma$ RI were conclusive: WT- and SELF-AgFc had similar MFIs indicating no impact of the SELF mutation on the already strong affinity of mIgG2a to Fc $\gamma$ RI [89].

#### 4.2 SELF mutation leads to better uptake into LSECs *in vitro* but not *in vivo*

In chapter 3.3 the *in vitro* uptake of pre-formed immune complexes with WT- or SELF-AgFcs into primary LSECs was tested. The molar ratio of AgFc:mAb was 4:1 to create an excess of AgFc and avoid the point of equivalence (POE), where the immune complexes would build large lattice structures causing aggregation and precipitation of proteins [60]. We saw that the uptake was dependent on the Fc $\gamma$ RIIB, for it could be blocked by pre-incubation with a commercial blocking anti-CD32B antibody designed to inhibit Fc parts from any IgG subclass from binding to Fc $\gamma$ RIIB. SELF-AgFcs were taken up more efficiently than WT-AgFcs in complex with their corresponding mAb (Figure 10). MFIs can be influenced by the degree of labelling (DOL), which i) shows batch differences and ii) depends on the coupled protein and its composition [90]. While DOL of the same AgFcs species with different Fc backbones varied only slightly (3.7 moles dye/mole IgG to 3.5 moles dye/mole IgG in d1d2-SELF-AgFc and d1d2-WT-AgFc, respectively), the difference was greater between AgFcs constructs of different antigens e.g., DOL of CysFnII-SELF-AgFc was 60 moles dye/mole IgG compared to d1d2-SELF with 3.7 moles dye/mole IgG (Supplementary data). This explains the spread in MFI range from 40000 (CysFnII-SELF-AgFc) to 15000 (d1d2-WT-AgFc) between constructs but not why SELF-AgFcs were taken up more efficiently than WT counterparts (Figure 10). A significantly higher uptake of complexes containing SELF-AgFcs could not be observed in *in vivo* experiments (chapter 3.6), at least at the investigated time points, where the molar ratio was 2:1. The ratio was chosen because we found in experiments done for the establishment of the LSECs FACS panel that at least 20  $\mu$ g of monoclonal was needed to detect in LSECs 7 days after injection (data not shown). In a 4:1 ratio that would mean 66  $\mu$ g of AgFc-AF488 for every animal and for production and cost-effective reasons, we decided to decrease to a 2:1 ratio. With this ratio *in vivo* there was no significant difference between WT- or SELF-AgFc complexes at the same time point (Figure 13, 60 min). In contrast to the *in vitro* set up, where mostly one cell type is involved in the uptake depending on the purity of the isolation process, in the *in vivo* set up there are multiple cells that can influence how much immune complex reaches the LSECs in the liver: Kupffer cells also express Fc $\gamma$ RIIB and depending on the size phagocytose immune complexes as well [91]. FcRn can bind immune

complexes and shuffle them across polarized barriers, delaying transport to the liver [32; 92; 53]. Additionally, for the *in vitro* uptake primary LSECs were isolated from 40-week-old animals because with age the amount of LSECs per animal increases, reducing the number of animals that have to be sacrificed per *in vitro* uptake assay. Grosse and Bulavin [93] found that up until 1 year after birth the expression of scavenger receptors increases and therefore endocytic activity. After that, senescent LSECs accumulate inside the liver and decrease the endocytic activity. In contrast, animals in *in vivo* experiments ranged from 12 to 18 weeks of age, which is the normal age for immunization protocols [94]. These differences can account for small variances but we strongly suspect that age did not influence the results as much as the different molar ratios and timing. Yu et al. [95] injected LSECs targeting nanoparticles and observed in real time the uptake into LSECs. Three minutes' post injection particles already reached the LSECs and 10 min post injection a strong signal could be observed. Additionally, a lag phase was observed after saturation of LSECs: endocytosed receptor only returned to the surface unoccupied after 5 minutes [59]. All in all, the different ratios, time points and systems (*in vitro* vs. *in vivo*, Figure 10 and Figure 13), could influence the discrepancies we saw and need to be investigated further to find definite answers.

### 4.3 The impact of the SELF mutation on FcγRIII

In an effort to characterize different effector functions of AgFcs, we developed an antibody dependent cell-mediated cytotoxicity (ADCC) killing assay of luc<sup>+</sup> hybridomas from THSD7A (d2 and d15) and PLA2R (CysR) with mFcγRIII transfected NK cells. Here the killing is induced through the binding of the AgFc to the BCR on the surface of the hybridomas, which marks the cells for killing by the NK cells. We found that SELF-AgFcs induced ADCC more efficiently than WT-AgFcs and LALAPG was not able to induce ADCC at all (Figure 9). We used an effector:target ratio of 3:1 and the highest achieved percentage of dead cells was 65% (d1d2-SELF-AgFc on anti-d1\_d2 hybridoma). Naïve NK cells were found to have a low expression of cytotoxic proteins such as granzyme B and perforin [96]. For more advanced effector functions NK cells need “priming”, which can be triggered by IL-2 and IL-12. We supplemented IL-2 that is needed for proliferation and cytotoxicity of NK cells [97] to the media but not IL-12, a pro-inflammatory cytokine. The combination of IL-2 and IL-12 was shown to have a synergistic effect and increased cytotoxic activity of NK cells [98]. This might explain why ADCC-mediated killing could not reach the level of BCR expression (ca. 90 %) on the hybridomas. We saw that the expression of BCR directly influences ADCC effectiveness: the highest amount of achieved dead cells on anti-CysR hybridomas with lower BCR expression (59 %, Figure 7) was 30 % with CysFnII-SELF, less than on hybridomas with higher BCR expression such as the anti-d1\_d2 hybridoma (81% BCR expression and induced dead cells of 60%, Figure 7). This is to be expected

since lower BCR expression decreases the binding of AgFcs that mark the cells for ADCC.

Kipps et al. [99] found that with identical binding affinity and specificity, mIgG2a is more effective in inducing ADCC than the subtypes mIgG1 or mIgG3, which might explain why WT-AgFcs (mIgG2a subtype) could induce up to 40 % of killing. Even though it has not been described that the SELF mutation increases the affinity towards Fc $\gamma$ RIII, we found that in *in vitro* ADCC killing assays, AgFcs with the SELF mutations induced ADCC more efficiently (p<sup>\*\*\*</sup>) compared to WT IgG2a backbones (Figure 9). This discrepancy might result in previous affinity assays being executed with human IgG backbones on human Fc $\gamma$ Rs instead of mouse Fc $\gamma$ Rs. Chu et al. [36] described a higher affinity of SELF constructs to human Fc $\gamma$ RI, Fc $\gamma$ RIIA, Fc $\gamma$ RIIB, and Fc $\gamma$ RIIIA as 1.2-, 1.0-, 430-fold increased and not detectable, respectively. A comprehensive study of the structure of human IgG1 bound to different human Fc $\gamma$ Rs revealed that Ser267 has the highest interaction surface of Fc $\gamma$ RIIB (>10% of total buried surface area (BSA)) and an intermediate interaction surface for Fc $\gamma$ RIIIA (5-10% of BSA) [100]. The greater the surface area the more accessible it is to the solvent and therefore more accessible to binding partners. Since Ser267 is important for the binding of both receptors (Fc $\gamma$ RIIB and Fc $\gamma$ RIII) to IgG, it might explain why a mutation of Serine 627 that increases the affinity towards Fc $\gamma$ RIIB also has an impact on Fc $\gamma$ RIII binding. However, until affinity studies are available for this mutation and the respective Fc $\gamma$ Rs, this remains purely hypothetical.

#### 4.4 Kinetics of immune complex uptake in LSECs

To understand the kinetics of immune complex uptake in mice, either pre-formed immune complexes were injected into WT BALB/c mice and then tracked over time or monoclonals and AgFcs were injected consecutively to understand the uptake kinetics of *in vivo* formed complexes (Chapter 3.5). Both approaches revealed the uptake into LSECs to be a fast process: after 10 mins LSECs already took up complexes and achieved the highest MFIs between one to six hours (Figure 12). This finding was in accordance to other groups that already saw uptake into LSECs between 3 and 10 mins after i.v. injection [59; 95]. Differences between WT- and SELF-AgFcs that were found in *in vitro* uptake assays could not be confirmed *in vivo*: in animals that were injected with the pre-formed immune complexes MFIs of WT-AgFc-complexes were higher in LSECs after 60 min (Figure 12), while MFIs showed no difference in the *in vivo* formed set up (Figure 13). Lux et al. [101] discovered the same when they analysed the binding affinity of differently sized immune complexes towards Fc $\gamma$ Rs. WT monomers that normally have low affinity towards Fc $\gamma$ Rs, bound Fc $\gamma$ Rs strongly when added in complex.

We observed that already formed complexes were stable enough not to leak anti-d1\_d2 mAb to

glomeruli inside the kidney (3.5.1) and already bound anti-d1\_d2 mAb in the kidneys could be cleared by AgFcs over time (3.5.2). These findings indicate a desired clinical outcome when the AgFcs are used as therapeutic agents: they appear clear bound antibodies from the kidney and the formed immune complexes are stable enough to reach the LSECs in the liver where they can be degraded.

To further test our hypothesis, we developed AgFcs with yet another mutation in the Fc-part: L234A/L235A, P329G (LALAPG). This abolishes the binding to any Fc $\gamma$ R [102] and should hinder the degradation of immune complexes formed through autoantibody and therapeutic AgFc. Therefore, complexes with this AgFc variant should circulate longer compared to complexes including the WT or SELF variant. Interestingly, we observed quite the opposite in 3.5.2: immune complexes with the anti-d1\_d2 mAb + d1d2-LALAPG-AgFc were degraded similarly albeit slower as immune complexes containing WT- or SELF- instead of LALAPG-AgFcs. This can be explained through the composition of the immune complexes: Not only does it include the mIgG2a backbone with the LALAPG mutation which ablates binding to Fc $\gamma$ Rs but also the mIgG1 backbone from the anti-d1\_d2 mAb. The affinity of mIgG1 towards Fc $\gamma$ RIIB is higher than of mIgG2a ( $10^{-7}$  K<sub>D</sub> (M) to  $10^{-6}$  K<sub>D</sub> (M), respectively) [103] but since these IgG are presented in immune complexes, the avidity effect comes into play as well. While affinity is the strength of attraction between an antibody and its ligand, avidity describes the strength of all non-covalent interactions including the binding affinity of the complex, the valency of the proteins and the structure of the complex [104]. Lux et al. [101] reported similar observations with IgG1 molecules with substitution of D265A: even though the IgG backbones had strongly reduced affinity towards Fc $\gamma$ Rs as monomers, they could still bind hFc $\gamma$ RIIA if present in a large immune complex. This probably gives insight into why a LALAPG backbone might not influence the uptake of an immune complex even though as a monomer all binding is abolished through the mutation.

#### **4.5 The neonatal Fc receptor impacts immune complex degradation**

The neonatal Fc receptor (FcRn) builds the basis for the long half-life of serum proteins like albumin and IgG [54]. It shuffles both proteins across polarized barriers and rescues them from degradation through lysosomes. Inside the kidney it is expressed in the tubules to rescue escaped proteins from excretion and in podocytes where it prevents the accumulation of IgG at the filtration barrier [53]. To understand the relationship between uptake into LSECs for degradation and rescue of immune complexes through the FcRn, we compared the uptake and degradation of immune complexes in *FcRn*<sup>-/-</sup> and WT C57BL/6 mice *in vivo*. We found no impact of the degradation through Fc $\gamma$ RIIB<sup>+</sup> LSECs but a decreased half-life of IgG and AgFc in general (Chapter 3.7). When we put this in context with IgG and immune complex kinetics *in vivo*, an

important role for the FcRn became evident. While it binds IgG and albumin, adding to the remarkably long half-life of both molecules, in the absence of FcRn internalized IgG is directed into lysosomes and degraded. The absence of FcRn in the liver was found to increase IgG catabolism [105; 106], which we could confirm with our results (Figure 15). Although FcRn is mostly expressed by hepatocytes in the liver, when FcRn is knocked out in hepatocytes, the circulating levels of IgG were not affected [107]. Pyzik et al. [50] suspected that another receptor takes over, which might explain why the uptake into LSECs was not impaired in *FcRn*<sup>-/-</sup> mice. High doses of IgG were shown to increase the clearance through the FcRn in a concentration-dependent manner [108], which might have an effect on the half-life of our AgFcs when injected in high doses. The rescue of circulating immune complexes, which can occur in the diseased state, creates a pro-inflammatory environment. Liu and colleagues [109; 110; 44] found that the expression of the FcRn can be up-regulated in inflammatory environments by TNF- $\alpha$  and IFN- $\gamma$  through the NF- $\kappa$ B pathways. This might prolong the half-life of immune complexes but also activates immune complex uptake through Fc $\gamma$ RI expressing cells: van der Poel et al. [44] discovered that IL-3 induced the uptake of immune complexes through Fc $\gamma$ RI. This could add to the degradation of pathogenic immune complexes in diseased animals and increase the uptake of otherwise inflammatory immune complexes. While Akilesh et al. [53] found that *FcRn*<sup>-/-</sup> mice accumulated IgG at the GBM, they also suggested that in healthy conditions the FcRn in podocytes transports IgG from the filtration barrier to prevent immune complex-mediated renal damage and clogging of the filter. This might be another reason why IgG deposition increases with podocyte effacement: for one the filtration barrier is physically destroyed and begins to leak proteins into the urine but also podocytes that are damaged cannot transport IgG from the barrier adding insult to injury. Overall, we found that FcRn does not have effect on the immune complex degradation inside LSECs but plays a vital role in the metabolism of IgG molecules.

Of note, *FcRn*<sup>-/-</sup> mice have a C57BL/6 genetic background. The control animals for this experiment were therefore C57BL/6 WT mice. There are several differences between C57BL/6 and BALB/c mice used for the EAMN-model that could influence results: Immunoglobulin heavy chain variable (IGHV) gene repertoires are different between the two strains [87]. Moreover, BALB/c mice express IGHG2A resulting in mIgG2a but not IGHG2C which results in mIgG2c subclass. For C57BL/6 mice it is the opposite [111]. BALB/c mice have been found to favor T<sub>H</sub>2 responses, while C57BL/6 mice favor T<sub>H</sub>1 [112; 113]. Depending on the T<sub>H</sub> cells involved, different cytokines are expressed which determine the class switch of antibodies. For example, the engagement of T<sub>H</sub>2 cells leads to the production of IL-4, which initiates the class switch to IgG1 in mice, as compared to T<sub>H</sub>1 cells that produce INF $\gamma$ , which initiates the class switch to IgG2a and IgG3 [114]. Even though BALB/c mice are more efficient in BCR editing than

C57BL/6 mice, which makes the latter more susceptible to the development of autoimmune diseases [115], our THSD7A-EAMN model does not work in C57BL/6 mice. These mice develop antibody titers after immunization with complete and incompletes Freund's adjuvant and immune deposits inside the glomeruli but do not develop proteinuria (Seifert et al., unpublished data). The glycosylation between strains might influence the immune response, since C57BL/6 mice were found to have higher sialylation than BALB/c mice [116]. Sialylation was found to dampen immune responses, inhibit activation of B cells and decrease binding to the complement component C1q and consequently complement-mediated cytotoxicity [117–120]. All of these details have to be considered when analyzing data collected in different mouse strains.

#### **4.6 Administering AgFcs to healthy animals leads to mild antibody generation in a few mice**

WT BALB/c mice and chPLA2R mice were injected with small doses of either d1d2-SELF- or CysFnII-SELF-AgFc, respectively, over 6 consecutive weeks (Chapter 3.8). In a few animals, mild anti-THSD7A and anti-PLA2R titers were observed as well as faint mIgG staining along the GBM (Figure 16). However, no animal developed proteinuria. Compared to actively THSD7A-immunized animals, anti-THSD7A or anti-PLA2R titer were very low (<1 in non-immunized animals, >100 in actively immunized animals, <5 in AgFc-injected animals). Still, immune reactions to any therapeutical agent are concerning. Since the AgFcs are Fc fusion peptides it could explain why they are more immunogenic than full murine antibodies [121]. The domains providing antigen-specific binding towards autoantibodies could be subject to misfolding: THSD7A contains intra-molecular disulfide bonds throughout the protein [24], which could be required for correct full-length protein folding. In an AgFc where two domains are isolated from the full-length protein and its structure, disulfide mispairing might occur increasing the immunogenicity of the construct. We observed this in other double domain constructs of THSD7A where d15\_d16 formed multimers in a non-reducing SDS-PAGE while single domains as d15 occur as one band (Supplementary data, Figure 24A). Autoantibodies formed against our AgFcs might be cross-reactive with naturally folded THSD7A, causing the slight positive mIgG staining inside the kidneys. To determine whether the mIgG binding inside the kidneys is transient and reversible, animals would need to be analyzed several weeks after the last AgFc injections. Improvement on the structure of AgFcs could lead to less undesired side effects, which is discussed in 4.10.

#### **4.7 Clearance of large amounts of immune complexes does not lead to immune complex deposition**

Since administration of immune complexes can cause serum sickness including characteristic findings of glomerulonephritis [122], we wanted to examine the effects of large amounts of immune complexes inside the animals (Chapter 3.9). Therefore, we injected d1\_d2 (THSD7A) immunized *THSD7A*<sup>-/-</sup> mice with 300 µg of d1d2-SELF-AgFc or as a control, with an in this setting irrelevant AgFc (CysFnII-SELF). We observed high amounts of both AgFcs inside the FcγRIIB<sup>+</sup> LSECs, which was unexpected since CysFnII-SELF-AgFc cannot bind autoantibodies generated against domains d1\_d2 of THSD7A and consequently binds FcγRIIB on LSECs with low affinity (Figure 17). But when we accounted for the different degree of labeling (DOL) of d1d2-SELF-AgFc (3.5 moles dye/mole IgG) and CysFnII SELF-AgFc (60 moles dye/mol IgG), it explains why the MFI of CysFnII-SELF-AgFc injected animals inside the liver is the same as in animals that were able to form immune complexes which are taken up more efficiently than monomers of IgG. Degree of labeling describes how many molecules of the dye, in this case AF647, are bound to one mole of AgFc. The degree of labeling depends on the composition of the target proteins. The succinimidyl ester (NHS ester) couples to primary amines (R-NH<sub>2</sub>) in proteins and peptides [90]. Consequently, the coupling efficiency is dependent on the compositions of proteins and can differ greatly according to accessible primary amines [90]. We did not choose to correct for the DOL by injecting less AgFcs because that would result in different molar ratios to be compared in one experiment. Overall, we could not observe any immune complex deposition during our experiment, which indicates that in a healthy system large amounts of immune complexes can be degraded through LSECs and other protein degradation pathways. How that is influenced in a diseased state, we cannot say at this point.

#### **4.8 Treatment success depends on the limitations of the mouse models**

After uptake experiments and investigating the kinetics of immune complexes *in vivo*, we wanted to assess if early administration of AgFcs could lead to ameliorated disease progression. Therefore, we treated WT BALB/c that were immunized with d1\_d2 of THSD7A with AgFcs before they developed symptoms of MN. In this pre-treatment of THSD7A-associated MN mice, autoantibody titers and proteinuria could be reduced (p\* and p\*\*\*\*, respectively, Figure 19). Serum parameters such as cholesterol, triglycerides and BUN were unaffected in all groups which points to a mild disease progression also in control animals. We did not observe a significant reduction of mIgG deposition in the kidney (Figure 20). In accordance with the temporal pathogenesis model of Akiyama et al. [123], our mice developed autoantibody titers first which

correlates to phase A of the model (Figure 19C, week 6). Plasma cells produce autoantibodies against the podocyte antigens PLA2R or THSD7A, which then cause damage to the podocytes through immune deposit formation and slit diaphragm disruption in phase B and C. Here, the proteinuria sets in (Figure 19C, week 8). During remission of the immunological disease activity, autoantibody titers decrease while proteinuria temporarily lags behind (phase D). Most importantly though, IgG deposits remain until the podocyte injury has been repaired (phase E). In the four weeks of our pre-treatment experiment, mIgG deposits remained unaffected (Figure 20). So, while we were able to stop the clinically active phase (phase C) in decreasing autoantibody titers and proteinuria, we likely stopped the experiment too early to determine an effect on the mIgG clearance in the kidney coherent with phase E.

The Treatment of THSD7A-immunized WT BALB/c mice (domains d1\_d2 and d15\_d16) after the development of proteinuria (>3 g/g) was successful in decreasing the autoantibody titer as well as the proteinuria (Chapter 3.12). Only 8 out of 20 immunized mice exceeded 3 g/g so 3 mice were treated with CysFnII-SELF- and 5 with d1d2 SELF-AgFc and d15 SELF-AgFc twice a week for four consecutive weeks. The results of this experiment can only be interpreted with care due to the small number of experimented animals and have to be investigated further. The De-Ritis ratio revealed no significant increase in either group, which indicates no liver toxicity during the treatment time in adult animals (Figure 21). An increased De-Ritis ratio indicates not only acute or chronic hepatitis but also chronic kidney disease [124]. CKD can be caused by drug induced liver injury (DILI), which can be induced by the therapeutic itself, its metabolites, or through its mechanism of action [125]. mIgG deposition inside the kidneys could not be decreased through AgFc treatment but as aforementioned, this could be due to timing consistent with Akiyama's temporal pathogenesis model [117]. Of note, in the absence of complement C3b, the hepatic uptake is increased [126]. Since Seifert et al. (unpublished data) found immune complexes containing complement components deposited along the GBM in actively immunized WT BALB/c mice, this could influence the degradation of AgFc/autoantibody complexes inside the liver and ameliorate treatment effects. Interestingly, we observed spontaneous remission in animals or a general mild disease progression. This is in accordance with other cohorts our group has experimented (Seifert et al., unpublished data). The more double domains are used for immunization the more severe the disease progression. In this cohort we immunized with only two double domains of THSD7A: d1\_d2 and d15\_d16. Higher ACRs can be achieved when immunizing with at least 4 double domains: d1\_d2, d9\_d10, d11\_d12, and d15\_d16 (Seifert et al., unpublished data). We decided against immunizing with 4 double domains because the d9d10- and d13d14-AgFcs presented as multimers in a non-reducing SDS-PAGE (Supplementary data, Figure 24A). This misfolding can influence immune complex size and also increase

immunogenicity [127]. For further experiments, a better compromise between i) a stable mouse model with high ACRs and no spontaneous remissions and ii) properly folded AgFc that block all epitopes needs to be made to assess the therapeutic potential for THSD7A-associated MN.

Treatment of hPLA2R autoimmune mice was partially successful (Chapter 3.13): though animals injected with CysFnII-WT-, CTLD1/2-WT- and CTLD7/8-WT-AgFc (treated) showed less proteinuria ( $p=0.0526$ ) and a delayed onset of autoantibody titers, we saw an increase in the De-Ritis ratio in treated animals compared to healthy controls or d15-WT-AgFc treated ones (Figure 22). Since we did not observe an increased De-Ritis ratio in adult WT BALB/c immunized with d1\_d2 and d15\_d16 of THSD7A, which were treated with higher doses of AgFc, it indicates that the increased De-Ritis ratio is due to the young age of the transgenic hPLA2R mice and the severity of the disease progression, not necessarily the impact of the AgFc treatment. In this particular mouse model, treatment begins at 3 weeks after birth when autoantibody titers emerge and mice are weaned off from their mothers. According to Fresquet et al.'s [19] “kidney as a sink” theory, mice could produce autoantibodies before that time and are bound on podocytes expressing PLA2R so they cannot be detected inside the serum until the amount of produced autoantibody exceeds the binding capacity to their target. Only after that the antibodies would be detected in the serum. If that is the case, our treatment might be too late to ameliorate the damage already done to the kidney in combination with an immature immune complex degradation system in these young animals. Furthermore, as stated by Tomas et al. [74] the “majority” of animals did not show IgG deposition along the GBM at 3 weeks of age, which indicates that there might be exceptions. Some animals were severely sick by week 5 after birth, while some were still without prominent proteinuria until week 6. The age of these animals might also have an impact on the treatment results: B cells display a premature phenotype until week 4 [128] and T and B cell development is ongoing until week 26 [129]. Jeong et al. [130] found that younger mice (week 2) are more susceptible to drug-induced liver injury (DILI) than older mice (week 8). Considering all these factors this might explain the ambiguous treatment results in these animals.

Lastly, the translation to the human system is challenging: diversity of B cells is introduced through the rearrangement of VD and DJ junctions. On average, 7.7 and 6.5 nucleotides are added in the human VD and DJ junctions [131]. Consequently, the diversity of the human naïve B cell repertoire is expanded through somatic point mutations, which results in an average of mutations of 16.5 in hIgG3 and 21.8 in hIgG4 [88]. This leads to a vast diversity among CDR3 regions and deep sequencing revealed that in thousands of human samples not one shared CDR3 sequence could be found [132]. Mice on the other hand, have a more germline focused repertoire resulting on average in 3 or 4 added nucleotides. So more sequences tend to be unmutated [87].

Autoantibodies generated against podocytes antigens in mice therefore do not reflect the human autoantibodies in MN when it comes to diversity.

Our findings of the ambiguous effects of antigen-specific AgFcs as a therapy for MN need further investigations, in order to understand the intricate pathomechanisms of disease development and how to treat it effectively.

#### **4.9 Enhancements of AgFcs in combination with new antigen-specific therapies could increase therapeutic potency**

To increase the potency of the AgFcs as an antigen-specific therapy multiple adjustments to the fusion peptides could be made: first, since wrong protein fusion linkers can lead to misfolding of the proteins [133], low yield in protein production [134], and impaired bioreactivity [135], the design of the linkers could be improved. The AgFcs are fused to the Fc part through a short connector peptide linker AAA. Generally, linkers can be divided into two categories: rigid and flexible. Rigid linkers provide a stable structure and often form  $\alpha$ -helices, resulting in a closely packed backbone [136]. They are used to separate different protein domains fused together and reduce their intermolecular interactions [137]. Flexible linkers like the Glycine/Serine (GS) linker provide flexibility, improve solubility and are used to increase spatial separations between domains as in e.g., single chain variable fragments (scFvs) [138]. For the AgFcs an increased spatial separation of domains and Fc part could lead to simultaneous binding of BCR and Fc $\gamma$ RIIB on autoreactive B cells. Whenever BCR and Fc $\gamma$ RIIB are engaged simultaneously on a pre-B cell, it leads to apoptosis of the respective autoreactive B cell and is a mechanism of central tolerance [48]. Since mature plasma cells do not express a BCR anymore, this approach would be rather pre-emptive than therapeutic. Glycosylation pattern should also be considered to enhance the potency of AgFcs: IgGs are glycosylated at Asn297 of the C<sub>H</sub>2 domain and the glycans act as spacers between the two heavy chains. They are important for structural integrity as well as influencing the immune response [139]. Differential glycosylation leads to adjustments in affinity of IgG subtypes to Fc $\gamma$ Rs [41]. For example, defucosylated IgG2a and IgG2b was found to have an increased affinity towards Fc $\gamma$ RIIB and Fc $\gamma$ RIV resulting in more mediated ADCC [140]. In contrast, glycans rich in terminal sialic acid and galactose residues had an anti-inflammatory effect [141]. Additionally, cell culture media and the choice of expression system influences the glycosylation of recombinant produced IgGs [142; 143], in our case AgFcs. Secondly, with deeper knowledge of the target antigen structures, the size of the domains coupled to the Fc part could be decreased. With solving of the protein crystal structure of PLA2R just recently this route is now accessible. Fresquet et al. [23] determined two peptide sequences VIQSES and SVLTLENC inside the CysR domain as the amino acids involved in the binding of autoantibodies, which narrowed

down the epitope region from the former P28mer sequence. Hence, antibodies binding these peptides could be selected by phage panning from libraries of PLA2R-positive patients. Recombinant antibodies created in this manner can be cloned into IgG format or scFv-Fc, affinity maturation can lead to even better binders with higher affinities, while yields in production can be increased. Further modifications could include insertions of FcγRIIB and/or FcRn increasing affinity mutations as well as histidine mutagenesis to create a “sweeping antibody” as designed by Igawa et al. [39]. This would be an improvement to the AgFcs presented in this study, for sweeping antibodies with pH dependent binding are recycled to the surface without the antigen still bound to it, therefore reducing the amount of therapeutic needed to deplete autoantibodies [38]. Additionally, immunogenicity could be reduced since full mouse or human antibodies are less immunogenic than fusion peptides like the AgFcs [144]. Thirdly, the size of the generated immune complexes *in vivo* should be assessed. While Ganesan et al. [59] found that antigen excess is essential to avoid the point of equivalence (POE) and therefore deposition of insoluble immune complexes in the kidney, Lux et al. [101] found that larger immune complexes have a higher affinity towards FcγRs but also trigger more IL-6 release than smaller complexes. For the treatment of mice or patients that would result in smaller doses of therapeutic AgFcs to avoid the POE and subsequent immune complex deposition as well as the increase of IL-6, a pro-inflammatory cytokine. For this, other applications could be explored like subcutaneous depots for humans or miniature osmotic pumps for mice that can be loaded with AgFc solution and implanted beneath the skin for continuous release of AgFc. Lastly, another antigen-specific therapy for MN could lie in bispecific antibodies: Normally antibodies contain two analogous antigen-binding sites and are monospecific and bivalent. Bispecific antibodies contain two different antigen-binding sites and can therefore bind more than one target. In MN patients where multiple domains are targeted along the extracellular part of the protein [24], multiple bispecific antibodies could connect CD3 expressing cytotoxic T cells with every domain-specific autoantibody producing B cells (Figure 23A). Similar to the approved therapeutic bispecific antibody Catumaxomab, which connects CD3 T cells with tumor cells expressing EpCam [145], a MN-bispecific antibody could connect CD3 T cells with B cells expressing the BCR to d1\_d2 on their surface. The Fc part binds a FcγR (either FcγRI, FcγRIIa or FcγRIII) on an accessory immune cell. Effector functions could then be edited by insertion of mutations like SELF (higher affinity towards FcγRIIB) [36] or YTE (higher affinity towards FcRn at pH 6) [146].

Since we saw only the depletion of autoantibodies from the circulation and could not assess the impact on B cells or autoantibody producing plasma cells, a combination therapy of AgFcs and consecutively injected chimeric autoantibody receptor (CAAR) T-cells might improve the outcome and decrease the chance of relapse for patients. Similar to the CAR T cell approach used

for B cell lymphomas [147], peripheral blood mononuclear cells (PBMCs) are isolated from the patients' blood and induced to proliferate through IL-2 and anti-CD3 antibody administration. T cells are then transduced with the CAAR of interest e.g., immuno-dominant domains of THSD7A or PLA2R, and transfused back into the patient. CAAR T cells bind to B cells that express the corresponding BCR of their CAAR. Through intracellular signaling domains such as CD3 $\zeta$ , the CAAR T cells produce granzyme B and perforins thus eliminating THSD7A- or PLA2R-specific autoantibody producing B cells (Figure 23B). This approach has been successful in a pemphigus vulgaris model mouse model eliminating anti-desmoglein 3 antibodies [148; 73; 149].

Additionally, to specifically deplete autoantibodies from the circulation even smaller molecules like immunodominant domains of THSD7A or PLA2R coupled to the ApoB-100 sequence RLTRKRGLK could be used. Akhter et al. [150] found that this sequence of ApoB-100, which is a mediator for the association of LDL and its receptor, enabled maleimide-PEG-DSPE to be taken up rapidly and efficiently into LSECs. LSECs express the low-density lipoprotein receptor protein-1 (LRP-1) and take up LDL as well [151]. They identified the mechanism of uptake through an unknown target receptor rather than a non-specific binding to the cell surface, which they hypothesized in the beginning. Liu et al. [95] took these findings and developed nanoparticles decorated with ovalbumin (OVA) to sensitize mice that were later challenged with the aerosolized antigen. They also observed the nanoparticles specifically targeted LSECs, which act as antigen presenting cells (APCs), through the ApoB-100 sequence. LSECs took up the particles and presented OVA-fragments through MHCII to CD4<sup>+</sup> T cells and produced IL-10 and TGF- $\beta$ . In this anti-inflammatory environment regulatory T cells (Tregs) were formed, which induced antigen-specific immune tolerance to the later introduced OVA (Figure 23C). Both approaches could be used to clear the blood of autoantibody-domain/ApoB-100 complexes through LSECs without involving the Fc $\gamma$ Rs allowing for less unwanted side effects targeting Fc $\gamma$ Rs might ensure and restore tolerance against the self-antigens.

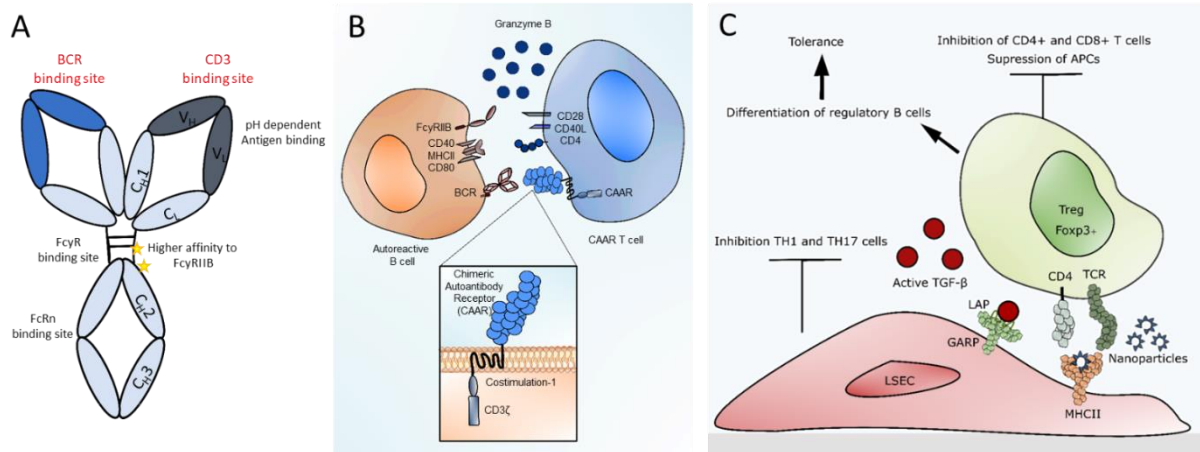


**Figure 23: Antigen-specific therapies for MN.** (A) Potential bispecific antibody combining CD3 antigen binding (dark grey) and specific anti-podocyte BCR (dark blue) binding. Mutations to increase affinity towards FcγRIIB are indicated by stars. FcγR binding site is located in the hinge region while FcRn binding site is between C<sub>H</sub>2 and C<sub>H</sub>3. pH dependent antigen binding can be achieved through histidine mutagenesis in the antigen binding region to create a sweeping antibody. (B) Chimeric autoantibody receptor (CAAR) T-cells could be used in a combination therapy of MN. The CAAR (magnified box) provides specific binding to autoreactive B cells through immuno-dominant domains of THSD7A or PLA2R. Upon binding the intracellular costimulation-1 and CD3ζ domains induce the release of granzyme B and perforins, eliminating the autoreactive B cell. (B) Nanoparticles coated with antigens target LSECs through their ApoB-100 sequence. TGF-β is produced as a precursor form, including latency-associated peptide (LAP) and mature TGF-β, anchored by the glycoprotein A repetitions predominant (GARP), a transmembrane protein. Upon cleavage active TGF-β is released and inhibits T<sub>H</sub>1 and T<sub>H</sub>17 cells. After endocytosis of the nanoparticles, peptides of the coated antigens, e.g. immuno-dominant domains of THSD7A or PLA2R, are presented by MHCII. Foxp3 expressing Tregs are engaged by CD4 and TCR co-stimulation and initiate the suppression of APCs, CD4<sup>+</sup> and CD8<sup>+</sup> cells, while simultaneously triggering regulatory B cells. All this leads to tolerance towards the antigens coated to the nanoparticles, in the case of MN patient's domains of THSD7A or PLA2R.

## 5 Conclusion and Outlook

To sum up our findings, we developed domain-specific AgFcs that bind antibodies against THSD7A and PLA2R and help degrade them through the endogenous degradation systems inside the liver. For the translation to human patients, more experiments have to be conducted. To portray the human situation better, human IgG backbones would have to be fused to human domains of THSD7A or PLA2R. For similar *in vitro* uptake experiments as we performed in this thesis, patient's autoantibodies can be purified through an AminoLink™ resin coupled to THSD7A or PLA2R and the domain recognition pattern of each patient could be identified. Fitting AgFcs can be built to accommodate each patient's needs. The purified autoantibodies can be linked to fluorescent dyes and human primary LSECs can be used to investigate the *in vitro* uptake of immune complexes consisting of human AgFcs and the patients' autoantibodies. For *in vivo* experiments, chimeric PLA2R-mice could be used for they can be immunized with human PLA2R and develop typical signs of MN (Tomas et al., data not published). Furthermore, mice with humanized FcγRs can be utilized, e.g. to correctly reflect affinities of the SELF mutation towards the FcγRs. With the rise of new technologies such as TCR and BCR epitope sequencing, epitopes of patient's autoantibodies could be identified which in turn leads to the generation of "sweeping antibodies" as therapeutics. They have several advantages compared to the AgFcs we created: a whole human IgG molecule is less immunogenic than our peptide Fc-fusion proteins, folding and stability are also likely to improve due to the structural changes. Through histidine mutagenesis pH dependent binding can be introduced to the antigen binding domain. This creates molecules that can direct autoantibodies towards degradation multiple times without being degraded themselves, reducing the amount and interval they would have to be administered to the patients. With more research, we are certain that potency can be increased while adverse effects minimized. Overall, we created a new antigen-specific therapeutic agent that could on day improve the care for patients and prevent disease progression to end-stage kidney disease and dialysis.

## 6 Annex

### 6.1 Supplementary data

The sequences of all used AgFcs are listed beneath. AAA: Linker between peptide and mIgG Fc part; green: cysteine in the upper hinge was mutated to serine; yellow: cysteines needed for structural integrity through disulphide bonds; turquoise: amino acids mutated to create the SELF-Fc IgG.

d1d2-SELF

AAQGDTEVPTLYLWKTGPWGRCMGDDCGPGGIQTRAVWCAHVEGWTTLHTNCKQAVRPSNQ  
 QNCFKVC DWHKELYDWRLGTWDR CQPVISKSLEKSRECVKGEEGIQVREIMCIQKDKDIPAEDI  
 ICEYFEPKPLLEQA CLIPCQAAAPT IKPSPPCKCPAPNLLGGPSVFIFPPKIKDVL MISLSPIVT CVV  
 VDV EEDDPDVQISW FVNNVEVHTAQTQTHREDY NSTLRVVSALPIQH QDWMSGKEFK CKVNN  
 KDFPAPIERTSKPKGSVRAPQVYVLPPEEEMTKKQVTLT CMVTDFMPEDIYVEWTNNGKTELN  
 YKNTEPVLDSGSYFMYSKLRVEKKNWVERNSYS CSVVHEGLHNHHTTKSFSRTPGK

d1d2-WT

AAQGDTEVPTLYLWKTGPWGRCMGDDCGPGGIQTRAVWCAHVEGWTTLHTNCKQAVRPSNQ  
 QNCFKVC DWHKELYDWRLGTWDR CQPVISKSLEKSRECVKGEEGIQVREIMCIQKDKDIPAEDI  
 ICEYFEPKPLLEQA CLIPCQAAAPT IKPSPPCKCPAPNLLGGPSVFIFPPKIKDVL MISLSPIVT CVV  
 VDVS EDDPDVQISW FVNNVEVHTAQTQTHREDY NSTLRVVSALPIQH QDWMSGKEFK CKVNN  
 KDL PAPIERTISKPKGSVRAPQVYVLPPEEEMTKKQVTLT CMVTDFMPEDIYVEWTNNGKTEL  
 NYKNTEPVLDSGSYFMYSKLRVEKKNWVERNSYS CSVVHEGLHNHHTTKSFSRTPGK

d15-SELF

MGDNDIHFAFLSTGAH SMAQYIWVTEPWSVCKVTFVDMRDNCGEGVQTRKVR CMQNTADGP  
 SEHVEDYLC DPEDMPLGSRECKLPCPAAAPT IKPSPPCKCPAPNLLGGPSVFIFPPKIKDVL MISLS  
 PIVT CVVV DV EEDDPDVQISW FVNNVEVHTAQTQTHREDY NSTLRVVSALPIQH QDWMSGKEF  
 K CKVNNKDFPAPIERTISKPKGSVRAPQVYVLPPEEEMTKKQVTLT CMVTDFMPEDIYVEWTN  
 NGKTELNYKNTEPVLDSGSYFMYSKLRVEKKNWVERNSYS CSVVHEGLHNHHTTKSFSRTPG  
 K

d15-WT

MGDNDIHFAFLSTGAH SMAQYIWVTEPWSVCKVTFVDMRDNCGEGVQTRKVR CMQNTADGP  
 SEHVEDYLC DPEDMPLGSRECKLPCPAAAPT IKPSPPCKCPAPNLLGGPSVFIFPPKIKDVL MISLS  
 PIVT CVVV DVSEDDPDVQISW FVNNVEVHTAQTQTHREDY NSTLRVVSALPIQH QDWMSGKEF  
 K CKVNNKDL PAPIERTISKPKGSVRAPQVYVLPPEEEMTKKQVTLT CMVTDFMPEDIYVEWTN  
 NGKTELNYKNTEPVLDSGSYFMYSKLRVEKKNWVERNSYS CSVVHEGLHNHHTTKSFSRTPG  
 K

CysFnII-WT

MGDNDIHFAFLSTGAH SMAEGVAAALTPERLLEWQDKGIFVIQSESLKKCIQAGKSVLTLENCK  
 QANKHMLWKVWSNHGLFNIGGSGCLGLNFSAPEQPLSLYECDSTLVSLRWRCNRKMITGPLQY  
 SVQVAHDNTVVASRKYIHKWISYSGGGDICEYLHKDLHTIKGNTHGMPCMFPPQYNHQWHH  
 ECTREGREDDLWCATTSRYERDEKWFPCDPTSAEAAAPT IKPSPPCKCPAPNLLGGPSVFIFPP  
 KIKDVL MISLSPIVT CVVV DVSEDDPDVQISW FVNNVEVHTAQTQTHREDY NSTLRVVSALPIQH  
 QDWMSGKEFK CKVNNKDL PAPIERTISKPKGSVRAPQVYVLPPEEEMTKKQVTLT CMVTDFM  
 PEDIYVEWTNNGKTELNYKNTEPVLDSGSYFMYSKLRVEKKNWVERNSYS CSVVHEGLHNH  
 HTTKSFSRTPGK

## CysFnII-SELF

MGDNDIHFAFLSTGAHSM AEGVAAALTPERLLEWQDKGIFVIQSESLKKCIQAGKSVLTLENCK  
 QANKHMLWKWVSNHGLFNIGGSGCLGLNFSAPEQPLSLYECDSTLVSLRWRCNRKMITGPLQY  
 SVQVAHDNTVVASRKYIHKWISYSGGGDICEYLHKDLHTIKGNTHGMPCMFPPQYNHQQWHH  
 ECTREGREDDLLWCATTSRYERDEKWFPCPDPTSAEAAAPTIKPSPPCCKCPAPNLLGGPSVFIFPP  
 KIKDVLMLISLPIVTCVVVDVEEDDPDVQISWVFNVEVHTAQTQTHREDYNSTLRVVSALPIQ  
 HQDWMSGKEFKCKVNNKDFPAPIERTISKPKGSVRAPQVYVLPPEEEMTKKQVTLT<sup>C</sup>CVMTDF  
 MPEDIYVEWTNNGKTELNYKNTEPVLDSGYSYFMYSKLRVEKKNWVERNSYS<sup>C</sup>SVVHEGLHN  
 HHTTKSFSRTPGK

## CTLD1/2-WT

MGDNDIHFAFLSTGAHSMATSAEVGCDTIWEKDLNSHICYQFNLLSSLSWSEAHSSCQMGGTL  
 LSTITETEENFIREHMSSKTVEVWMGLNQLDEHAGWQWSDGTPLNYLNWSPEVNFEPFVEDHC  
 GTFSSFMPSAWRSRDCESTLPYICKKYLNHIDHEIVEKDAWKYYATHCEPGWNPYNRNCYKLO  
 KEEKTWHEALRSCQADNSALIDITSLAEVEFLVTLGDNASETWIGLSSNKIPVSFEWSNDSSVI  
 FTNWHITLPHIFPNRSQLCVSAEQSEGHWKVKNCEERLFYICKKAGHVLSDAEAAAPTIKPSPPC<sup>C</sup>  
 KCPAPNLLGGPSVFIFPPKIKDVLMLISLPIVTCVVVDVSEDDPDVQISWVFNVEVHTAQTQTH  
 REDYNSTLRVVSALPIQHQDWMSGKEFKCKVNNKDLPAPIERTISKPKGSVRAPQVYVLPPEEE  
 MTKKQVTLT<sup>C</sup>CVMTDFMPEDIYVEWTNNGKTELNYKNTEPVLDSGYSYFMYSKLRVEKKNWV  
 ERNSYS<sup>C</sup>SVVHEGLHNHHTTKSFSRTPGK

## CTLD7/8-WT

MGDNDIHFAFLSTGAHSMAPNTLEYGNRTYKIINANMTWYAAIKTCLMHKAQLVSITDQYHQSF  
 LTVVLNRLGYAHWIGLFTTDNGLNFDWSDGTKSSFTFWKDEESSLLGDCVFADSNRWHSTAC  
 ESFLQGAICHVPPETROQSEHPELCSETSIPWIKFKSNCYSFSTVLDSMSFEAAHEFCCKEKSNTLTI  
 KDEAENAFLEELFAFGSSVQMVWLNAQFDGNNETIKWFDGTPTDQSNWGIRKPDTDYFKPHH  
 CVALRIPEGLWQLSPCQEKKGFKMEAAAPTIKPSPPCCKCPAPNLLGGPSVFIFPPKIKDVLMLISL  
 SPIVTCVVVDVSEDDPDVQISWVFNVEVHTAQTQTHREDYNSTLRVVSALPIQHQDWMSGKE  
 FKCKVNNKDLPAPIERTISKPKGSVRAPQVYVLPPEEEMTKKQVTLT<sup>C</sup>CVMTDFMPEDIYVEWT  
 NNGKTELNYKNTEPVLDSGYSYFMYSKLRVEKKNWVERNSYS<sup>C</sup>SVVHEGLHNHHTTKSFSRTP  
 GK

Figure 24 shows the remaining AgFcs in a non-reducing SDS-PAGE. The d15d16-AgFc constructs showed multiple bands with non-reducing sample buffer in contrary to all other constructs which presented as a single band (Figure 24A). For that reason, d15-AgFcs were cloned and used throughout the experiments. The constructs used for treatment of the transgenic human PLA2R-mice are shown in Figure 24B.

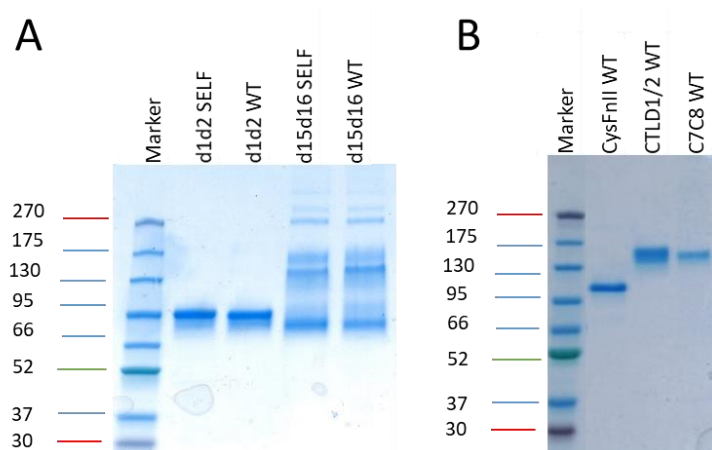


**Figure 24: Non-reducing SDS-PAGE of remaining AgFcs.** (A) Coomassie blue staining of the d1d2- and d15d16-AgFc constructs. While d1d2-AgFc presents as a single band in the non-reducing SDS-PAGE, d15d16-AgFcs formed multimers and presented with multiple bands due to intramolecular cysteine bridging. Therefore, d15-AgFc constructs were built, which do not form multimers. (B) Coomassie blue staining of AgFcs used to treat transgenic human PLA2R-mice. CysFnII-WT-AgFc is about 103 kDa in size and runs between the 95 and 130 kDa bands of the marker, while CTLD1/2- and CTLD7/8-WT-AgFc are 116 kDa in size and run between the marker bands 130 and 170 kDa under non-reducing conditions.

Table 6-1 shows the different batches of AgFcs couple to fluorochromes and their degree of labelling.

*Table 6-1: Degree of labelling for fluorochrome coupled AgFcs*

AgFc	degree of labelling (DOL) [mole dye/mole IgG]
d1d2-WT	2,69
d1d2-SELF	4,5
d1d2-LALAPG	46
d15-WT	0,96
d15-SELF	3,25
CysFnII-WT	34,3
CysFnII-SELF	60,8

## 6.2 Abbreviations

*Table 6-2: List of abbreviations used in this study*

### Abbreviation

%	Percent
°C	Degree Celsius
µg	Microgram(s)
µL	Microliter(s)
µM	Micro molar
3' UTR	3' untranslated region
ACR	Albumin creatinine ratio
ADCC	antibody dependent cellular cytotoxicity
AF	Alexa Fluor
AgFc	antigen Fc fusion construct

<b>ALT</b>	alanine aminotransferase
<b>anti-d1_d2 mAb</b>	monoclonal antibody binding domains 1 and 2 of THSD7A
<b>anti-d15 mAb</b>	monoclonal antibody binding domain 15 of THSD7A
<b>anti-CysR mAb</b>	monoclonal antibody binding domain CysR of PLA2R
<b>APC</b>	antigen presenting cell
<b>AST</b>	Aspartate aminotransferase
<b>BCR</b>	B cell receptor
<b>bp</b>	Basepair(s)
<b>BSA</b>	Bovine serum albumine
<b>bsa</b>	Buried surface area
<b>BUN</b>	blood urea nitrogen
<b>CAAR</b>	chimeric autoantobody receptor
<b>CDR3</b>	Complementarity-determining region 3
<b>CFA</b>	complete freund's adjuvants
<b>CH2</b>	constant heavy chain 2
<b>CTLD</b>	C-type lectin-like domain
<b>CTLD1/2-AgFc</b>	AgFc with domains CTLD 1 and 2 of PLA2R as Fab part
<b>CTLD7/8-AgFc</b>	AgFc with domains CTLD 7 and 8 of PLA2R as Fab part
<b>CysFnII-AgFc</b>	AgFc with domains CysR and FnII of PLA2R as Fab part, binds anti-CysR mAb
<b>CysR</b>	Cysteine-rich domain
<b>d1_d2</b>	domains 1 and 2 of THSD7A
<b>d1d2-AgFc</b>	AgFc with domains 1 and 2 of THSD7A as Fab part, binds anti-d1_d2 mAb
<b>d15-AgFc</b>	AgFc with domain 15 of THSD7A as Fab part, binds anti-d15 mAb
<b>DC</b>	dendritic cell
<b>DJ</b>	Diversity-joining
<b>DNA</b>	Deoxyribonucleic acid
<b>DOL</b>	degree of labeling
<b>E. coli</b>	Escherichia coli
<b>EAMN</b>	experimental autoimmune membranous nephropathy
<b>EDTA</b>	Ethylenediaminetetraacetic acid
<b>EEA</b>	Early Endosome Antigen
<b>ELISA</b>	Enzyme linked immunosorbent assay
<b>EpCam</b>	epithelial cell adhesion molecule
<b>EXT</b>	exotosin
<b>FACS</b>	Fluorescence Activated Cell Sorting
<b>FcRn</b>	neonatal Fc receptor
<b>FcRn-/-</b>	neonatal Fc receptor knock out
<b>FcyR</b>	Fc gamma receptor
<b>FITC</b>	fluorescein-5-isothiocyanate
<b>FnII</b>	fibronectin II domain
<b>g</b>	Gram(s), earth acceleration
<b>GARP</b>	Glycoprotein A repetitions predominant
<b>GBM</b>	glomerular basement membrane
<b>GS</b>	glycine/serine
<b>h</b>	Hour(s)
<b>HEK</b>	human embryonic kidney cells

<b>hpi</b>	hours post injection
<b>HRP</b>	Horse reddish peroxidase
<b>ICD</b>	immune complex disease
<b>IF</b>	Immunofluorescence
<b>IFA</b>	incomplete freund's adjuvats
<b>IgG</b>	Immunoglobuline G
<b>IGHV</b>	Immunoglobuline heavy chain variable
<b>IgM</b>	Immunoglobuline M
<b>IHC</b>	immunohistochemistry
<b>IL-2</b>	interleukin-2
<b>IL-6R</b>	interleukin-6 receptor
<b>INF-<math>\gamma</math></b>	interferone gamma
<b>ip</b>	intraperitoneally
<b>ITAM</b>	immunoreceptor tyrosine-based activation motif
<b>iv</b>	intravenous
<b>IVIS</b>	in vivo imaging system
<b>kb</b>	Kilobase(s)
<b>kDa</b>	Kilodalton(s)
<b>KO</b>	knock out
<b>LALAPG</b>	L234A/L235A, P329G
<b>LAP</b>	latency-associated peptide
<b>LDL</b>	low density lipoprotein
<b>LRP-1</b>	low-density lipoprotein receptor protein 1
<b>LSEC</b>	liver sinusoidal endothelial cell
<b>M</b>	Molar
<b>mA</b>	Miliampere(s)
<b>mAb</b>	monoclonal antibody
<b>MFI</b>	mean fluorescent intensity
<b>mg</b>	Milligram(s)
<b>MHCII</b>	major histocompatibility complex II
<b>min</b>	Minute(s)
<b>mL</b>	Milliliter(s)
<b>mM</b>	Milimolar
<b>MN</b>	Membranous nephropathy
<b>mRNA</b>	Messenger RNA
<b>MTP</b>	Microtiterplate
<b>MW</b>	Molecular weight
<b>NELL-1</b>	Neural epidermal growth factor-like 1 protein
<b>ng</b>	Nanogram(s)
<b>NHS</b>	N-Hydroxysuccinimide
<b>NK</b>	natural killer cells
<b>nM</b>	Nanomolar(s)
<b>nm</b>	Nanometer(s)
<b>nt</b>	Nucleotide(s)
<b>OD450</b>	Optical density at wave length 450 nm
<b>ORF</b>	Open reading frame

<b>OVA</b>	ovalbumin
<b>PAGE</b>	Polyacrylamide gelectrophoresis
<b>PBMC</b>	Peripheral Blood Mononuclear Cell
<b>PBS</b>	Phosphate buffered saline
<b>PCDH7</b>	Protocadherin-7
<b>PCR</b>	Polymerase chain reaction
<b>PE</b>	phycoerythrin
<b>PLA2R</b>	Phospholipase A2 receptor
<b>pLSEC</b>	primary LSECs
<b>POE</b>	point of equivalence
<b>rb</b>	rabbit
<b>RNA</b>	Ribonucleic acid
<b>rpm</b>	Rounds per minute
<b>s</b>	Second(s)
<b>sc</b>	subcutaneous
<b>scFv</b>	Single chain fragment variable
<b>SDS</b>	Sodium dodecyl sulfate
<b>SELF</b>	S267E/L328F
<b>SIC</b>	small immune complex
<b>sPLA2</b>	Secretory phospholipase A2
<b>TCR</b>	T cell receptor
<b>TH cells</b>	T helper cells
<b>THBS1</b>	Thrombospondin-1
<b>THSD7A</b>	thrombospondin type 1 domain-containing protein 7A
<b>THSD7A-/-</b>	thrombospondin type 1 domain-containing protein 7A knock out
<b>TNF-a</b>	tumor necrose factor a
<b>TRE</b>	Total radiant efficiency
<b>TRE/g</b>	Total radiant efficiency per g organ weight
<b>U</b>	Unit(s)
<b>V</b>	Volt(s)
<b>v/v</b>	Volume per volume
<b>VD</b>	Variable-diversity
<b>w/v</b>	Weight per volume
<b>WT</b>	Wildtype

## 7 References

- [1] J.K.J. Deegens and J.F.M. Wetzels, Membranous nephropathy in the older adult: epidemiology, diagnosis and management, *Drugs & aging*, 24 (9) (2007), 717–732.
- [2] M. Uhlén, L. Fagerberg, B.M. Hallström, C. Lindskog, P. Oksvold, A. Mardinoglu, Å. Sivertsson, C. Kampf, E. Sjöstedt, A. Asplund, I. Olsson, K. Edlund, E. Lundberg, S. Navani, C.A.-K. Szigartyo, J. Odeberg, D. Djureinovic, J.O. Takanen, S. Hober, T. Alm, P.-H. Edqvist, H. Berling, H. Tegel, J. Mulder, J. Rockberg, P. Nilsson, J.M. Schwenk, M. Hamsten, K. von Feilitzen, M. Forsberg, L. Persson, F. Johansson, M. Zwahlen, G. von Heijne, J. Nielsen and F. Pontén, Proteomics. Tissue-based map of the human proteome, *Science (New York, N.Y.)*, 347 (6220) (2015), 1260419.
- [3] J. Reiser and M.M. Altintas, *Podocytes*, F1000Research, 5 (2016).
- [4] R.J. Glassock, Secondary membranous glomerulonephritis, *Nephrology, dialysis, transplantation : official publication of the European Dialysis and Transplant Association - European Renal Association*, 7 Suppl 1 (1992), 64–71.
- [5] F. von Haxthausen, L. Reinhard, H.O. Pinnschmidt, M. Rink, A. Soave, E. Hoxha and R.A.K. Stahl, Antigen-Specific IgG Subclasses in Primary and Malignancy-Associated Membranous Nephropathy, *Frontiers in immunology*, 9 (2018), 3035.
- [6] G. Haddad, J.M. Lorenzen, H. Ma, N. de Haan, H. Seeger, C. Zaghrini, S. Brandt, M. Kölling, U. Wegmann, B. Kiss, G. Pál, P. Gál, R.P. Wüthrich, M. Wuhrer, L.H. Beck, D.J. Salant, G. Lambeau and A.D. Kistler, Altered glycosylation of IgG4 promotes lectin complement pathway activation in anti-PLA2R1-associated membranous nephropathy, *The Journal of clinical investigation*, 131 (5) (2021).
- [7] L. Seifert, Dissertation, Universität Hamburg (2020).
- [8] N.M. Tomas, L.H. Beck, C. Meyer-Schwesinger, B. Seitz-Polski, H. Ma, G. Zahner, G. Dolla, E. Hoxha, U. Helmchen, A.-S. Dabert-Gay, D. Debayle, M. Merchant, J. Klein, D.J. Salant, R.A.K. Stahl and G. Lambeau, Thrombospondin type-1 domain-containing 7A in idiopathic membranous nephropathy, *The New England journal of medicine*, 371 (24) (2014), 2277–2287.
- [9] L.H. Beck, R.G.B. Bonegio, G. Lambeau, D.M. Beck, D.W. Powell, T.D. Cummins, J.B. Klein and D.J. Salant, M-type phospholipase A2 receptor as target antigen in idiopathic membranous nephropathy, *The New England journal of medicine*, 361 (1) (2009), 11–21.
- [10] S. Sethi, B.J. Madden, H. Debiec, M.C. Charlesworth, L. Gross, A. Ravindran, A.M. Hummel, U. Specks, F.C. Fervenza and P. Ronco, Exostosin 1/Exostosin 2-Associated Membranous Nephropathy, *Journal of the American Society of Nephrology : JASN*, 30 (6) (2019), 1123–1136.
- [11] S. Sethi, H. Debiec, B. Madden, M. Vivarelli, M.C. Charlesworth, A. Ravindran, L. Gross, T. Ulinski, D. Buob, C.L. Tran, F. Emma, F. Diomedi-Camassei, F.C. Fervenza and P. Ronco, Semaphorin 3B-associated membranous nephropathy is a distinct type of disease predominantly present in pediatric patients, *Kidney international*, 98 (5) (2020), 1253–1264.
- [12] S. Sethi, H. Debiec, B. Madden, M.C. Charlesworth, J. Morelle, L. Gross, A. Ravindran, D. Buob, M. Jadoul, F.C. Fervenza and P. Ronco, Neural epidermal growth factor-like 1 protein (NELL-1) associated membranous nephropathy, *Kidney international*, 97 (1) (2020), 163–174.
- [13] S. Sethi, B. Madden, H. Debiec, J. Morelle, M.C. Charlesworth, L. Gross, V. Negron, D. Buob, S. Chaudhry, M. Jadoul, F.C. Fervenza and P. Ronco, Protocadherin 7-Associated Membranous Nephropathy, *Journal of the American Society of Nephrology : JASN*, 32 (5) (2021), 1249–1261.
- [14] G. Lambeau, Receptors for a growing family of secreted phospholipases A2, *Trends in Pharmacological Sciences*, 20 (4) (1999), 162–170.
- [15] E. Zvaritch, G. Lambeau and M. Lazdunski, Endocytic properties of the M-type 180-kDa receptor for secretory phospholipases A2, *The Journal of biological chemistry*, 271 (1) (1996), 250–257.
- [16] J. Boskovic, J.N. Arnold, R. Stilson, S. Gordon, R.B. Sim, A. Rivera-Calzada, D. Wienke, C.M. Isacke, L. Martinez-Pomares and O. Llorca, Structural model for the mannose receptor family uncovered by electron microscopy of Endo180 and the mannose receptor, *The Journal of biological chemistry*, 281 (13) (2006), 8780–8787.

- [17] Y. Dong, L. Cao, H. Tang, X. Shi and Y. He, Structure of Human M-type Phospholipase A2 Receptor Revealed by Cryo-Electron Microscopy, *Journal of molecular biology*, 429 (24) (2017), 3825–3835.
- [18] B.S. Gully, H. Venugopal, A.J. Fulcher, Z. Fu, J. Li, F.A. Deuss, C. Llerena, W.R. Heath, M.H. Lahoud, I. Caminschi, J. Rossjohn and R. Berry, The cryo-EM structure of the endocytic receptor DEC-205, *The Journal of biological chemistry*, 296 (2021), 100127.
- [19] M. Fresquet, T.A. Jowitt, J. Gummadova, R. Collins, R. O'Cualain, E.A. McKenzie, R. Lennon and P.E. Brenchley, Identification of a major epitope recognized by PLA2R autoantibodies in primary membranous nephropathy, *Journal of the American Society of Nephrology : JASN*, 26 (2) (2015), 302–313.
- [20] L. Kao, V. Lam, M. Waldman, R.J. Glasscock and Q. Zhu, Identification of the immunodominant epitope region in phospholipase A2 receptor-mediated autoantibody binding in idiopathic membranous nephropathy, *Journal of the American Society of Nephrology : JASN*, 26 (2) (2015), 291–301.
- [21] B. Seitz-Polski, G. Dolla, C. Payré, C.A. Girard, J. Polidori, K. Zorzi, E. Birgy-Barelli, P. Jullien, C. Courivaud, T. Krummel, S. Benzaken, G. Bernard, S. Burtey, C. Mariat, V.L.M. Esnault and G. Lambeau, Epitope Spreading of Autoantibody Response to PLA2R Associates with Poor Prognosis in Membranous Nephropathy, *Journal of the American Society of Nephrology : JASN*, 27 (5) (2016), 1517–1533.
- [22] L. Reinhard, G. Zahner, S. Menzel, F. Koch-Nolte, R.A.K. Stahl and E. Hoxha, Clinical Relevance of Domain-Specific Phospholipase A2 Receptor 1 Antibody Levels in Patients with Membranous Nephropathy, *Journal of the American Society of Nephrology : JASN*, 31 (1) (2020), 197–207.
- [23] M. Fresquet, M.P. Lockhart-Cairns, S.J. Rhoden, T.A. Jowitt, D.C. Briggs, C. Baldock, P.E. Brenchley and R. Lennon, Structure of PLA2R reveals presentation of the dominant membranous nephropathy epitope and an immunogenic patch, *Proceedings of the National Academy of Sciences of the United States of America*, 119 (29) (2022), e2202209119.
- [24] L. Seifert, E. Hoxha, A.M. Eichhoff, G. Zahner, S. Dehde, L. Reinhard, F. Koch-Nolte, R.A.K. Stahl and N.M. Tomas, The Most N-Terminal Region of THSD7A Is the Predominant Target for Autoimmunity in THSD7A-Associated Membranous Nephropathy, *Journal of the American Society of Nephrology : JASN*, 29 (5) (2018), 1536–1548.
- [25] S.G. Sharma and C.P. Larsen, Tissue staining for THSD7A in glomeruli correlates with serum antibodies in primary membranous nephropathy: a clinicopathological study, *Modern Pathology*, 31 (4) (2018), 616–622.
- [26] M.E. Reff, K. Carner, K.S. Chambers, P.C. Chinn, J.E. Leonard, R. Raab, R.A. Newman, N. Hanna and D.R. Anderson, Depletion of B cells in vivo by a chimeric mouse human monoclonal antibody to CD20, *Blood*, 83 (2) (1994), 435–445.
- [27] D.R. Anderson, A. Grillo-López, C. Varns, K.S. Chambers and N. Hanna, Targeted anti-cancer therapy using rituximab, a chimaeric anti-CD20 antibody (IDEC-C2B8) in the treatment of non-Hodgkin's B-cell lymphoma, *Biochemical Society transactions*, 25 (2) (1997), 705–708.
- [28] M.J. Glennie, R.R. French, M.S. Cragg and R.P. Taylor, Mechanisms of killing by anti-CD20 monoclonal antibodies, *Molecular immunology*, 44 (16) (2007), 3823–3837.
- [29] B. Coiffier, S. Lefretre, L.M. Pedersen, O. Gadeberg, H. Fredriksen, M.H.J. van Oers, J. Wooldridge, J. Kloczko, J. Holowiecki, A. Hellmann, J. Walewski, M. Flensburg, J. Petersen and T. Robak, Safety and efficacy of ofatumumab, a fully human monoclonal anti-CD20 antibody, in patients with relapsed or refractory B-cell chronic lymphocytic leukemia: a phase 1-2 study, *Blood*, 111 (3) (2008), 1094–1100.
- [30] M. de Weers, Y.-T. Tai, M.S. van der Veer, J.M. Bakker, T. Vink, D.C.H. Jacobs, L.A. Oomen, M. Peipp, T. Valerius, J.W. Slootstra, T. Mutis, W.K. Bleeker, K.C. Anderson, H.M. Lokhorst, J.G.J. van de Winkel and P.W.H.I. Parren, Daratumumab, a novel therapeutic human CD38 monoclonal antibody, induces killing of multiple myeloma and other hematological tumors, *Journal of immunology (Baltimore, Md. : 1950)*, 186 (3) (2011), 1840–1848.
- [31] J. Deckert, M.-C. Wetzel, L.M. Bartle, A. Skaletskaya, V.S. Goldmacher, F. Vallée, Q. Zhou-Liu, P. Ferrari, S. Pouzieux, C. Lahoute, C. Dumontet, A. Plesa, M. Chiron, P. Lejeune, T. Chittenden, P.U. Park and V. Blanc, SAR650984, a novel humanized CD38-targeting antibody, demonstrates potent

- antitumor activity in models of multiple myeloma and other CD38+ hematologic malignancies, *Clinical cancer research : an official journal of the American Association for Cancer Research*, 20 (17) (2014), 4574–4583.
- [32] K.P. Baker, B.M. Edwards, S.H. Main, G.H. Choi, R.E. Wager, W.G. Halpern, P.B. Lappin, T. Riccobene, D. Abramian, L. Sekut, B. Sturm, C. Poortman, R.R. Minter, C.L. Dobson, E. Williams, S. Carmen, R. Smith, V. Roschke, D.M. Hilbert, T.J. Vaughan and V.R. Albert, Generation and characterization of LymphoStat-B, a human monoclonal antibody that antagonizes the bioactivities of B lymphocyte stimulator, *Arthritis and rheumatism*, 48 (11) (2003), 3253–3265.
- [33] B. Basu, Ofatumumab for rituximab-resistant nephrotic syndrome, *The New England journal of medicine*, 370 (13) (2014), 1268–1270.
- [34] MorphoSys AG, A Phase Ib/IIa, Open-Label, Multicenter Clinical Trial to Assess Safety and Efficacy of the Human Anti-CD38 Antibody MOR202 in Anti-PLA2R Antibody Positive Membranous Nephropathy (aMN), <https://clinicaltrials.gov/ct2/show/NCT04145440> (11 November 2022).
- [35] National Institute of Allergy and Infectious Diseases (NIAID), Immune Tolerance Network (ITN), GlaxoSmithKline, PPD and Rho Federal Systems Division, Inc., Efficacy of Belimumab and Rituximab Compared to Rituximab Alone for the Treatment of Primary Membranous Nephropathy (ITN080AI), <https://clinicaltrials.gov/ct2/show/NCT03949855> (11 November 2022).
- [36] S.Y. Chu, I. Vostiar, S. Karki, G.L. Moore, G.A. Lazar, E. Pong, P.F. Joyce, D.E. Szymkowski and J.R. Desjarlais, Inhibition of B cell receptor-mediated activation of primary human B cells by coengagement of CD19 and FcγRIIb with Fc-engineered antibodies, *Molecular immunology*, 45 (15) (2008), 3926–3933.
- [37] J. Desjarlais, S. Chu, H. Horton, H. Chen, S. Karki, I. Leung and D. Szymkowski, Reduction of Total IgE by Targeted Coengagement of IgE-BCR and FcγRIIb with Fc-Engineered Antibodies, *Journal of Allergy and Clinical Immunology*, 127 (2) (2011), AB164-AB164.
- [38] Y. Iwayanagi, T. Igawa, A. Maeda, K. Haraya, N.A. Wada, N. Shibahara, K. Ohmine, T. Nambu, G. Nakamura, F. Mimoto, H. Katada, S. Ito, T. Tachibana, K. Jishage and K. Hattori, Inhibitory FcγRIIb-Mediated Soluble Antigen Clearance from Plasma by a pH-Dependent Antigen-Binding Antibody and Its Enhancement by Fc Engineering, *Journal of immunology (Baltimore, Md. : 1950)*, 195 (7) (2015), 3198–3205.
- [39] T. Igawa, A. Maeda, K. Haraya, T. Tachibana, Y. Iwayanagi, F. Mimoto, Y. Higuchi, S. Ishii, S. Tamba, N. Hironiwa, K. Nagano, T. Wakabayashi, H. Tsunoda and K. Hattori, Engineered monoclonal antibody with novel antigen-sweeping activity in vivo, *PLoS ONE*, 8 (5) (2013), e63236.
- [40] T. Igawa, K. Haraya and K. Hattori, Sweeping antibody as a novel therapeutic antibody modality capable of eliminating soluble antigens from circulation, *Immunological reviews*, 270 (1) (2016), 132–151.
- [41] F. Nimmerjahn and J.V. Ravetch, Divergent immunoglobulin g subclass activity through selective Fc receptor binding, *Science (New York, N.Y.)*, 310 (5753) (2005), 1510–1512.
- [42] J.G. van de Winkel and C.L. Anderson, Biology of human immunoglobulin G Fc receptors, *Journal of leukocyte biology*, 49 (5) (1991), 511–524.
- [43] J.C. Unkeless and H.N. Eisen, Binding of monomeric immunoglobulins to Fc receptors of mouse macrophages, *The Journal of experimental medicine*, 142 (6) (1975), 1520–1533.
- [44] C.E. van der Poel, R.A. Karssemeijer, P. Boross, J.A. van der Linden, M. Blokland, J.G.J. van de Winkel and J.H.W. Leusen, Cytokine-induced immune complex binding to the high-affinity IgG receptor, FcγRI, in the presence of monomeric IgG, *Blood*, 116 (24) (2010), 5327–5333.
- [45] F. Nimmerjahn, A. Lux, H. Albert, M. Woigk, C. Lehmann, D. Dudziak, P. Smith and J.V. Ravetch, FcγRIV deletion reveals its central role for IgG2a and IgG2b activity in vivo, *Proceedings of the National Academy of Sciences of the United States of America*, 107 (45) (2010), 19396–19401.
- [46] P. Bruhns, B. Iannascoli, P. England, D.A. Mancardi, N. Fernandez, S. Jorieux and M. Daëron, Specificity and affinity of human Fcγ receptors and their polymorphic variants for human IgG subclasses, *Blood*, 113 (16) (2009), 3716–3725.
- [47] S. Latour, W.H. Fridman and M. Daëron, Identification, molecular cloning, biologic properties, and tissue distribution of a novel isoform of murine low-affinity IgG receptor homologous to human FcγRIIB1, *Journal of immunology (Baltimore, Md. : 1950)*, 157 (1) (1996), 189–197.

- [48] F. Nimmerjahn and J.V. Ravetch, Fcγ receptors: old friends and new family members, *Immunity*, 24 (1) (2006), 19–28.
- [49] M.D. Hulett and P.M. Hogarth, Molecular Basis of Fc Receptor Function, *Advances in immunology*, 57 (1994), 1–127.
- [50] M. Pyzik, K.M.K. Sand, J.J. Hubbard, J.T. Andersen, I. Sandlie and R.S. Blumberg, The Neonatal Fc Receptor (FcRn): A Misnomer?, *Frontiers in immunology*, 10 (2019), 1540.
- [51] T. Peters *Advances in protein chemistry*, in: C.B. Anfinsen, J.T. Edsall and F.M. Richards (Eds.) *Advances in protein chemistry*, Academic Press, Orlando u. a., 1985, pp. 161–245.
- [52] H.L. Spiegelberg and B.G. Fishkin, The catabolism of human G immunoglobulins of different heavy chain subclasses. 3. The catabolism of heavy chain disease proteins and of Fc fragments of myeloma proteins, *Clinical and Experimental Immunology*, 10 (4) (1972), 599–607.
- [53] S. Akilesh, T.B. Huber, H. Wu, G. Wang, B. Hartleben, J.B. Kopp, J.H. Miner, D.C. Roopenian, E.R. Unanue and A.S. Shaw, Podocytes use FcRn to clear IgG from the glomerular basement membrane, *Proceedings of the National Academy of Sciences of the United States of America*, 105 (3) (2008), 967–972.
- [54] K.M.K. Sand, M. Bern, J. Nilsen, H.T. Noordzij, I. Sandlie and J.T. Andersen, Unraveling the Interaction between FcRn and Albumin: Opportunities for Design of Albumin-Based Therapeutics, *Frontiers in immunology*, 5 (2014), 682.
- [55] E. Dobrinskikh, L. Lewis, R. Brian Doctor, K. Okamura, M.G. Lee, C. Altmann, S. Faubel, J.B. Kopp and J. Blaine, Shank2 Regulates Renal Albumin Endocytosis, *Physiological reports*, 3 (9) (2015).
- [56] H. Birn and E.I. Christensen, Renal albumin absorption in physiology and pathology, *Kidney international*, 69 (3) (2006), 440–449.
- [57] C. Géraud, K. Evdokimov, B.K. Straub, W.K. Peitsch, A. Demory, Y. Dörflinger, K. Schledzewski, A. Schmieder, P. Schemmer, H.G. Augustin, P. Schirmacher and S. Goerdts, Unique cell type-specific junctional complexes in vascular endothelium of human and rat liver sinusoids, *PLoS ONE*, 7 (4) (2012), e34206.
- [58] E. Wisse, R.B. de Zanger, K. Charels, P. van der Smissen and R.S. McCuskey, The liver sieve: considerations concerning the structure and function of endothelial fenestrae, the sinusoidal wall and the space of Disse, *Hepatology (Baltimore, Md.)*, 5 (4) (1985), 683–692.
- [59] L.P. Ganesan, J. Kim, Y. Wu, S. Mohanty, G.S. Phillips, D.J. Birmingham, J.M. Robinson and C.L. Anderson, FcγRIIb on liver sinusoidal endothelium clears small immune complexes, *Journal of immunology (Baltimore, Md. : 1950)*, 189 (10) (2012), 4981–4988.
- [60] M. Heidelberger and F.E. Kendall, A QUANTITATIVE THEORY OF THE PRECIPITIN REACTION : III. THE REACTION BETWEEN CRYSTALLINE EGG ALBUMIN AND ITS HOMOLOGOUS ANTIBODY, *The Journal of experimental medicine*, 62 (5) (1935), 697–720.
- [61] A.O. Haakenstad, Removal of glomerular deposits induced by either preformed immune complexes or by a chronic immune complex model in NZB/W mice, *Journal of immunology (Baltimore, Md. : 1950)*, 138 (12) (1987), 4192–4199.
- [62] M.H. Wener and M. Mannik, Mechanisms of immune deposit formation in renal glomeruli, *Springer seminars in immunopathology*, 9 (2-3) (1986), 219–235.
- [63] H.M. Miettinen, J.K. Rose and I. Mellman, Fc receptor isoforms exhibit distinct abilities for coated pit localization as a result of cytoplasmic domain heterogeneity, *Cell*, 58 (2) (1989), 317–327.
- [64] S.A. Mousavi, M. Sporstøl, C. Fladeby, R. Kjekken, N. Barois and T. Berg, Receptor-mediated endocytosis of immune complexes in rat liver sinusoidal endothelial cells is mediated by FcγRIIb2, *Hepatology (Baltimore, Md.)*, 46 (3) (2007), 871–884.
- [65] M. Berg, G. Wingender, D. Djandji, S. Hegenbarth, F. Momburg, G. Hämmerling, A. Limmer and P. Knolle, Cross-presentation of antigens from apoptotic tumor cells by liver sinusoidal endothelial cells leads to tumor-specific CD8<sup>+</sup> T cell tolerance, *European journal of immunology*, 36 (11) (2006), 2960–2970.
- [66] A. Carambia, C. Frenzel, O.T. Bruns, D. Schwinge, R. Reimer, H. Hohenberg, S. Huber, G. Tiegs, C. Schramm, A.W. Lohse and J. Herkel, Inhibition of inflammatory CD4 T cell activity by murine liver sinusoidal endothelial cells, *Journal of hepatology*, 58 (1) (2013), 112–118.

- [67] Y. Takabe, S. Yagi, T. Koike and N. Shiojiri, Immunomagnetic exclusion of E-cadherin-positive hepatoblasts in fetal mouse liver cell cultures impairs morphogenesis and gene expression of sinusoidal endothelial cells, *Journal of anatomy*, 221 (3) (2012), 229–239.
- [68] A. Schrage, C. Loddenkemper, U. Erben, U. Lauer, G. Hausdorf, P.R. Jungblut, J. Johnson, P.A. Knolle, M. Zeitz, A. Hamann and K. Klugewitz, Murine CD146 is widely expressed on endothelial cells and is recognized by the monoclonal antibody ME-9F1, *Histochemistry and cell biology*, 129 (4) (2008), 441–451.
- [69] N. Despoix, T. Walzer, N. Jouve, M. Blot-Chabaud, N. Bardin, P. Paul, L. Lyonnet, E. Vivier, F. Dignat-George and F. Vély, Mouse CD146/MCAM is a marker of natural killer cell maturation, *European journal of immunology*, 38 (10) (2008), 2855–2864.
- [70] O. Strauss, A. Phillips, K. Ruggiero, A. Bartlett and P.R. Dunbar, Immunofluorescence identifies distinct subsets of endothelial cells in the human liver, *Scientific reports*, 7 (2017), 44356.
- [71] K. Su, H. Yang, X. Li, X. Li, A.W. Gibson, J.M. Cafardi, T. Zhou, J.C. Edberg and R.P. Kimberly, Expression profile of FcγRIIb on leukocytes and its dysregulation in systemic lupus erythematosus, *Journal of immunology* (Baltimore, Md. : 1950), 178 (5) (2007), 3272–3280.
- [72] S. Bhandari, R. Li, J. Simón-Santamaría, P. McCourt, S.D. Johansen, B. Smedsrød, I. Martinez-Zubiaurre and K.K. Sørensen, Transcriptome and proteome profiling reveal complementary scavenger and immune features of rat liver sinusoidal endothelial cells and liver macrophages, *BMC molecular and cell biology*, 21 (1) (2020), 85.
- [73] Q. Su, S.Y. Kim, F. Adewale, Y. Zhou, C. Aldler, M. Ni, Y. Wei, M.E. Burczynski, G.S. Atwal, M.W. Sleeman, A.J. Murphy, Y. Xin and X. Cheng, Single-cell RNA transcriptome landscape of hepatocytes and non-parenchymal cells in healthy and NAFLD mouse liver, *iScience*, 24 (11) (2021), 103233.
- [74] N.M. Tomas, S. Dehde, C. Meyer-Schwesinger, M. Huang, I. Hermans-Borgmeyer, J. Maybaum, R. Lucas, J.L. von der Heide, O. Kretz, S.M.S. Köllner, L. Seifert, T.B. Huber and G. Zahner, Podocyte expression of human phospholipase A2 receptor 1 causes immune-mediated membranous nephropathy in mice, *Kidney international* (2022).
- [75] N.M. Tomas, C. Meyer-Schwesinger, H. von Spiegel, A.M. Kotb, G. Zahner, E. Hoxha, U. Helmchen, N. Endlich, F. Koch-Nolte and R.A.K. Stahl, A Heterologous Model of Thrombospondin Type 1 Domain-Containing 7A-Associated Membranous Nephropathy, *Journal of the American Society of Nephrology : JASN*, 28 (11) (2017), 3262–3277.
- [76] C. Meyer-Schwesinger, T.N. Meyer, H. Sievert, E. Hoxha, M. Sachs, E.-M. Klupp, S. Münster, S. Balabanov, L. Carrier, U. Helmchen, F. Thaiss and R.A.K. Stahl, Ubiquitin C-terminal hydrolase-11 activity induces polyubiquitin accumulation in podocytes and increases proteinuria in rat membranous nephropathy, *The American Journal of Pathology*, 178 (5) (2011), 2044–2057.
- [77] T. Schirrmann and K. Büsow *Antibody Engineering*, in: R. Kontermann and S. Dübel (Eds.) *Antibody Engineering*, Scholars Portal, Berlin, Heidelberg, 2010, pp. 387–398.
- [78] W.C. Skarnes, B. Rosen, A.P. West, M. Koutsourakis, W. Bushell, V. Iyer, A.O. Mujica, M. Thomas, J. Harrow, T. Cox, D. Jackson, J. Severin, P. Biggs, J. Fu, M. Nefedov, P.J. de Jong, A.F. Stewart and A. Bradley, A conditional knockout resource for the genome-wide study of mouse gene function, *Nature*, 474 (7351) (2011), 337–342.
- [79] F. Schwenk, U. Baron and K. Rajewsky, A cre-transgenic mouse strain for the ubiquitous deletion of loxP-flanked gene segments including deletion in germ cells, *Nucleic acids research*, 23 (24) (1995), 5080–5081.
- [80] J.M. Wilson, M. de Hoop, N. Zorzi, B.H. Toh, C.G. Dotti and R.G. Parton, EEA1, a tethering protein of the early sorting endosome, shows a polarized distribution in hippocampal neurons, epithelial cells, and fibroblasts, *Molecular biology of the cell*, 11 (8) (2000), 2657–2671.
- [81] F. de Ritis, M. Coltorti and G. Giusti, An enzymic test for the diagnosis of viral hepatitis: The transaminase serum activities, *Clinica chimica acta; international journal of clinical chemistry*, 2 (1) (1957), 70–74.
- [82] F. de Ritis, M. Coltorti and G. Giusti, An enzymic test for the diagnosis of viral hepatitis: the transaminase serum activities. 1957, *Clinica chimica acta; international journal of clinical chemistry*, 369 (2) (2006), 148–152.

- [83] S. Agrawal, J.J. Zaritsky, A. Fornoni and W.E. Smoyer, Dyslipidaemia in nephrotic syndrome: mechanisms and treatment, *Nature reviews. Nephrology*, 14 (1) (2018), 57–70.
- [84] S.C. Devanaboyina, P. Khare, D.K. Challa, R.J. Ober and E.S. Ward, Engineered clearing agents for the selective depletion of antigen-specific antibodies, *Nat Commun*, 8 (1) (2017), 15314.
- [85] W. Sun, P. Khare, X. Wang, D.K. Challa, B.M. Greenberg, R.J. Ober and E.S. Ward, Selective Depletion of Antigen-Specific Antibodies for the Treatment of Demyelinating Disease, *Molecular therapy : the journal of the American Society of Gene Therapy*, 29 (3) (2021), 1312–1323.
- [86] C.-H. Lee, G. Romain, W. Yan, M. Watanabe, W. Charab, B. Todorova, J. Lee, K. Triplett, M. Donkor, O.I. Lungu, A. Lux, N. Marshall, M.A. Lindorfer, O.R.-L. Goff, B. Balbino, T.H. Kang, H. Tanno, G. Delidakis, C. Alford, R.P. Taylor, F. Nimmerjahn, N. Varadarajan, P. Bruhns, Y.J. Zhang and G. Georgiou, IgG Fc domains that bind C1q but not effector Fc $\gamma$  receptors delineate the importance of complement-mediated effector functions, *Nature immunology*, 18 (8) (2017), 889–898.
- [87] A.M. Collins, Y. Wang, K.M. Roskin, C.P. Marquis and K.J.L. Jackson, The mouse antibody heavy chain repertoire is germline-focused and highly variable between inbred strains, *Philosophical transactions of the Royal Society of London. Series B, Biological sciences*, 370 (1676) (2015).
- [88] K.J.L. Jackson, Y. Wang and A.M. Collins, Human immunoglobulin classes and subclasses show variability in VDJ gene mutation levels, *Immunology and cell biology*, 92 (8) (2014), 729–733.
- [89] J. Lu, J. Chu, Z. Zou, N.B. Hamacher, M.W. Rixon and P.D. Sun, Structure of Fc $\gamma$ RI in complex with Fc reveals the importance of glycan recognition for high-affinity IgG binding, *Proceedings of the National Academy of Sciences of the United States of America*, 112 (3) (2015), 833–838.
- [90] P.R. Banks and D.M. Paquette, Comparison of three common amine reactive fluorescent probes used for conjugation to biomolecules by capillary zone electrophoresis, *Bioconjugate chemistry*, 6 (4) (1995), 447–458.
- [91] A.V. Elchaninov, T.K. Fatkhudinov, P.A. Vishnyakova, A.V. Lokhonina and G.T. Sukhikh, Phenotypical and Functional Polymorphism of Liver Resident Macrophages, *Cells*, 8 (9) (2019).
- [92] E.S. Ward, S.C. Devanaboyina and R.J. Ober, Targeting FcRn for the modulation of antibody dynamics, *Molecular immunology*, 67 (2 Pt A) (2015), 131–141.
- [93] L. Grosse and D.V. Bulavin, LSEC model of aging, *Aging*, 12 (11) (2020), 11152–11160.
- [94] J.G. Hu, T. Yokoyama and T. Kitagawa, Studies on the optimal immunization schedule of experimental animals. IV. The optimal age and sex of mice, and the influence of booster injections, *Chemical & pharmaceutical bulletin*, 38 (2) (1990), 448–451.
- [95] X. Yu, L. Chen, J. Liu, B. Dai, G. Xu, G. Shen, Q. Luo and Z. Zhang, Immune modulation of liver sinusoidal endothelial cells by melittin nanoparticles suppresses liver metastasis, *Nat Commun*, 10 (1) (2019), 574.
- [96] T.A. Fehniger, S.F. Cai, X. Cao, A.J. Bredemeyer, R.M. Presti, A.R. French and T.J. Ley, Acquisition of murine NK cell cytotoxicity requires the translation of a pre-existing pool of granzyme B and perforin mRNAs, *Immunity*, 26 (6) (2007), 798–811.
- [97] C.S. Henney, K. Kuribayashi, D.E. Kern and S. Gillis, Interleukin-2 augments natural killer cell activity, *Nature*, 291 (5813) (1981), 335–338.
- [98] M. Aste-Amezaga, A. D'Andrea, M. Kubin and G. Trinchieri, Cooperation of natural killer cell stimulatory factor/interleukin-12 with other stimuli in the induction of cytokines and cytotoxic cell-associated molecules in human T and NK cells, *Cellular immunology*, 156 (2) (1994), 480–492.
- [99] T.J. Kipps, P. Parham, J. Punt and L.A. Herzenberg, Importance of immunoglobulin isotype in human antibody-dependent, cell-mediated cytotoxicity directed by murine monoclonal antibodies, *The Journal of experimental medicine*, 161 (1) (1985), 1–17.
- [100] M. Kiyoshi, J.M.M. Caaveiro, T. Kawai, S. Tashiro, T. Ide, Y. Asaoka, K. Hatayama and K. Tsumoto, Structural basis for binding of human IgG1 to its high-affinity human receptor Fc $\gamma$ RI, *Nat Commun*, 6 (2015), 6866.
- [101] A. Lux, X. Yu, C.N. Scanlan and F. Nimmerjahn, Impact of immune complex size and glycosylation on IgG binding to human Fc $\gamma$ Rs, *Journal of immunology (Baltimore, Md. : 1950)*, 190 (8) (2013), 4315–4323.
- [102] T. Schlothauer, S. Herter, C.F. Koller, S. Grau-Richards, V. Steinhart, C. Spick, M. Kubbies, C. Klein, P. Umaña and E. Mössner, Novel human IgG1 and IgG4 Fc-engineered antibodies with

- completely abolished immune effector functions, *Protein engineering, design & selection : PEDS*, 29 (10) (2016), 457–466.
- [103] G. Dekkers, A.E.H. Bentlage, T.C. Stegmann, H.L. Howie, S. Lissenberg-Thunnissen, J. Zimring, T. Rispens and G. Vidarsson, Affinity of human IgG subclasses to mouse Fc gamma receptors, *mAbs*, 9 (5) (2017), 767–773.
- [104] P.I. Kitov and D.R. Bundle, On the nature of the multivalency effect: a thermodynamic model, *Journal of the American Chemical Society*, 125 (52) (2003), 16271–16284.
- [105] V. Yip, E. Palma, D.B. Tesar, E.E. Mundo, D. Bumbaca, E.K. Torres, N.A. Reyes, B.Q. Shen, P.J. Fielder, S. Prabhu, L.A. Khawli and C.A. Boswell, Quantitative cumulative biodistribution of antibodies in mice: effect of modulating binding affinity to the neonatal Fc receptor, *mAbs*, 6 (3) (2014), 689–696.
- [106] N. Chen, W. Wang, S. Fauty, Y. Fang, L. Hamuro, A. Hussain and T. Prueksaritanont, The effect of the neonatal Fc receptor on human IgG biodistribution in mice, *mAbs*, 6 (2) (2014), 502–508.
- [107] M. Pyzik, T. Rath, T.T. Kuo, S. Win, K. Baker, J.J. Hubbard, R. Grenha, A. Gandhi, T.D. Krämer, A.R. Mezo, Z.S. Taylor, K. McDonnell, V. Nienaber, J.T. Andersen, A. Mizoguchi, L. Blumberg, S. Purohit, S.D. Jones, G. Christianson, W.I. Lencer, I. Sandlie, N. Kaplowitz, D.C. Roopenian and R.S. Blumberg, Hepatic FcRn regulates albumin homeostasis and susceptibility to liver injury, *Proceedings of the National Academy of Sciences of the United States of America*, 114 (14) (2017), E2862-E2871.
- [108] J.L. FAHEY and A.G. ROBINSON, FACTORS CONTROLLING SERUM GAMMA-GLOBULIN CONCENTRATION, *The Journal of experimental medicine*, 118 (1963), 845–868.
- [109] X. Liu, L. Ye, Y. Bai, H. Mojidi, N.E. Simister and X. Zhu, Activation of the JAK/STAT-1 signaling pathway by IFN-gamma can down-regulate functional expression of the MHC class I-related neonatal Fc receptor for IgG, *Journal of immunology (Baltimore, Md. : 1950)*, 181 (1) (2008), 449–463.
- [110] X. Liu, L. Ye, G.J. Christianson, J.-Q. Yang, D.C. Roopenian and X. Zhu, NF-kappaB signaling regulates functional expression of the MHC class I-related neonatal Fc receptor for IgG via intronic binding sequences, *Journal of immunology (Baltimore, Md. : 1950)*, 179 (5) (2007), 2999–3011.
- [111] E. Jouvin-Marche, M.G. Morgado, C. Leguern, D. Voegtle, F. Bonhomme and P.A. Cazenave, The mouse Igh-1a and Igh-1b H chain constant regions are derived from two distinct isotypic genes, *Immunogenetics*, 29 (2) (1989), 92–97.
- [112] T.R. Mosmann and R.L. Coffman, TH1 and TH2 cells: different patterns of lymphokine secretion lead to different functional properties, *Annual review of immunology*, 7 (1989), 145–173.
- [113] S.L. Reiner and R.M. Locksley, The regulation of immunity to *Leishmania major*, *Annual review of immunology*, 13 (1995), 151–177.
- [114] K.M. Murphy and C. Weaver, *Janeway Immunologie*, 9th ed. (Springer Berlin Heidelberg, Berlin, Heidelberg, 2018).
- [115] H. Fukuyama, F. Nimmerjahn and J.V. Ravetch, The inhibitory Fc gamma receptor modulates autoimmunity by limiting the accumulation of immunoglobulin G+ anti-DNA plasma cells, *Nature immunology*, 6 (1) (2005), 99–106.
- [116] N. de Haan, K.R. Reiding, J. Krištić, A.L. Hipgrave Ederveen, G. Lauc and M. Wuhrer, The N-Glycosylation of Mouse Immunoglobulin G (IgG)-Fragment Crystallizable Differs Between IgG Subclasses and Strains, *Frontiers in immunology*, 8 (2017), 608.
- [117] R.M. Anthony, F. Wermeling, M.C.I. Karlsson and J.V. Ravetch, Identification of a receptor required for the anti-inflammatory activity of IVIG, *Proceedings of the National Academy of Sciences of the United States of America*, 105 (50) (2008), 19571–19578.
- [118] M.B. Jones, D.M. Oswald, S. Joshi, S.W. Whiteheart, R. Orlando and B.A. Cobb, B-cell-independent sialylation of IgG, *Proceedings of the National Academy of Sciences of the United States of America*, 113 (26) (2016), 7207–7212.
- [119] C. Hess, A. Winkler, A.K. Lorenz, V. Holeccka, V. Blanchard, S. Eiglmeier, A.-L. Schoen, J. Bitterling, A.D. Stoehr, D. Petzold, T. Schommartz, M.M.M. Mertes, C.T. Schoen, B. Tiburzy, A. Herrmann, J. Köhl, R.A. Manz, M.P. Madaio, M. Berger, H. Wardemann and M. Ehlers, T cell-independent B cell activation induces immunosuppressive sialylated IgG antibodies, *The Journal of clinical investigation*, 123 (9) (2013), 3788–3796.

- [120] I. Quast, C.W. Keller, M.A. Maurer, J.P. Giddens, B. Tackenberg, L.-X. Wang, C. Münz, F. Nimmerjahn, M.C. Dalakas and J.D. Lünemann, Sialylation of IgG Fc domain impairs complement-dependent cytotoxicity, *The Journal of clinical investigation*, 125 (11) (2015), 4160–4170.
- [121] L. Grassi and C. Cabrele, Susceptibility of protein therapeutics to spontaneous chemical modifications by oxidation, cyclization, and elimination reactions, *Amino Acids*, 51 (10-12) (2019), 1409–1431.
- [122] R.T. MCCLUSKEY, B. BENACERRAF, J.L. POTTER and F. MILLER, The pathologic effects of intravenously administered soluble antigen-antibody complexes. I. Passive serum sickness in mice, *The Journal of experimental medicine*, 111 (1960), 181–194.
- [123] S. Akiyama, E. Imai and S. Maruyama, Immunology of membranous nephropathy, *F1000Research*, 8 (2019).
- [124] H. Ochiai, T. Shirasawa, T. Yoshimoto, S. Nagahama, A. Watanabe, K. Sakamoto and A. Kokaze, Elevated alanine aminotransferase and low aspartate aminotransferase/alanine aminotransferase ratio are associated with chronic kidney disease among middle-aged women: a cross-sectional study, *BMC Nephrol*, 21 (1) (2020), 471.
- [125] S. David and J.P. Hamilton, Drug-induced Liver Injury, *US gastroenterology & hepatology review*, 6 (2010), 73–80.
- [126] T. Skogh, R. Blomhoff, W. Eskild and T. Berg, Hepatic uptake of circulating IgG immune complexes, *Immunology*, 55 (4) (1985), 585–594.
- [127] K.D. Ratanji, J.P. Derrick, R.J. Dearman and I. Kimber, Immunogenicity of therapeutic proteins: influence of aggregation, *Journal of Immunotoxicology*, 11 (2) (2014), 99–109.
- [128] P. Ghia, E. ten Boekel, A.G. Rolink and F. Melchers, B-cell development: a comparison between mouse and man, *Immunology today*, 19 (10) (1998), 480–485.
- [129] M.M. Kay, J. Mendoza, J. Diven, T. Denton, N. Union and M. Lajiness, Age-related changes in the immune system of mice of eight medium and long-lived strains and hybrids. I. Organ, cellular, and activity changes, *Mechanisms of ageing and development*, 11 (5-6) (1979), 295–346.
- [130] T.B. Jeong, D. Kwon, S.W. Son, S.H. Kim, Y.-H. Lee, M.-S. Seo, K.S. Kim and Y.-S. Jung, Weaning Mice and Adult Mice Exhibit Differential Carbon Tetrachloride-Induced Acute Hepatotoxicity, *Antioxidants (Basel, Switzerland)*, 9 (3) (2020).
- [131] K.J.L. Jackson, B.A. Gaëta and A.M. Collins, Identifying highly mutated IGHD genes in the junctions of rearranged human immunoglobulin heavy chain genes, *Journal of immunological methods*, 324 (1-2) (2007), 26–37.
- [132] J. Glanville, T.C. Kuo, H.-C. von Büdingen, L. Guey, J. Berka, P.D. Sundar, G. Huerta, G.R. Mehta, J.R. Oksenberg, S.L. Hauser, D.R. Cox, A. Rajpal and J. Pons, Naive antibody gene-segment frequencies are heritable and unaltered by chronic lymphocyte ablation, *Proceedings of the National Academy of Sciences of the United States of America*, 108 (50) (2011), 20066–20071.
- [133] H. Zhao and M. Sokabe, Tuning the mechanosensitivity of a BK channel by changing the linker length, *Cell Res*, 18 (8) (2008), 871–878.
- [134] N. Amet, H.-F. Lee and W.-C. Shen, Insertion of the designed helical linker led to increased expression of tf-based fusion proteins, *Pharmaceutical research*, 26 (3) (2009), 523–528.
- [135] X. Bai, J. Zhang, A. Ewing, S.A. Miller, A. Jancso Radek, D.V. Shevchenko, K. Tsukerman, T. Walunas, A. Lapidus, J.W. Campbell and S.A. Hogenhout, Living with genome instability: the adaptation of phytoplasmas to diverse environments of their insect and plant hosts, *Journal of bacteriology*, 188 (10) (2006), 3682–3696.
- [136] R. Aurora, T.P. Creamer, R. Srinivasan and G.D. Rose, Local interactions in protein folding: lessons from the alpha-helix, *The Journal of biological chemistry*, 272 (3) (1997), 1413–1416.
- [137] X. Chen, J.L. Zaro and W.-C. Shen, Fusion protein linkers: property, design and functionality, *Advanced drug delivery reviews*, 65 (10) (2013), 1357–1369.
- [138] R.E. Bird, K.D. Hardman, J.W. Jacobson, S. Johnson, B.M. Kaufman, S.M. Lee, T. Lee, S.H. Pope, G.S. Riordan and M. Whitlow, Single-chain antigen-binding proteins, *Science (New York, N.Y.)*, 242 (4877) (1988), 423–426.
- [139] D.R. Burton and R.A. Dwek, Immunology. Sugar determines antibody activity, *Science (New York, N.Y.)*, 313 (5787) (2006), 627–628.

- [140] J.N. Arnold, M.R. Wormald, R.B. Sim, P.M. Rudd and R.A. Dwek, The impact of glycosylation on the biological function and structure of human immunoglobulins, *Annual review of immunology*, 25 (2007), 21–50.
- [141] I. Schwab, M. Seeling, M. Biburger, S. Aschermann, L. Nitschke and F. Nimmerjahn, B cells and CD22 are dispensable for the immediate antiinflammatory activity of intravenous immunoglobulins in vivo, *European journal of immunology*, 42 (12) (2012), 3302–3309.
- [142] P.A. Blundell, D. Lu, A. Dell, S. Haslam and R.J. Pleass, Choice of Host Cell Line Is Essential for the Functional Glycosylation of the Fc Region of Human IgG1 Inhibitors of Influenza B Viruses, *The Journal of Immunology Author Choice*, 204 (4) (2020), 1022–1034.
- [143] J. Ehret, M. Zimmermann, T. Eichhorn and A. Zimmer, Impact of cell culture media additives on IgG glycosylation produced in Chinese hamster ovary cells, *Biotechnology and bioengineering*, 116 (4) (2019), 816–830.
- [144] J. Davda, P. Declerck, S. Hu-Lieskovan, T.P. Hickling, I.A. Jacobs, J. Chou, S. Salek-Ardakani and E. Kraynov, Immunogenicity of immunomodulatory, antibody-based, oncology therapeutics, *j. immunotherapy cancer*, 7 (1) (2019), 105.
- [145] R. Zeidler, G. Reisbach, B. Wollenberg, S. Lang, S. Chaubal, B. Schmitt and H. Lindhofer, Simultaneous activation of T cells and accessory cells by a new class of intact bispecific antibody results in efficient tumor cell killing, *The Journal of Immunology Author Choice*, 163 (3) (1999), 1246–1252.
- [146] W.F. Dall'Acqua, R.M. Woods, E.S. Ward, S.R. Palaszynski, N.K. Patel, Y.A. Brewah, H. Wu, P.A. Kiener and S. Langemann, Increasing the affinity of a human IgG1 for the neonatal Fc receptor: biological consequences, *The Journal of Immunology Author Choice*, 169 (9) (2002), 5171–5180.
- [147] S.J. Schuster, N.L. Bartlett, S. Assouline, S.-S. Yoon, F. Bosch, L.H. Sehn, C.Y. Cheah, M. Shadman, G.P. Gregory, M. Ku, M.C. Wei, S. Yin, A. Kwan, K. Yousefi, G. Hernandez, C.-C. Li, C. O'Hear and L.E. Budde, Mosunetuzumab Induces Complete Remissions in Poor Prognosis Non-Hodgkin Lymphoma Patients, Including Those Who Are Resistant to or Relapsing After Chimeric Antigen Receptor T-Cell (CAR-T) Therapies, and Is Active in Treatment through Multiple Lines, *Blood*, 134 (Supplement\_1) (2019), 6.
- [148] C.T. Ellebrecht, V.G. Bhoj, A. Nace, E.J. Choi, X. Mao, M.J. Cho, G. Di Zenzo, A. Lanzavecchia, J.T. Seykora, G. Cotsarelis, M.C. Milone and A.S. Payne, Reengineering chimeric antigen receptor T cells for targeted therapy of autoimmune disease, *Science (New York, N.Y.)*, 353 (6295) (2016), 179–184.
- [149] R. Li, C. Ma, H. Cai and W. Chen, The CAR T-Cell Mechanoimmunology at a Glance, *Advanced science (Weinheim, Baden-Wurttemberg, Germany)*, 7 (24) (2020), 2002628.
- [150] A. Akhter, Y. Hayashi, Y. Sakurai, N. Ohga, K. Hida and H. Harashima, A liposomal delivery system that targets liver endothelial cells based on a new peptide motif present in the ApoB-100 sequence, *International journal of pharmaceutics*, 456 (1) (2013), 195–201.
- [151] C.I. Øie, R.S. Appa, I. Hilden, H.H. Petersen, A. Gruhler, B. Smedsrød and J.-B. Hansen, Rat liver sinusoidal endothelial cells (LSECs) express functional low density lipoprotein receptor-related protein-1 (LRP-1), *Journal of hepatology*, 55 (6) (2011), 1346–1352.

“Don’t adventures ever have an end?

I suppose not.

Someone else always has to carry on the story.”

J.R.R. Tolkien